ACID FUNCTIONALIZED MESOPOROUS SILICA KIT-6 CATALYST FOR DEHYDRATION, ESTERIFICATION AND ETHERIFICATION

BY

MISS TRAN THI TUONG VI

A DISSERTATION SUBMITTED IN PARTIAL FULFILLMENT OF
THE REQUIREMENTS FOR THE DEGREE OF
DOCTOR OF PHILOSOPHY (CHEMISTRY)
DEPARTMENT OF CHEMISTRY
FACULTY OF SCIENCE AND TECHNOLOGY
THAMMASAT UNIVERSITY
ACADEMIC YEAR 2019

COPYRIGHT OF THAMMASAT UNIVERSITY

Ref. code: 25625909320250YIN

ACID FUNCTIONALIZED MESOPOROUS SILICA KIT-6 CATALYST FOR DEHYDRATION, ESTERIFICATION AND ETHERIFICATION

BY

MISS TRAN THI TUONG VI

A DISSERTATION SUBMITTED IN PARTIAL FULFILLMENT OF

THE REQUIREMENTS FOR THE DEGREE OF

DOCTOR OF PHILOSOPHY (CHEMISTRY)

DEPARTMENT OF CHEMISTRY

FACULTY OF SCIENCE AND TECHNOLOGY

THAMMASAT UNIVERSITY

ACADEMIC YEAR 2019

COPYRIGHT OF THAMMASAT UNIVERSITY

Ref. code: 25625909320250YIN

THAMMASAT UNIVERSITY

FACULTY OF SCIENCE AND TECHNOLOGY

DISSERTATION

BY

MISS TRAN THI TUONG VI

ENTITLED

ACID FUNCTIONALIZED MESOPOROUS SILICA KIT-6 CATALYST FOR DEHYDRATION, ESTERIFICATION AND ETHERIFICATION

was approved as partial fulfillment of the requirements for the degree of Doctor of Philosophy (Chemistry)

on June 8, 2020

Chairman _____ (Assistant Professor Suwadee Kongparakul, Ph.D.)

Member and Advisor _____ (Associate Professor Chanatip Samart, D.Eng.)

Member and Co-Advisor _____ (Professor Guoqing Guan, Ph.D.)

Member _____ (Associate Professor Prasert Reubroycharoen, D.Eng.)

Member _____ (Associate Professor Peerasak Paoprasert, Ph.D.)

Dean _____ (Assistant Professor Nuttanont Hongwarittorrn, Ph.D.)

Ref. code: 25625909320250YIN

Dissertation Title	ACID FUNCTIONALIZED MESOPOROUS SILICA KIT-6 CATALYST FOR DEHYDRATION, ESTERIFICATION AND ETHERIFICATION
Author	Miss Tran Thi Tuong Vi
Degree	Doctor of Philosophy (Chemistry)
Department/Faculty/University	Department of Chemistry Faculty of Science and Technology Thammasat University
Dissertation Advisor	Associate Professor Chanatip Samart, D.Eng.
Dissertation Co-Advisor	Professor Guoqing Guan, Ph.D.
Academic Year	2019

ABSTRACT

The KIT-6 (a highly ordered mesoporous silica with cubic Ia3d symmetry) and acid functionalized KIT-6 as a solid acid catalyst have been studied extensively for dehydration of xylose to furfural, esterification of fusel oil (isoamyl alcohol) to isoamyl acetate and etherification of glycerol to glycerol n-butyl ether. The KIT-6-SO_3H catalysts were synthesized by co-condensation method in different ratios of tetraethyl orthosilicate (TEOS, 99%) to 3-(mercaptopropyl) methyldimethoxysilane (MPMDS, 99%) and subsequent oxidation. Highly performance and selective dehydration of xylose to furfural were achieved using KIT-6-SO_3H as a catalyst in a water/toluene biphasic system. The highest xylose conversion and furfural selectivity were reached 97.50 and 94.65%, respectively at the optimized condition at 170 °C for 2 h of 0.2-KIT-6-SO_3H catalyst. This catalyst could be reused up to three cycles without any treatment. The KIT-6-SO_3H catalyst presented a high turnover frequency in the xylose dehydration reaction due to the three-dimensional structure of the KIT-6 mesoporous silica.

In the second part, the production of isoamyl acetate using KIT-6-SO_3H as a heterogeneous catalyst in the esterification reaction of fusel oil and acetic acid was achieved. The highest yield of isoamyl acetate was reached at 95.05% in the reaction condition of reaction temperature at 80 °C for 3 h. Moreover, the turnover frequency

Ref. code: 25625909320250YIN

(TOF) was controlled by accessibility and the amount of acid site which was manipulated by variation the ratio of MPMDS:TEOS and the highest TOF were achieved by 0.1-SO_3H-KIT-6. Whereas, 0.3-SO_3H-KIT-6 catalyst performed the excellent reusability over three cycles with the decrease in isoamyl acetate yield is not significant in each cycle.

In the last part, the etherification of glycerol and n-butanol using KIT-6-SO_3H as a heterogeneous catalyst was achieved. The 0.3-KIT-6-SO_3H catalyst contained the highest acidity would be selected as a catalyst for this reaction. The highest di glycerol n-butyl ether (di-GNBEs) selectivity was 51.50% at the optimized reaction condition of 140 ℃ for 6 h.

In this research, the KIT-6-SO_3H catalyst was prepared by sequential co-condensation and oxidation method. The KIT-6-SO_3H played the good performance in acid catalysis reaction including furfural production from xylose dehydration, isoamyl acetate production from fusel oil esterification and glycerol n-butyl ether production from glycerol etherification.

Keywords: KIT-6-SO_3H; Acid catalyst; Dehydration of xylose; Esterification of fusel oil; Etherification of glycerol; Fuel additive

Ref. code: 25625909320250YIN

ACKNOWLEDGEMENTS

The research work has been conducted in the Petrochem group in the Department of Chemistry, Faculty of Science and Technology, Thammasat University for the duration 2017-2020. I would like to extend my acknowledgment to the Thammasat University's Scholarship for Foreign Students Studying towards a Degree and the Faculty of Science and Technology, Thammasat University for supporting to study doctoral degree program in chemistry. Thanks go towards the instrument support provided by the Central Scientific Instrument Center, Faculty of Science and Technology and Center of Scientific Equipment for Advance Science Research, Office of Advanced Science and Technology, Thammasat University.

During the time to study at Thammasat University as a student of a doctoral degree, I wish to sincerely express for everyone who shared the knowledge, the experience, suggestions, and the advice throughout to complete my thesis.

Firstly, I would like to express my sincere gratitude to my advisor Associate Professor Chanatip Samart for giving me this opportunity to study and for all his valuable advice, motivation, encouragement. His great knowledge, enthusiasm and inspired in keeping my progress on schedule and I came to learn about so many new things for my future career. My thanks are also expressed to my co-advisor, Professor Guoqing Guan (Institute of Regional Innovation, Hirosaki University) for all the support, guidance and kindness. I express special thanks to Assistant Professor Suwadee Kongparakul for her gently support, comments and take care throughout the time in the Petrochem group. Thanks for the time being with you.

Besides, my sincere thanks to Assistant Professor Suwadee Kongparakul (Department of Chemistry, Faculty of Science and Technology, Thammasat University), Associate Professor Prasert Reubroycharoen (Department of Chemical Technology, Faculty of Science, Chulalongkorn University) and Associate Professor Peerasak Paoprasert (Department of Chemistry, Faculty of Science and Technology, Thammasat University) attending as chairman and member of my thesis committee, as well as for their constructive discussion, comments, and suggestions. And Dr. Narong Chanlek from

Ref. code: 25625909320250YIN

the Thailand Synchrotron Light Research Institute for his kindness assistance in XPS analysis. And I would love to all my lab-mates and friends for their kindness, friendly and helps directly and indirectly way to complete my thesis. Many thanks for every one of you.

Finally, I would like to express my warmest gratitude to my parents and my family for loving, encouraging, understanding and supporting me spiritually throughout my life.

Much love!

Miss Tran Thi Tuong Vi

Ref. code: 25625909320250YIN

TABLE OF CONTENTS

Ref. code: 25625909320250YIN

Ref. code: 25625909320250YIN

Ref. code: 25625909320250YIN

Ref. code: 25625909320250YIN

Ref. code: 25625909320250YIN

LIST OF TABLES

Ref. code: 25625909320250YIN

LIST OF FIGURES

Ref. code: 25625909320250YIN

Ref. code: 25625909320250YIN

Ref. code: 25625909320250YIN

CHAPTER 1
INTRODUCTION

1.1 Dissertation motivation

In the issue of future energy, fossil resources are running out due to the high demand in many industries including energy, polymers, fine chemicals and materials with limited resources. Moreover, regarding environmental degradation, the use of fossil fuels also exerted a negative impact on the environment (Alipour, Omidvarborna, & Kim, 2017; Jezak, Dzida, & Zorebski, 2016; Yuan, Zhang, Zheng, & Lin, 2015; Zhou & Zhang, 2016). Against this background, the scientists must find new energy resources that were renewable and clean to replacement of conventional fossil fuel due to their low pollution, net-zero carbon emissions, complete recyclability and potential to mitigate global warming (Alipour et al., 2017; Jezak et al., 2016; Lam, Lee, & Mohamed, 2010; Sajid, Zhao, & Liu, 2018; Yuan et al., 2015; Zhou & Zhang, 2016). Therefore, these problems are becoming more significant for scientists to take the responsibility of searching for renewable and sustainable resources.

Among renewable resources, biomass plays the most potential renewable resources due to its abundance and viability. In addition, biomass also presents an important role in carbon balance to capture CO_2 through photosynthesis and completely carbon cycle (Alipour et al., 2017; Jezak et al., 2016; Yuan et al., 2015; Zhang & Deng, 2015; Zhou & Zhang, 2016). Biomass is an organic material that was widely available in waste materials and plants such as crops, forestry wastes, agricultural residues, urban solid waste, animal residues, industrial residues, etc. (Kumar, Kumar, Baredar, & Shukla, 2015; Saidur, Abdelaziz, Demirbas, Hossain, & Mekhilef, 2011). Moreover, it is one of the most important renewable energy sources that don't affect food supply although competition for arable land use between biomass and edible biomass occurs in some cases and widely available in a various agricultural countries such as Viet Nam, Thailand, Indonesia, Malaysia, etc. (Kumar et al., 2015; Saidur et al., 2011). Generally, the utilization of biomass as a feedstock for

Ref. code: 25625909320250YIN

valuable platform chemicals and fuels is called "*biorefinery or bio-base green chemistry*". The biomass composed of three main different components of cellulose, hemicellulose and lignin. These components could be used as feedstock for synthesis different products through catalytic transformation including dehydration, hydrolysis, isomerization, reforming, aldol condensation, hydrogenation and esterification reactions, etc. (Tong, Ma, & Li, 2010). The catalyst development plays a key role to improve the production efficiency in biofuels and biorefineries (Mitsutani, 2002; Sheldon & Van Bekkum, 2008). Many of these processes involved the use of traditional Brønsted acids (H_2SO_4, HF, HCl, p-toluenesulfonic acid) or Lewis acids ($AlCl_3$, $ZnCl_2$, BF_3) in liquid-phase homogeneous systems or acid on inorganic supports in vapor phase systems. However, this catalyst has many drawbacks which have a serious impact on the environment, process instrument and cost of separation and cleaning (Corma & Garcia, 2003; Hoelderich, 2000). An obvious solution to this problem is the replacement of traditional Brønsted and Lewis acids with reusable solid acids. Acid catalyst constitute one of the most important for the heterogeneous catalyst (Hoelderich, 2000). They include mixed oxides such as silica–alumina and sulfated zirconia, acidic clays, zeolite (Yoshida et al., 2017), supported heteropoly acids (Dias, Pillinger, & Valente, 2005; Guo et al., 2018), organic ion exchange resin, polymer resin (Aellig, Scholz, Dapsens, Mondelli, & Perez-Ramirez, 2015), acid carbon (Antonyraj & Haridas, 2018), hybrid organic–inorganic materials such as mesoporous oxides containing organic sulfonic acid moieties and acidic mesoporous silica (Hu et al., 2018). Solid acid catalysts can be divided into three groups: amorphous mixed oxides including acid treated clays, the crystalline zeolites and related materials (zeotype) catalyst, and solid acids catalyst containing surface sulfonic acid group. The solid acids catalyst containing sulfonic acid groups such as Amberlyst®-15, Amberlyst®-35, Nafion® resins, and Nafion-silica composites were used in various reactions. However, a serious drawback is their limited thermal stability and low surface area (< 0.02 $m^2\ g^{-1}$) (Sheldon, Arends, & Hanefeld, 2007; Sheldon & Van Bekkum, 2008).

One of the most interesting types is highly ordered mesoporous silica framework with one-dimensional (1D), two-dimensional (2D) and three-dimensional (3D) channels which could be presented high selective to the product. In this research,

Ref. code: 25625909320250YIN

the KIT-6 with three-dimensional structure containing sulfonic groups as shown in **Figure 1.1** would be the main catalyst. It was prepared by a sol–gel technique involving copolymerization of functionalized and non-functionalized silanes. The sol–gel process affords material with a high surface area (300 – 800 m^2 g^{-1}), high porosity and large mesopore. This material combines a high surface area, high thermal stability and acid strength with excellent accessibility to the active site and orderly mesopores of the uniform pore size distribution (Sheldon et al., 2007). The functionalization method is one of the most important factors that affect the catalyst properties. There are three different functionalization techniques including post-synthetic functionalization silica or grafting, co-condensation and preparation of periodic mesoporous with organosilicas. However, there are many advantages of co-condensation method including non-pore blocking, and homogeneous distributed of the acid site. The direct co-condensation of tetraethoxysilane (TEOS) with 3-(mercaptopropyl)-methyldimethoxysilane (MPMDS) in the presence of poly(ethylene oxide)–poly(propylene oxide) block copolymer, commercially (Pluronic 123) as a templating agent have been use under acidic conditions. When hydrogen peroxide is added to the sol–gel mixture, the -SH groups are oxidized, affording the -SO_3H functionalized mesoporous silica within one step. In addition, the modification of surface hydrophobicity affected rate of conversion and reusability of catalyst (Kaiprommarat, Kongparakul, Reubroycharoen, Guan, & Samart, 2016).

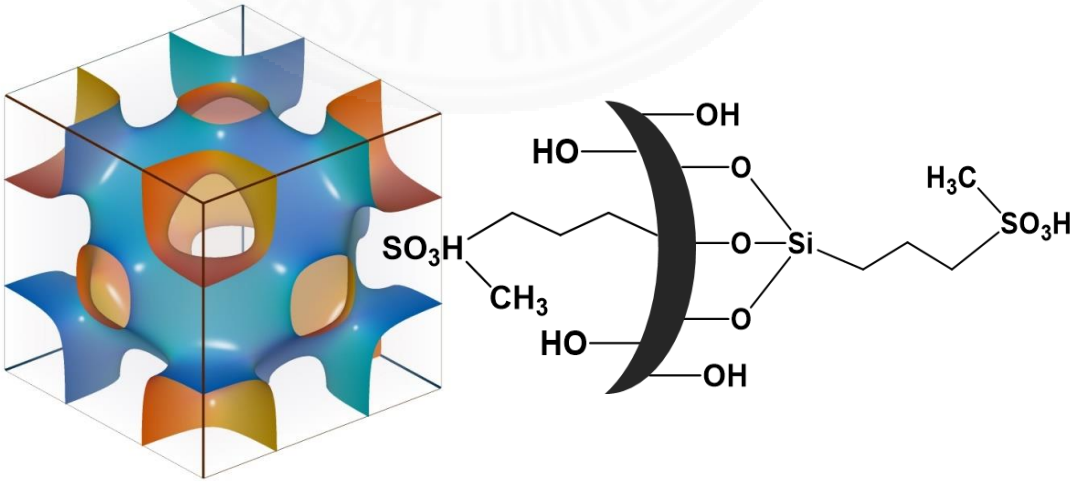

Figure 1.1 Schematic diagram of three-dimensional structure of KIT-6-SO_3H catalyst

Ref. code: 25625909320250YIN

Among these mesoporous silica, KIT-6 type mesoporous silica presents attractive properties including its pore selective properties, well-ordered structure, high surface area, high thermal stability and good molecular transport inside the pore (Ayad, Salahuddin, El-Nasr, & Torad, 2016; Pirez, Caderon, Dacquin, Lee, & Wilson, 2012). Therefore, KIT-6 mesoporous silica is interesting mesoporous silica for catalyst support. In this research, the author focused on using the KIT-6 mesoporous silica with acid functional group as a catalyst for xylose dehydration to produce furfural, esterification of fusel oil and glycerol etherification with n-butanol. In addition, the effect of reaction condition including reaction temperature (°C), reaction time (h), catalyst loading (wt.%) on catalyst performance would be investigated.

1.2 Review of literature

Currently, KIT-6 mesoporous silica catalyst has received more attention for potential acid catalysts. Many research papers interested in KIT-6 in various applications.

(Merkache et al., 2015) studied the first catalytic behavior of conversion of methylcyclopentane (MCP) and hydrogenation of carbon dioxide (CO_2) with Fe-KIT-6 catalyst. The mesopore structure helped to improve the loading of iron molecules. The author suggested that the molar ratio of Si/Fe mainly affected to form CO products from CO_2 hydrogenation at high reaction temperature (500 °C). The catalytic activity significantly increased with decreasing of Si/Fe molar ratio. Moreover, the low reaction temperature provides high selectivity (100%) to n-hexane from methylcyclopentane conversion.

(Xu et al., 2014) synthesized an acid-based bifunctional Al-KIT-6-NH_2 catalyst through post-grafting and alumination method. The 3D structure of KIT-6 preferred more active sites distribution along the pore channels and prevented agglomeration. The acid site of Al-KIT-6-NH_2 was varied by the aluminum concentration. The catalytic performance in Knoevenagel condensation reaction was investigated. As the results, the catalytic activity significantly increased with increasing number of both weak acid and weak basic sites.

Ref. code: 25625909320250YIN

(Ma et al., 2012) synthesized a Co_3O_4-KIT-6 catalyst by sol-gel and impregnation method for N_2O decomposition. The author studied the effect of hydrothermal treatment temperature in range 45 to 120 ℃ on pore size distribution of KIT-6 support catalyst and different amounts of Co_3O_4 loading. The catalyst showed high thermal stability at reaction temperature of 350 ℃ and time on stream for 20 h with 51.2% N_2O conversion. As the results, the pore size and pore volume of catalyst was affected by hydrothermal temperature which increased from 3.6 nm to 8.7 nm when increased hydrothermal temperature from 45 to 120 ℃. The author also suggested this catalyst would approach other reactions such as oxidation of CO.

In addition, the Ag/KIT-6 catalyst was prepared by a one-pot co-condensation method and applied to the CO oxidation reaction (Yang et al., 2017). The co-condensation method showed well-dispersed Ag nanoparticles on KIT-6 structure which gave good catalytic activity with CO conversion up to 100% at 90 ℃. Besides, the three-dimensional mesopore structure also helped to enhance turnover frequency (TOF).

(Zhou et al., 2013) studied CuO/KIT-6 catalyst in acetaldehyde production from ethanol oxidation. The highly ordered bicontinuous mesoporous structure and well-dispersed CuO particles on the KIT-6 presented the excellent catalytic activity in ethanol conversion and acetaldehyde selectivity up to 93.8% and 96.6%, respectively.

(Pirez et al., 2012) investigated the catalytic behavior to $PrSO_3H$-KIT-6. Both KIT-6 and $PrSO_3H$-KIT-6 catalysts presented a three-dimensional mesopore structure and a large surface area up to 600 $m^2\ g^{-1}$. This catalyst was applied to the fatty acid esterification process under mild conditions. The three-dimensional structure of the $PrSO_3H$-KIT-6 catalyst enhanced the turnover frequency (TOF) to compare with the Amberlyst-15 catalyst and $PrSO_3H$-SBA-15 catalyst with a 2D structure. The pore accessibility affected the rate reaction of the lauric and palmitic acid esterification process.

(Hafizi et al., 2016) synthesized the mesoporous silica KIT-6 functionalized with propylsulfonic acid by sol-gel method for production of 5-hydroxymethylfurfural (HMF) from fructose. The highest HMF yield and fructose conversion was 84.1% and

Ref. code: 25625909320250YIN

100%, respectively at 165 ℃ after 30 min. In addition, this catalyst could be reused five times without losing catalytic activity.

(Najafi-Chermahini & Assar, 2019) studied a mesoporous KIT-6 catalyst functionalized with sulfonic acid (KIT-6-SO_3H) and alumina-incorporated KIT-6 (Al-KIT-6) by post-grafting and alumination method, respectively. The catalytic activity of the Brønsted acid catalyst (KIT-6-SO_3H) and Lewis acid catalyst (Al-KIT-6) were compared to the with esterification reaction between levulinic acid and n-butanol. As the results, the Al-KIT-6 catalyst presented higher thermal stability than KIT-6-SO_3H catalyst. Moreover, the Al-KIT-6 catalyst could be reused up to the six cycles and slightly deceased after the fifth cycle. However, the KIT-6-SO_3H catalyst was signification decreased after the fourth cycle. Besides that, the KIT-6-SO_3H catalyzed for esterification reaction could be carried out under milder conditions than Al-KIT-6.

(Najafi-Chermahini et al., 2018) prepared a mesoporous KIT-6 silica functionalized with sulfonic acid (–SO_3H) groups by post-grafting method. The KIT-6-PrSO_3H catalyst was applied to synthesis of aryl tetrazoles derivatives from aromatic nitrilesaryl. As the results, the aprotic solvents such as DMF was achieved a highest yield of product (89%) at optimize conditions. The catalyst could be reused up to five times.

For the above-mentioned, the author has expressed interest and conducted studies on the KIT-6 mesoporous catalyst and developed this catalyst for the conversion of biomass to fuel and fine chemicals. This catalyst was prepared by the sol-gel method and functionalization by consequent co-condensation and oxidation method. Moreover, the surface of KIT-6 mesoporous silica was modified with 3-(mercaptopropyl)-methyldimethoxysilane (MPMDS), which contains the alkyl group to increase their surface hydrophobicity. The accumulation of polar compounds on the catalyst surface would be decreased.

1.3 Objectives of the research

The main objective of this dissertation has investigated the synthesis and application of the KIT-6 catalyst to biomass conversion.

Ref. code: 25625909320250YIN

1. To synthesis the KIT-6 mesoporous acid catalyst by a co-condensation method and the effect of different molar ratios between tetraethyl orthosilicate (TEOS) and 3-(mercaptopropyl)methyldimethoxysilane (MPMDS).

2. To study the physicochemical characteristics of acid functionalized KIT-6 catalyst by using small-angle X-ray scattering (SAXS), N_2 sorption analysis, X-ray photoelectron spectroscopy (XPS), and ammonia temperature-programmed desorption (NH_3-TPD).

3. To apply the acid-functionalized KIT-6 mesoporous silica (KIT-6-SO_3H) catalyst for furfural production from xylose dehydration in a biphasic system. The effect of experimental condition in xylose dehydration by KIT-6 SO_3H catalyst including reaction temperature (130 – 170 °C) and reaction time (1 – 3 h), and catalyst loading (10, 25, 50 wt.%) were investigated.

4. To study the catalytic activity of KIT-6-SO_3H catalyst in esterification between fusel oil and acetic acid. The effect of experimental condition in fusel oil esterification comprises reaction temperature (60 – 120 °C), reaction time (1 – 5 h), the molar ratio of acetic acid/fusel oil (1:1 – 4:1) and catalyst loading (3, 5, 7 wt.%) has been investigated.

5. To study the catalytic activity of KIT-6-SO_3H catalyst in glycerol etherification with n-butanol. The effect of experimental condition in glycerol etherification consists of reaction temperature (120 – 160 °C), reaction time (2 – 10 h), the molar ratio of n-butanol/glycerol (6:1 – 12:1) and catalyst loading (5, 10, 15 wt.%) were investigated.

Ref. code: 25625909320250YIN

1.4 References

Aellig, C., Scholz, D., Dapsens, P. Y., Mondelli, C., & Perez-Ramirez, J. (2015). When catalyst meets reactor: continuous biphasic processing of xylan to furfural over GaUSY/Amberlyst-36. *Catalysis Science & Technology, 5* (1), 142-149. doi:10.1039/C4CY00973H

Alipour, S., Omidvarborna, H., & Kim, D.S. (2017). A review on synthesis of alkoxymethyl furfural, a biofuel candidate. *Renewable and Sustainable Energy Reviews, 71*, 908-926. doi:https://doi.org/10.1016/j.rser.2016.12.118

Antonyraj, C. A., & Haridas, A. (2018). A lignin-derived sulphated carbon for acid catalyzed transformations of bio-derived sugars. *Catalysis Communications, 104*, 101-105. doi:https://doi.org/10.1016/j.catcom.2017.10.029

Ayad, M. M., Salahuddin, N. A., El-Nasr, A. A., & Torad, N. L. (2016). Amine-functionalized mesoporous silica KIT-6 as a controlled release drug delivery carrier. *Microporous and Mesoporous Materials, 229*, 166-177. doi:https://doi.org/10.1016/j.micromeso.2016.04.029

Corma, A., & Garcia, H. (2003). Lewis acids: from conventional homogeneous to green homogeneous and heterogeneous catalysis. *Chemical Reviews, 103* (11), 4307-4366.

Dias, A. S., Pillinger, M., & Valente, A. A. (2005). Liquid phase dehydration of D-xylose in the presence of Keggin-type heteropolyacids. *Applied Catalysis A: General, 285* (1), 126-131. doi:https://doi.org/10.1016/j.apcata.2005.02.016

Guo, X., Guo, F., Li, Y., Zheng, Z., Xing, Z., Zhu, Z., . . . Jin, Y. (2018). Dehydration of D-xylose into furfural over bimetallic salts of heteropolyacid in DMSO/H_2O mixture. *Applied Catalysis A: General, 558*, 18-25. doi:https://doi.org/10.1016/j.apcata.2018.03.027

Hafizi, H., Najafi Chermahini, A., Saraji, M., & Mohammadnezhad, G. (2016). The catalytic conversion of fructose into 5-hydroxymethylfurfural over acid-functionalized KIT-6, an ordered mesoporous silica. *Chemical Engineering Journal, 294*, 380-388. doi:https://doi.org/10.1016/j.cej.2016.02.082

Hoelderich, W. F. (2000). Environmentally benign manufacturing of fine and intermediate chemicals. *Catalysis Today, 62* (1), 115-130. doi:https://doi.org/10.1016/S0920-5861(00)00413-2

Ref. code: 25625909320250YIN

Hu, S., Zhu, J., Wu, Y., Xie, R., Wu, K., & Yang, M. (2018). Preparation of packing type catalysts AAO@Al/Meso-SiO_2-SO_3H for the dehydration of xylose into furfural. *Microporous and Mesoporous Materials, 262*, 112-121. doi:https://doi.org/10.1016/j.micromeso.2017.11.021

Jezak, S., Dzida, M., & Zorebski, M. (2016). High pressure physicochemical properties of 2-methylfuran and 2,5-dimethylfuran – second generation biofuels. *Fuel, 184*, 334-343. doi:https://doi.org/10.1016/j.fuel.2016.07.025

Kaiprommarat, S., Kongparakul, S., Reubroycharoen, P., Guan, G., & Samart, C. (2016). Highly efficient sulfonic MCM-41 catalyst for furfural production: Furan-based biofuel agent. *Fuel, 174*, 189-196. doi:https://doi.org/10.1016/j.fuel.2016.02.011

Kumar, A., Kumar, N., Baredar, P., & Shukla, A. (2015). A review on biomass energy resources, potential, conversion and policy in India. *Renewable and Sustainable Energy Reviews, 45*, 530-539. doi:https://doi.org/10.1016/j.rser.2015.02.007

Lam, M. K., Lee, K. T., & Mohamed, A. R. (2010). Homogeneous, heterogeneous and enzymatic catalysis for transesterification of high free fatty acid oil (waste cooking oil) to biodiesel: a review. *Biotechnology advances, 28* (4), 500-518.

Ma, Z., Ren, Y., & Bruce, P. G. (2012). Co_3O_4-KIT-6 composite catalysts: synthesis, characterization, and application in catalytic decomposition of N_2O. *Journal of Nanoparticle Research, 14* (8), 874. doi:10.1007/s11051-012-0874-9

Merkache, R., Fechete, I., Maamache, M., Bernard, M., Turek, P., Al-Dalama, K., & Garin, F. (2015). 3D ordered mesoporous Fe-KIT-6 catalysts for methylcyclopentane (MCP) conversion and carbon dioxide (CO_2) hydrogenation for energy and environmental applications. *Applied Catalysis A: General, 504*, 672-681. doi:https://doi.org/10.1016/j.apcata.2015.03.032

Mitsutani, A. (2002). Future possibilities of recently commercialized acid/base-catalyzed chemical processes. *Catalysis Today, 73* (1), 57-63. doi:https://doi.org/10.1016/S0920-5861(01)00518-1

Najafi Chermahini, A., Andisheh, N., & Teimouri, A. (2018). KIT-6-anchored sulfonic acid groups as a heterogeneous solid acid catalyst for the synthesis of aryl tetrazoles. *Journal of the Iranian Chemical Society, 15* (4), 831-838. doi:10.1007/s13738-017-1282-y

Najafi Chermahini, A., & Assar, M. (2019). Production of n-butyl levulinate over modified KIT-6 catalysts: comparison of the activity of KIT-SO_3H and Al-KIT-6 catalysts. *Journal of the Iranian Chemical Society, 16* (9), 2045-2053. doi:10.1007/s13738-019-01677-4

Pirez, C., Caderon, J.M., Dacquin, J.P., Lee, A. F., & Wilson, K. (2012). Tunable KIT-6 Mesoporous Sulfonic Acid Catalysts for Fatty Acid Esterification. *ACS Catalysis, 2* (8), 1607-1614. doi:10.1021/cs300161a

Saidur, R., Abdelaziz, E. A., Demirbas, A., Hossain, M. S., & Mekhilef, S. (2011). A review on biomass as a fuel for boilers. *Renewable and Sustainable Energy Reviews, 15* (5), 2262-2289. doi:https://doi.org/10.1016/j.rser.2011.02.015

Sajid, M., Zhao, X., & Liu, D. (2018). Production of 2,5-furandicarboxylic acid (FDCA) from 5-hydroxymethylfurfural (HMF): Recent progress focusing on the chemical-catalytic routes. *Green Chemistry, 20* (24), 5427-5453. doi:10.1039/C8GC02680G

Sheldon, R. A., Arends, I., & Hanefeld, U. (2007). *Green chemistry and catalysis*: John Wiley & Sons.

Sheldon, R. A., & Van Bekkum, H. (2008). *Fine chemicals through heterogeneous catalysis*: John Wiley & Sons.

Tong, X., Ma, Y., & Li, Y. (2010). Biomass into chemicals: Conversion of sugars to furan derivatives by catalytic processes. *Applied Catalysis A: General, 385* (1), 1-13. doi:https://doi.org/10.1016/j.apcata.2010.06.049

Xu, L., Wang, C., & Guan, J. (2014). Preparation of acid-base bifunctional mesoporous KIT-6 (KIT: Korea Advanced Institute of Science and Technology) and its catalytic performance in Knoevenagel reaction. *Journal of Solid State Chemistry, 213*, 250-255. doi:https://doi.org/10.1016/j.jssc.2014.03.010

Yang, Y., Hou, F., Li, H., Liu, N., Wang, Y., & Zhang, X. (2017). Facile synthesis of Ag/KIT-6 catalyst via a simple one pot method and application in the CO oxidation. *Journal of Porous Materials, 24* (6), 1661-1665. doi:10.1007/s10934-017-0406-1

Yoshida, K., Nanao, H., Kiyozumi, Y., Sato, K., Sato, O., Yamaguchi, A., & Shirai, M. (2017). Furfural production from xylose and bamboo powder over chabazite-type zeolite prepared by interzeolite conversion method. *Journal of the Taiwan Institute of Chemical Engineers, 79*, 55-59. doi:https://doi.org/10.1016/j.jtice.2017.05.035

Yuan, Z., Zhang, Z., Zheng, J., & Lin, J. (2015). Efficient synthesis of promising liquid fuels 5-ethoxymethylfurfural from carbohydrates. *Fuel, 150*, 236-242. doi:https://doi.org/10.1016/j.fuel.2015.02.020

Zhang, Z., & Deng, K. (2015). Recent advances in the catalytic synthesis of 2,5-furandicarboxylic acid and its derivatives. *ACS Catalysis, 5* (11), 6529-6544. doi:10.1021/acscatal.5b01491

Zhou, G., Zhang, H., Xie, H., Wu, M., & Wei, M. (2013). Ethanol Catalytic Oxidation on Ordered Mesoporous CuO/KIT-6 Catalyst. *International Journal of Chemical Reactor Engineering, 11* (1), 259-263.

Zhou, P., & Zhang, Z. (2016). One-pot catalytic conversion of carbohydrates into furfural and 5-hydroxymethylfurfural. *Catalysis Science & Technology, 6* (11), 3694-3712. doi:10.1039/C6CY00384B

Ref. code: 25625909320250YIN

CHAPTER 2
SYNTHESIS OF SULFONIC ACID FUNCTIONALIZED KIT-6 CATALYST FOR FURFURAL PRODUCTION BY XYLOSE DEHYDRATION REACTION

2.1 Introduction

Recently, regarding environmental pollution, the uses of alternative and clean fuel sources also exerted a positive impact on the environment and mitigate global warming (Alipour et al., 2017; Jezak et al., 2016; Yuan, Zhang et al., 2015; Zhou & Zhang, 2016). In this concept, biomass has been interested in the field of "biorefinery or bio-based green chemistry" and considered as renewable resources for biofuels and bio-based chemicals. Biomass has consisted of various constituents such as cellulose (40 – 50%), hemicellulose (25 – 35%), lignin (15 – 25%) and other (protein, wax, etc.) as shown in **Figure 2.1**. Among these components, biomass hemicellulose is the second main composition behind cellulose which is composed of hetro-polysaccharides with different 5- and 6-carbon monosaccharide sugar monomers (xylose, mannose, glucose, galactose, uronic acid).

The technology of biomass conversion can be divided into thermal, thermochemical, chemical and biochemical methods. However, all of them either require high energy or come at a large cost (Tran et al., 2018). The catalytic conversion has been of interest in the biomass conversion to fuel and valuable platform chemicals. In addition, the catalytic process could selectively generate the desired product (Agirrezabal Telleria, Gandarias, & Arias, 2014). There are many different interests in biomass dehydration as shown in **Figure 2.2**. On the other hand, the production of furfural has drawn attention from scientists and has become a significant and valuable platform chemical in the furan-based biofuel and biorefinery industry. From these derivatives, furfural production from acid-catalyzed xylose dehydration is an important conversion process factor and has attracted a lot of attention from scientists (Titirici, White, Falco, & Sevilla, 2012; Zhou & Zhang, 2016). The process allows

Ref. code: 25625909320250YIN

not only low energy requires but also the residue that could be used as fertilizer on agricultural plantations (Hoydonckx, Van Rhijn, Van Rhijn, De Vos, & Jacobs, 2007).

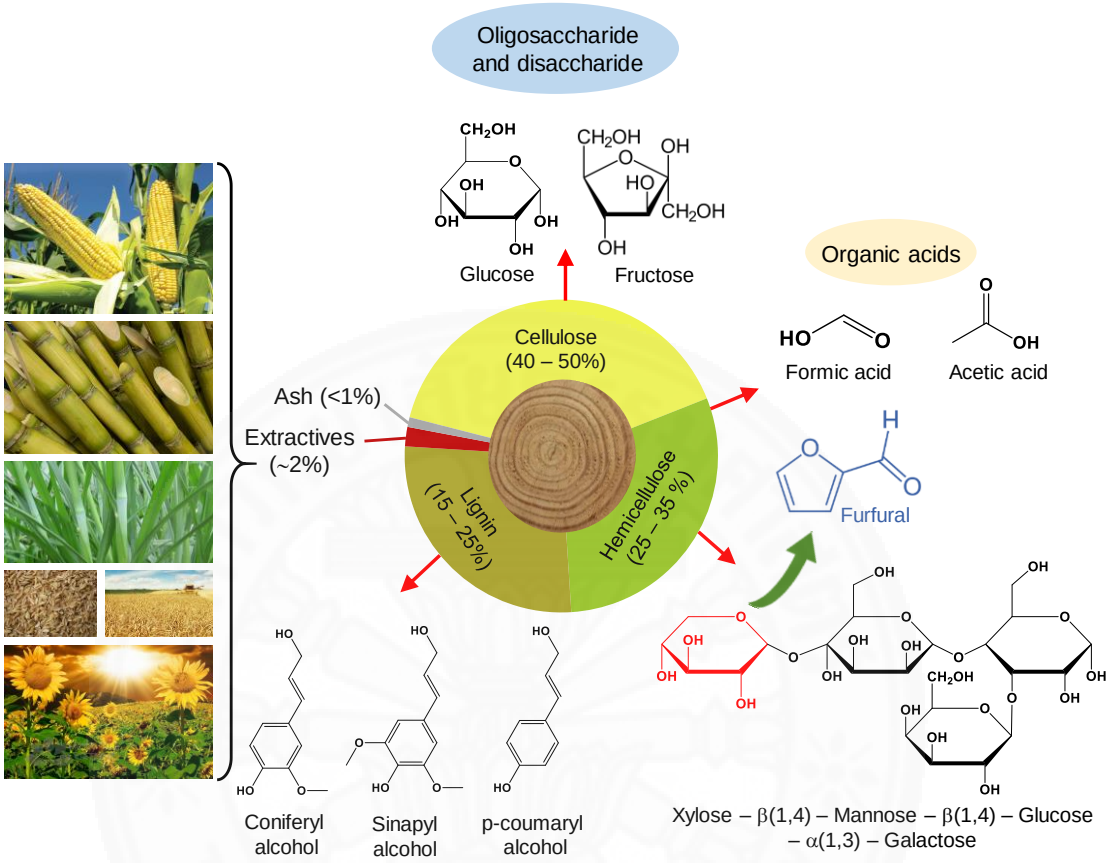

Figure 2.1 The representative structures of constituent components in biomass

Ref. code: 25625909320250YIN

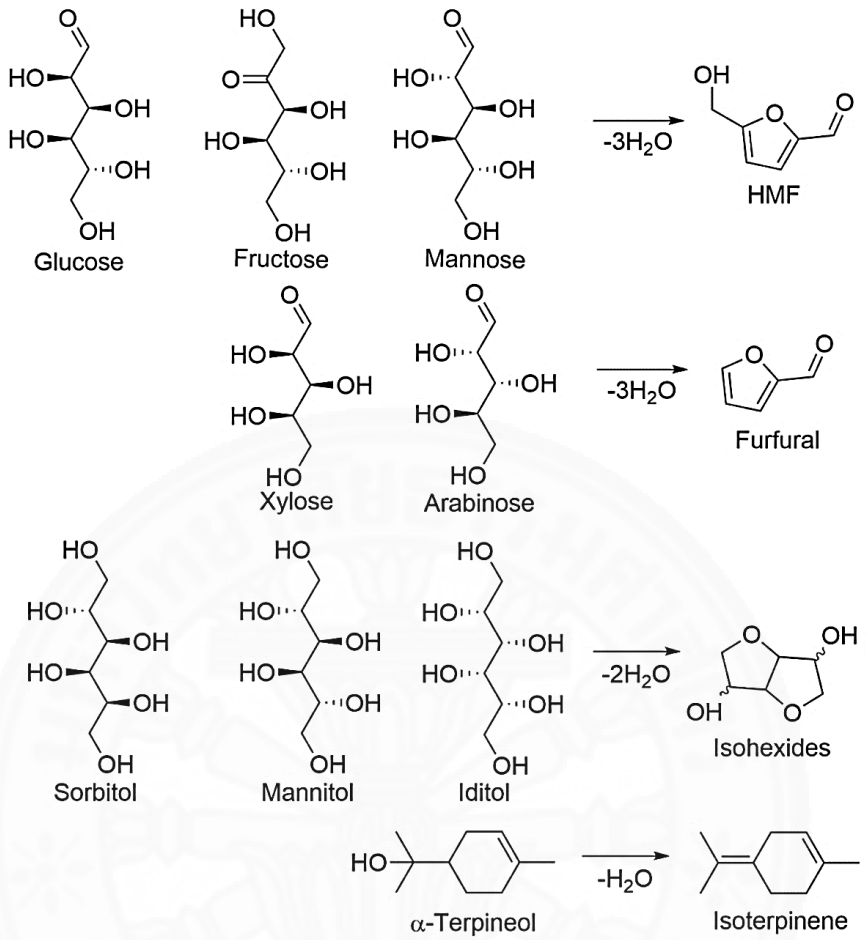

Figure 2.2 Chemicals derived through dehydration from biomass

Owing to the abundance of hydroxyl groups in a wide diversity of natural substances, dehydration reactions are one of the most important ways to modify and valorize biomass. Dehydration reaction is a condition that involves when reacting molecule has lost of water (typically an alcohol), produce an alkene or other unsaturated product depending on the reacting compound. Dehydration are common reaction under Lewis or Bronsted acids as shown in **Figure 2.3**. The Bronsted acid catalyst makes easier the dehydration by protonating the hydroxyl group as shown in step 1. The protonated alcohol group ($R\text{-}H_2O^+$) is a more wisely leaving group than the hydroxyl group and forms as water. Simultaneously, a carbon-carbon double bond (C=C) is formed in the carbon skeleton of the substrate, according to Zaitsev's rule, through release of the β-proton and concurrently closing the catalytic cycle (step 2) (Li, Assary, Atesin, Curtiss, & Marks, 2014). In addition, the dehydration can be active

Ref. code: 25625909320250YIN

under Lewis acid catalyst as well. This reaction occurs through the bonding of the Lewis acid to the lone pair electron of the hydroxyl oxygen (step 1). The electrophilic nature of the Lewis acid lowers the electron density in the alcohol C-O bond, resulting in segmentation of the alcohol C-O bond and the formation of alkene and Lewis acid hydroxide types (step 2). The Lewis acid hydroxide reacts with the released β-proton, forming water and the original catalyst types (step 3) (Li et al., 2014).

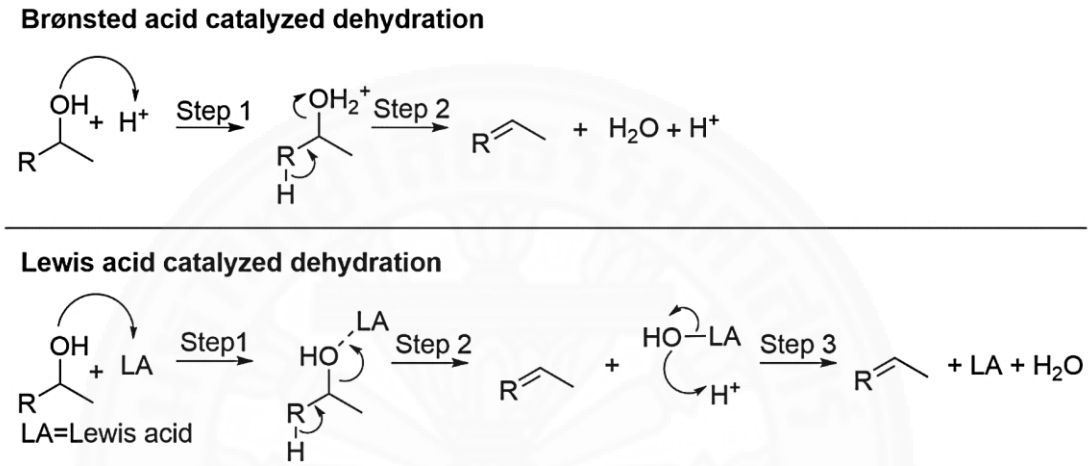

Figure 2.3 The dehydration mechanisms with Bronsted and Lewis acid catalysts

Xylose undergo dehydration to produce furfural with loss three molecules of water under simultaneous of heat and acid catalyzed reaction conditions. More than one reaction mechanism of furfural production from xylose dehydration has been studied based on different techniques and different reaction conditions could be discussed in three kinds as shown in **Figure 2.4** (Binder, Blank, Cefali, & Raines, 2010; Danon, Marcotullio, & de Jong, 2014). Firstly, from the acyclic of pentoses, either via a 1,2-enediol, intermediate (2) and then dehydration (Figure 2.4 a) or directly via a 2,3-(α, β-) unsaturated aldehyde (4) (**Figure 2.4 b)**. In addition, from the pyranose of pentoses, the acid catalyst coverts xylose to 2,5-anhydroxylose furanose intermediate and then dehydrates to forms furfural (**Figure 2.4 c**). The 1,2-enediol derivative would provide the 2,3-unsaturated aldehyde as a prime intermediate in the presumption of the acyclic pathway. At lower acidities, enolization and subsequent isomerization is favored, although the formation of furfural is decelerated and there are more options for undesirable reactions (Danon et al., 2014).

Ref. code: 25625909320250YIN

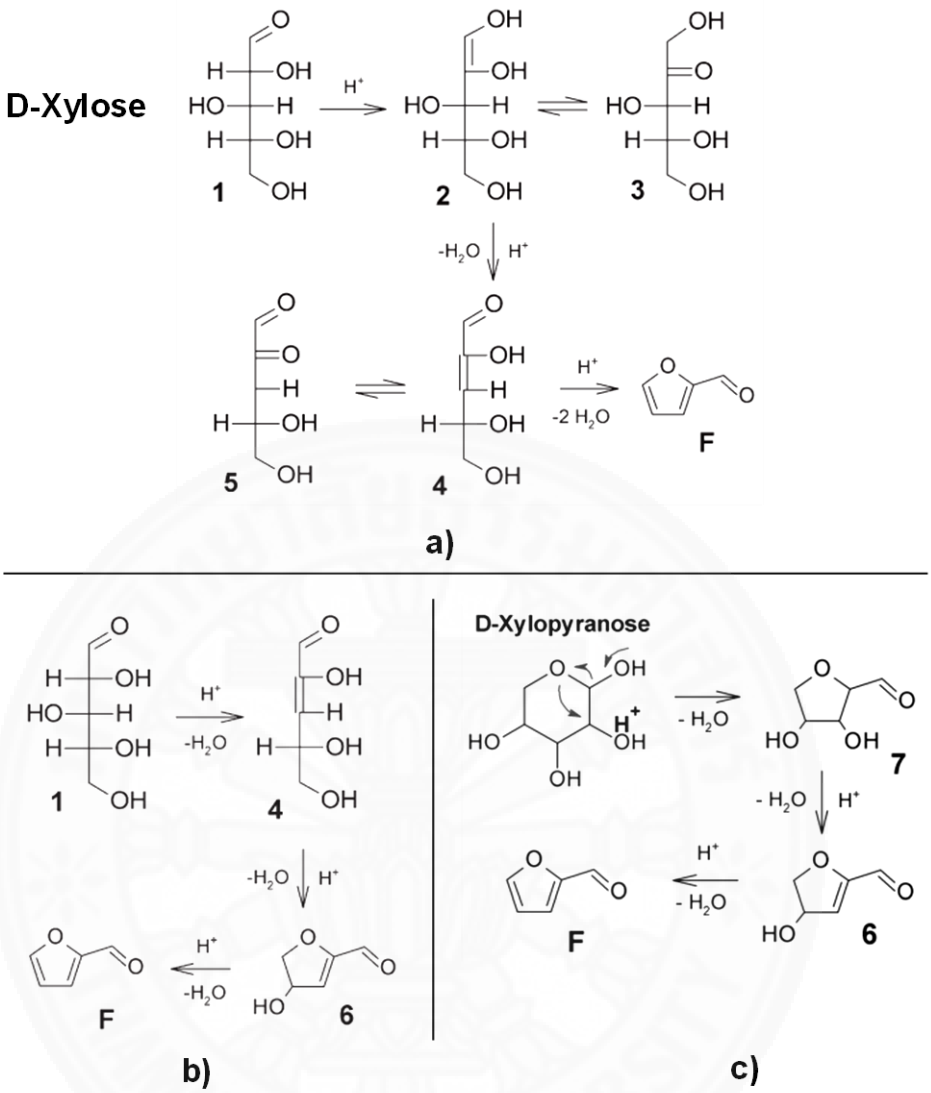

Figure 2.4 Mechanism of furfural production from xylose dehydration (a) via 1,2-enolization, (b) β-elimination, (c) via cyclic intermediates

Furfural has been recognized as "one of the top chemicals from biorefinery carbohydrates" by the US Department of Energy's in 2010 (Bozell & Petersen, 2010). In this sense, the researcher focuses on developing of homogeneous, heterogeneous acid catalysis and improving the reaction media. The homogeneous acid catalyst has effective and widely used for this process such as mineral acids (H_2SO_4 (Antal, Leesomboon, Mok, & Richards, 1991; Montané, Salvadó, Torras, & Farriol, 2002; Suxia et al., 2012), H_3PO_4, HCl, HNO_3 (Marzialetti et al., 2008), tungsten based Keggin-type heteropolyacid (Dias, Pillinger, & Valente, 2005b), etc). However, there appeared to have some drawbacks such as high reaction temperature, side reaction, costly, large

Ref. code: 25625909320250YIN

amount of toxic chemicals, and difficult catalyst recycling and environmental pollution (Isikgor & Becer, 2015; Li, Pan, Deng, Fu, & Xu, 2015). Against these drawbacks, the heterogeneous catalyst emerged as the potential of advancement solution to these problems. Many researchers have expressed their interest and conducted studies on zeolites (Galarneau et al., 2003), sulfonic ion-exchange resins (Agirrezabal-Telleria, Larreategui, Requies, Güemez, & Arias, 2011; Tuteja, Nishimura, & Ebitani, 2012) and mesoporous silica (Agirrezabal-Telleria, Gandarias, & Arias, 2014). The acid strength, acidity, surface area and porosity of catalyst can affect the yields, selectivity of product. In addition, the acid functional group with a hydrophobic surface and suitable pore size also affect the rate of conversion and furfural selectivity (Morales, Paniagua, Melero, & Iglesias, 2017). Hence, the growing interest in sulfonic acid mesoporous silica and its rapid development because of high surface area, high acid property, good thermal and chemical stability and adjustable in pore size. To avoid the undesired product and increase the selectivity to desired product, they replaced the solvent system of the reaction from single-phase to biphasic system. Accordingly, the water-immiscible organic solvent biphasic system to separate the product simultaneous. The organic solvent widely applied in this system such as n-butanol, 2-methyltetrahydrofuran (2-MTHF), dimethylsulfoxide (DMSO), methyl isobutyl ketone (MIBK) and toluene.

In this chapter, the methyl propyl sulfonic acid functionalized on mesoporous silica as KIT-6 catalyst (KIT-6-SO_3H) with a three-dimensional structure was used as catalyst for conversion of xylose to furfural under the biphasic system to expect increase the conversion rate. The study would investigate the effect of reaction condition on the catalytic performance. Furthermore, catalyst reusability was also investigated.

2.2 Review of literature

(Gairola & Smirnova, 2012) synthesized furfural from hemicellulose and D-xylose by simultaneous furfural extraction with supercritical CO_2 (SC-CO_2) technique without using catalyst. At the optimized conditions, 4% D-xylose loading with reaction

Ref. code: 25625909320250YIN

temperature 230 °C for 25 min under CO_2 flow rate (3.6 g/min) with the pressure of 12 MPa gave the highest yield of furfural (68%).

(Morais et al., 2016) produced furfural production from D-xylose without using catalyst in a biphasic system of the water, tetrahydrofuran (THF) and methyl isobutyl ketone (MIBK) mixture. The reaction was taking place at 180 °C for 1 h, 50 bar CO_2. The furfural yield and furfural selectivity were 56.6 mol% and 63.3 mol%, respectively. Moreover, the author also studied with hemicellulose hydrolysate dehydration at the same conditions, the results showed the furfural yield of 43 mol% and furfural selectivity of 44 mol%.

(Rong et al., 2012) studied furfural production from dehydration of D-xylose under mixture of sulfuric acid catalyst and an inorganic-salts (NaCl or $FeCl_3$) as a promoter under biphasic system (toluene/water). The highest furfural yield could reach 83% at the reaction conditions 10 wt.% of H_2SO_4 mixed with 2.4 g NaCl, 10wt.% of xylose and reaction time for 5 h. This research proposed that the biphasic system could enhance the selectivity of furfural. Moreover, the addition of $FeCl_3$ promoter decreased the ion activity in reaction system and thus, to develop more efficiency than NaCl.

(Zhang et al., 2013) studied the dehydration of different raw materials including lignocellulosic biomass, xylan and D-xylose under $AlCl_3$ catalyst in ionic liquid (1-butyl-3- methylimidazolium chloride). The highest furfural yield was 84.8 % at 170 °C for 10 seconds with dehydration of D-xylose. Besides, the furfural yields of lignocellulosic biomass were in the range of 16.0% to 33.0%. The low furfural yield caused by impurities in biomass.

(Choudhary et al., 2012) presented furfural production from xylose dehydration with HCl and $CrCl_3$ catalyst. Among these, the mixture of Bronsted acid (HCl) and Lewis ($CrCl_3$) catalyst have studied in aqueous phase and biphasic system (water and toluene) at 140 °C for 2 h. The furfural yield increased from 29.0 to 39.0% in aqueous phase and 76.3% in biphasic system. As the results, the Lewis acid sites could enhance the xylose conversion rate meanwhile, the Bronsted acid sites could improve the furfural selectivity (**Figure 2.5**). Moreover, the biphasic system performs a high percentage of furfural yield.

Ref. code: 25625909320250YIN

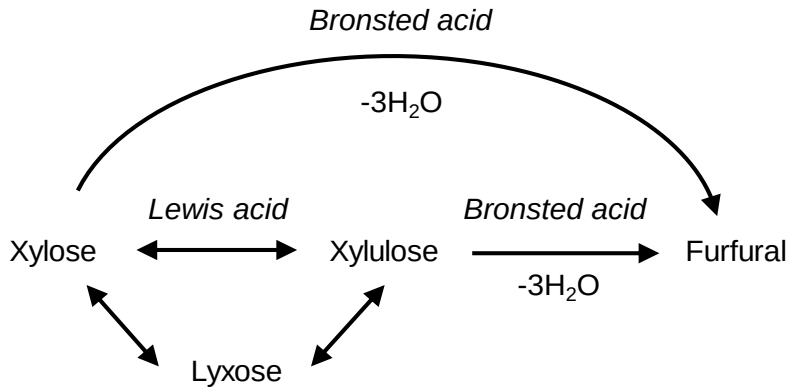

Figure 2.5 The pathway to form furfural production in the presence of a Bronsted acid catalyst and combination of Lewis and Bronsted acid catalysts (Choudhary et al., 2012)

(Lam et al., 2012) studied the effect of a different graphitic catalysts including graphene, graphene oxide, sulfonic acid functionalized graphene, and sulfonic acid functionalized graphene oxide for xylose dehydration. At the condition of 200 °C for 35 minutes and 2 wt.% catalyst, the sulfonic acid functionalized graphene oxide catalyst showed the highest furfural yield and furfural selectivity of 62.0% and 75.0%, respectively. The author suggested that the presence of sulfonic functional group ($-SO_3H$) improved the catalytic activity.

(Lourvanij & Rorrer, 1997) investigated the effect of pore size of catalyst on the catalytic activity in dehydration reaction of carbohydrates. The microporous structure zeolite Y gave less yield of 5-hydroxymethylfurfural (HMF) production than the mesoporous structure.

Recently, many researches have focused on the mesoporous structure to improve the catalytic activity of xylose dehydration. (Dias, Pillinger, & Valente, 2005a) investigated an acid functionalized with 2D hexagonally mesoporous structure (MCM-41) in xylose dehydration reaction. This was the first report for preparing a sulfonic functionalized mesoporous catalyst using (3-mercaptopropyl)-trimethoxysilane as the sulfonic precursor. This catalyst presented high catalytic activity in xylose dehydration. However, the reusability of catalyst was still low due to the low thermal stability.

(Kaiprommarat et al., 2016) investigated the sulfonated MCM-41 ($PrSO_3H$-MCM-41) and methyl-propyl sulfonated MCM-41 ($MPrSO_3H$-MCM-41) catalysts for producing furfural from xylose under biphasic system (water and toluene). The methyl-

Ref. code: 25625909320250YIN

propyl sulfonated MCM-41 catalyst could improve the xylose conversion rate because of the methyl group in anti-adsorption of furfural or water at active site, which enhances the number of converted xyloses per active site in terms of turn over frequency (TOF). At the optimized reaction conditions, 155 °C for 2 h, the yield and selectivity of furfural were 93.0%, 98.0%, respectively. The author also presented the effect of pore size on the product selectivity. The suitable pore diameter should be between 3-6 nm which could give over 93% of furfural selectivity.

(Agirrezabal-Telleria et al., 2012) investigated and tunable the porous structure of propyl sulfonated SBA-15 catalyst to produce furfural from xylose. The highest furfural yield of 82% could be achieved under biphasic system (water and toluene mixture). The author proposed that xylose diffusion was limited owing to the low catalyst pore size. However, toluene solvent as the extracting agent could be improved the furfural selectivity.

As mentioned above, the sulfonated functionalized mesoporous catalyst has attracted a lot of interest and has been selected as a catalyst to be used in xylose dehydration reaction in the biphasic system. The catalyst which contains the alkyl group helped to increase the hydrophobicity and decrease the agglomeration of polar compounds on the catalyst surface.

Ref. code: 25625909320250YIN

2.3 Materials

All chemicals and equipment used in this research are shown in **Table 2.1** and **Table 2.2**, respectively

2.3.1 Chemicals

Table 2.1 List of the chemicals used in this research

Chemicals	Manufacturer	Country
Acetone, Comercial grade	RCI Labscan	USA
Acetonitrile, HPLC grade	RCI Labscan	USA
n-butanol, AR grade	RCI Labscan	USA
D-Xylose	Sigma-Aldrich	USA
Ethanol Absolute, 99%	QReC	New Zealand
Hydrogen peroxide, AR grade, 30%	Sigma-Aldrich	USA
Hydrochloric acid, AR grade, 37%	QReC	New Zealand
Methanol, HPLC grade	RCI Labscan	USA
3-Mercaptopropyl methyldimethoxysilane, AR grade, 95%	Sigma-Aldrich	USA
Pluronic P123 triblock copolymer, poly (ethylene glycol)-block-poly (propylene glycol)-block-poly (ethylene glycol), Mw = 5800, AR grade	Sigma-Aldrich	USA
Tetraethyl orthosilicate, AR grade, 98%	Sigma-Aldrich	USA
Toluene, AR grade	RCI Labscan	USA
Sodium carbonate anhydrous (Na_2CO_3)	Ajax Finechem	Australia
Sodium sulfate anhydrous (Na_2SO_4)	Ajax Finechem	Australia
Sulfuric acid, 98%	QReC	New Zealand

Ref. code: 25625909320250YIN

2.3.2 Equipment

Table 2.2 List of the instrument used in this research

	Company
Autoclave reactor, 50ml	Parr, model 4744, USA
Autoclave reactor, 100ml	Custom made by company, Thailand
Autoclave reactor, 400 ml	Amar Equipment, India
Gas Chromatography-Mass Spectrometry (GC-MS)	Shimadzu, GCMS-QP 2010, Japan
High Performance Liquid Chromatograph (HPLC)	Shimadzu, Japan, LC-20AT (pump), SPD-20A (UV dectector)
Oven	Memmert UF 110
Surface area & Porosimetry analyzer	Gold App Instrument, V-sorb 2800P
Scanning Electron Microscope (SEM)	JEOL, Japan, JSM-6510LV
Temperature Programed Desorption of amonia (NH_3-TPD)	BET-CAT (BEL, Japan)
X-ray diffraction (SAXD)	Rigaku, TTRAX III and Bruker, D8 advance
X-ray photoelectron Spectroscopy (XPS)	ULVAC-PHI, PHI 500 VersaProbe II, Japan

2.4 Methods

2.4.1 Synthesis of sulfonic acid functionalized KIT-6-SO_3H catalyst

The sulfonic acid functionalized KIT-6 catalyst was synthesized by co-condensation method. The molar ratio of the mixture was (1-x) TEOS: xMPMDS: 0.017P123: 1.83HCl: 1.31Butanol: 195H_2O (Tran et al., 2019).

First, 2.0 g of Pluronic P123 triblock polymer was dissolved in 73.0 g of de-ionized water and 3.75 g of HCl 37 % at room temperature. After that, 2.0 g of n-butanol was added dropwise under stirred vigorously at 35 °C kept for 1 h. Then, the mixture of 4.3 g of tetraethyl orthosilicate (TEOS) and a g of 3-Mercaptopropyl methyldimethoxysilane (MPMDS) follow the ratio as mentioned before were added dropwise and kept agitated vigorously for 24 h. Thereafter, the mixture was heated to

Ref. code: 25625909320250YIN

a temperature 100 °C and maintained at this temperature for 24 h. The white solid powder obtained was filtered and dried at 60 °C for 16 h. The as-synthesized sample was removed the template by Soxhlet extraction with the mixture of ethanol/HCl solvent at 70 °C for 24 h. Finally, the catalyst was oxidized by 30% H_2O_2 solution for 24 h to obtain the methyl-propyl sulfonic acid functionalized KIT-6 catalyst (MPr-KIT-6-SO_3H). The catalyst was filtered, washed with DI water, and dried at 60 °C for 16 h. The sulfonic acid functionalized KIT-6 catalyst with an x molar content of MPMDS (x: 0.1 – 0.3) was denoted as x-KIT-6-SO_3H. The synthesis of this catalyst was illustrated by **Figure 2.6**.

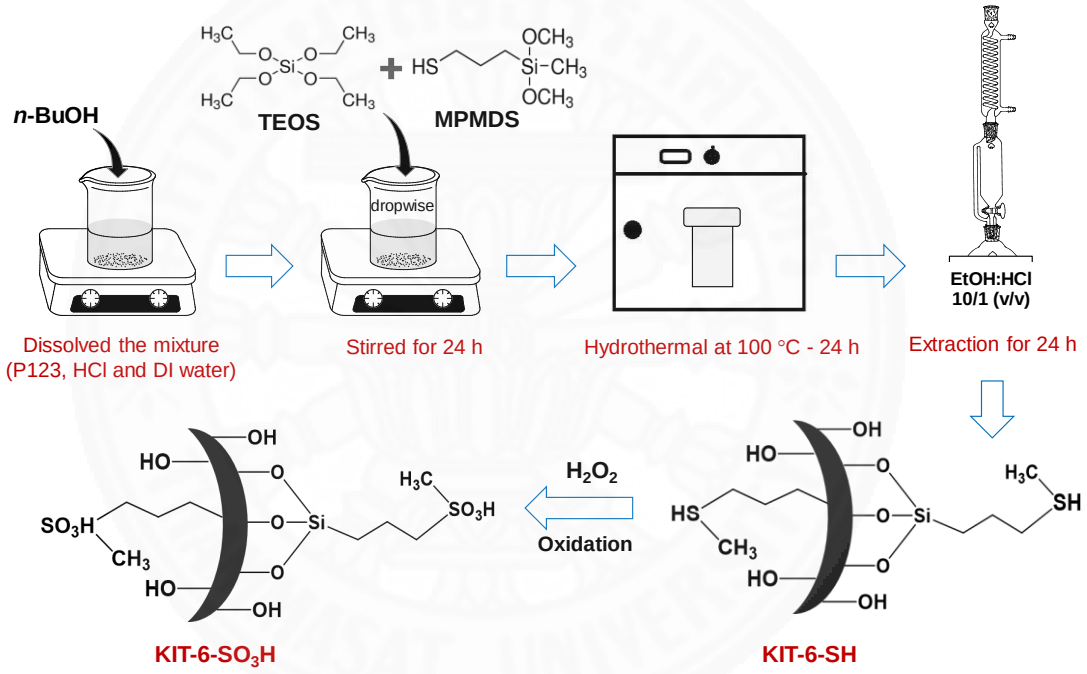

Figure 2.6 Synthesis scheme of the KIT-6-SO_3H catalyst by the co-condensation method

2.4.2 Characterization of KIT-6 and KIT-6-SO_3H catalyst

The structure ordering of KIT-6 and KIT-6-SO_3H catalyst were studied by small angle X-ray diffraction pattern (SAXD) on Rigaku TTRAX III X-Ray diffractometer using Cu Kα (λ = 0.154 nm) radiation, a 40kV beam voltage and a 40mA beam current in the 2θ angle of 0.5 – 5° with a resolution of 0.02° and scan speed 0.1 second per step.

The surface area and pore properties of KIT-6 and KIT-6-SO_3H catalysts were analyzed by N_2 sorption at -196 °C with a volumetric V-Sorb 2800P from Gold APP Instruments. Before analysis, the samples were degassed at 50 °C for 60

Ref. code: 25625909320250YIN

minutes, and next 60 °C for 960 minutes. The surface area was calculated by using the Brunauer–Emmett–Teller (BET) equation. The desorption isotherm was used to get the pore size distribution by Barrett-Joiner-Halender (BHJ) method. The total pore volume of sample depends on the adsorbed volume of N_2 at a relative pressure of 0.99.

The surface chemical compositions and functional groups of the catalysts were analyzed by X-ray photoelectron spectroscopy (XPS, ULVAC-PHI, PHI 500 VersaProbe II) with AlKα radiation (hν = 117.40 eV) radiation. The binding energy (BE) was corrected by the C1s peak at 284.5 eV, with S2p spectra fitted using a common Gaussian/Lorentzian peak shape to confirm the presence of sulfonic acid on the KIT-6 surface.

The acidity and acid strength of KIT-6 and KIT-6-SO_3H catalyst were studied by using temperature programed desorption of ammonia (NH_3-TPD), BETCAT (BEL). In a typical acidity measurement, the catalyst was placed in an u-shaped quartz cell and preheated at 750 °C for 1 h under He flow in order to get rid of moisture and impurities within the catalyst structure. Subsequently, the catalyst was saturated with a mixed of 5 % NH_3 and 95 % He at room temperature for 1 h with flow rate of 50 cm^3/min. After stabilization, NH_3 desorption was carried out by heating from 50 °C to 400 °C at heating rate of 5 °C/min under He flow. The NH_3-desorption peak was recorded using a TCD and the adsorbed NH_3 concentration was quantified from the peak area which was calibrated by the standard gas.

2.4.3 Catalytic activity in furfural production via xylose dehydration

2.4.3.1 Xylose dehydration

The mixture of xylose solution (0.5 g xylose dissolved in 12.5 mL DI water), 12.5 mL toluene and KIT-6-SO_3H catalysts was transferred in an autoclave reactor (Amar Equipments, India, 400.0 mL). Then, the reactor was heated to desired reaction temperature (130 °C, 150 °C and 170 °C) and stirred at a constant rate of 500 rpm for suspected reaction time (1 – 3 h). After being finished and cooled down, the product was washed from the reactor by 12.5 mL DI water and 12.5 mL toluene. Thereafter, the catalyst was separated by filtration and washed with 25 mL DI water and 25 mL toluene to obtain the liquid product with two layers in separatory funnel. The upper layer was collected and removed water by anhydrous sodium sulfate.

Ref. code: 25625909320250YIN

2.4.3.2 Product analysis

The furfural yield of both two phases (toluene and aqueous phase) were determined by high-performance liquid chromatography (Shimadzu, Japan) connected with UV detector at λmax equals 276 nm with Agilent Eclipse XDB-C18 column (4.6 mm ID, 250 mm length, prominence, Shimadzu, Japan) at column temperature of 40 °C. The mobile phase at flow 1.0 mL/min with volume ratio of acetonitrile/DI water (v/v) is 15/85, and 20.0 µL of sample would be injected.

The xylose conversion was determinized by headspace gas chromatography-mass spectrometry (GCMS-QP2010, Shimadzu, Japan) with HP-5 column (0.25 mm ID, 30 m length, 0.25 mm film thickness). The injection temperature was at 105 °C. The column oven temperature was started at 70 °C and heat up to 90 °C with 2 °C/min (Kaiprommarat et al., 2016; Li, Liu, Zhang, & Zhan, 2014; Tran et al., 2019).

The furfural yield, furfural selectivity, xylose conversion and turnover frequency were calculated by **Equation 2.1, 2.2, 2.3 and 2.4**, respectively (Kaiprommarat et al., 2016; Xu et al., 2015).

$$\text{Furfural yield} = \frac{\text{Moles of produced furfural}}{\text{Moles of initial xylose}} \times 100 \quad (2.1)$$

$$\text{Furfural selectivity} = \frac{\text{Moles of produced furfural}}{\text{Moles of reacted xylose}} \times 100 \quad (2.2)$$

$$\text{Xylose conversion} = \frac{\text{Moles of reacted xylose}}{\text{Moles of initial xylose}} \times 100 \quad (2.3)$$

$$\text{Turnover frequency (TOF)} = \frac{\text{Number of converted xylose}}{\text{Number of acid sites x reaction time}} \quad (2.4)$$

2.5 Results and discussion

2.5.1 Characterization of KIT-6-SO_3H catalyst

2.5.1.1 Small angle X-ray diffraction (SAXD)

The structure and three dimension bi-continuous cubic mesoporous silica of KIT-6 and KIT-6-SO_3H catalyst were investigated by SAXD as shown

Ref. code: 25625909320250YIN

in **Figure 2.7**. Both KIT-6 and KIT-6-SO_3H catalyst presented a distinct-peak and two weak broad peaks at 2θ of 0.76°, 0.89° and 1.53° which corresponded consecutively (211), (220), and (332) reflection plane (Liu et al., 2018; Pirez et al., 2012). However, the intensity of SAXD peak decreased with increasing molar ratio of MPMDS:TEOS resulting that the structure of KIT-6-SO_3H catalyst became disordered. The less order structure caused from stuffing of the mercaptoalkoxide (Si-O-R-SH) molecules hinder the formation of ordered porous structure (Ng, Mohd Subari, Marie, Mukti, & Juan, 2013; Wang, Lin, Chan, & Cheng, 2005). Besides, the reflection peak KIT-6-SO_3H catalyst was shifted to higher 2θ than KIT-6 due to the reduction of pore size. As the results, it could prove that functionalization has occurred inside the mesopore channel. Therefore, all x-KIT-6-SO_3H catalyst gave smaller pore size than pristine KIT-6.

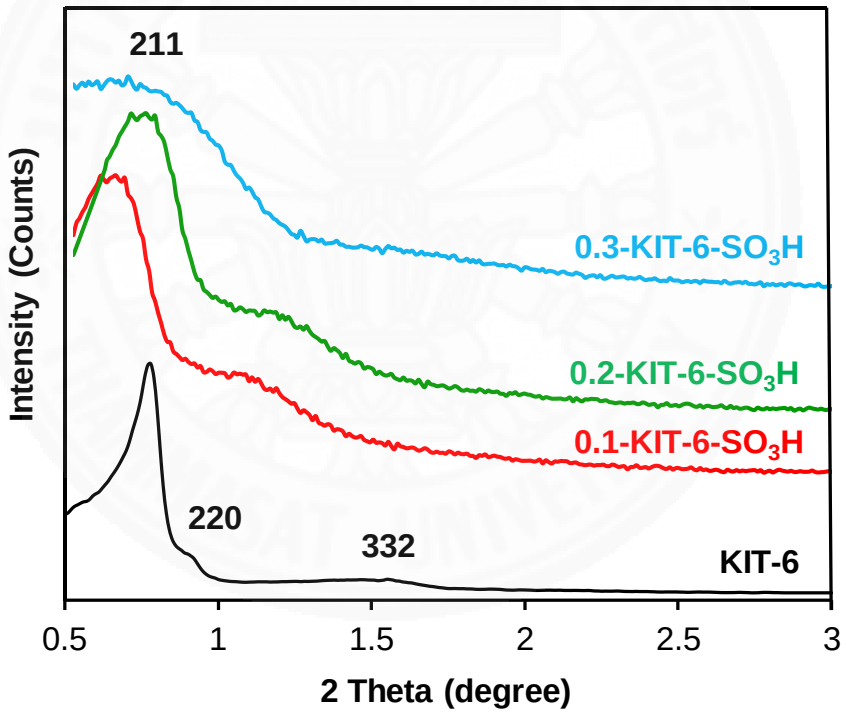

Figure 2.7 SAXD patterns of KIT-6 and KIT-6-SO_3H catalyst

2.5.1.2 N_2 sorption analysis

The textural properties of KIT-6 and KIT-6-SO_3H catalyst were studied by nitrogen sorption which their isotherms are presented in **Figure 2.8 (a)**. The isotherm of both KIT-6 and KIT-6-SO_3H catalyst revealed an IUPAC type IV indicating mesoporous structure. The isotherm of KIT-6 presented a hysteresis type H1 to imply

Ref. code: 25625909320250YIN

a well-defined open cylindrical pore structure and facile pore connectivity. Meanwhile, the KIT-6-SO_3H catalyst isotherm presented a hysteresis type H4 corresponded to a narrow-slit pore, particles with internal voids of regular shape and broad size distribution and disordered structure. An increase of MPMDS:TEOS ratio resulted in increased degree in the disorder mesoporous structure, perhaps because of the steric effect and close packing of the alkyl-sulfonic chain to prevent the pore arrangement (Rác, Molnár, Forgo, Mohai, & Bertóti, 2006; Wang et al., 2005). The increasing of MPMDS:TEOS molar ratio affected to decrease of the BET surface area, porosity was presented in **Figure 2.8 (b)** and **Table 2.3**. The KIT-6 presented large surface area (S_{BET} = 872 m^2/g) which was higher than the 0.3-KIT-6-SO_3H mesoporous silica catalyst (S_{BET} = 225 m^2/g). In addition, pore size of KIT-6-SO_3H catalyst decreased from 4.70 nm to 4.50 nm with increased MPMDS:TEOS molar ratio from 0.1 to 0.3. The excessive swelling MPMDS may destroy the mesoporous structure that reflected to continuously enlarge the pore size of KIT-6-SO_3H catalyst (Rác et al., 2006).

Table 2.3 Textural properties and acidity of KIT-6 and KIT-6-SO_3H catalysts

Catalyst	Surface area (m^2/g)	Pore size (nm)	BJH pore volume (cm^3/g)	Acidity (mmol/g)	Acid density ($mmol/m^2$)
KIT-6	872	6.2	0.88	0.02	n/d
0.1-KIT-6-SO_3H	269	4.7	0.21	0.69	0.003
0.2-KIT-6-SO_3H	157	4.6	0.13	1.25	0.008
0.3-KIT-6-SO_3H	225	4.5	0.10	1.53	0.007
3^{rd} used of 0.2-KIT-6-SO_3H	17	2.8	0.12	n/d	n/d

Ref. code: 25625909320250YIN

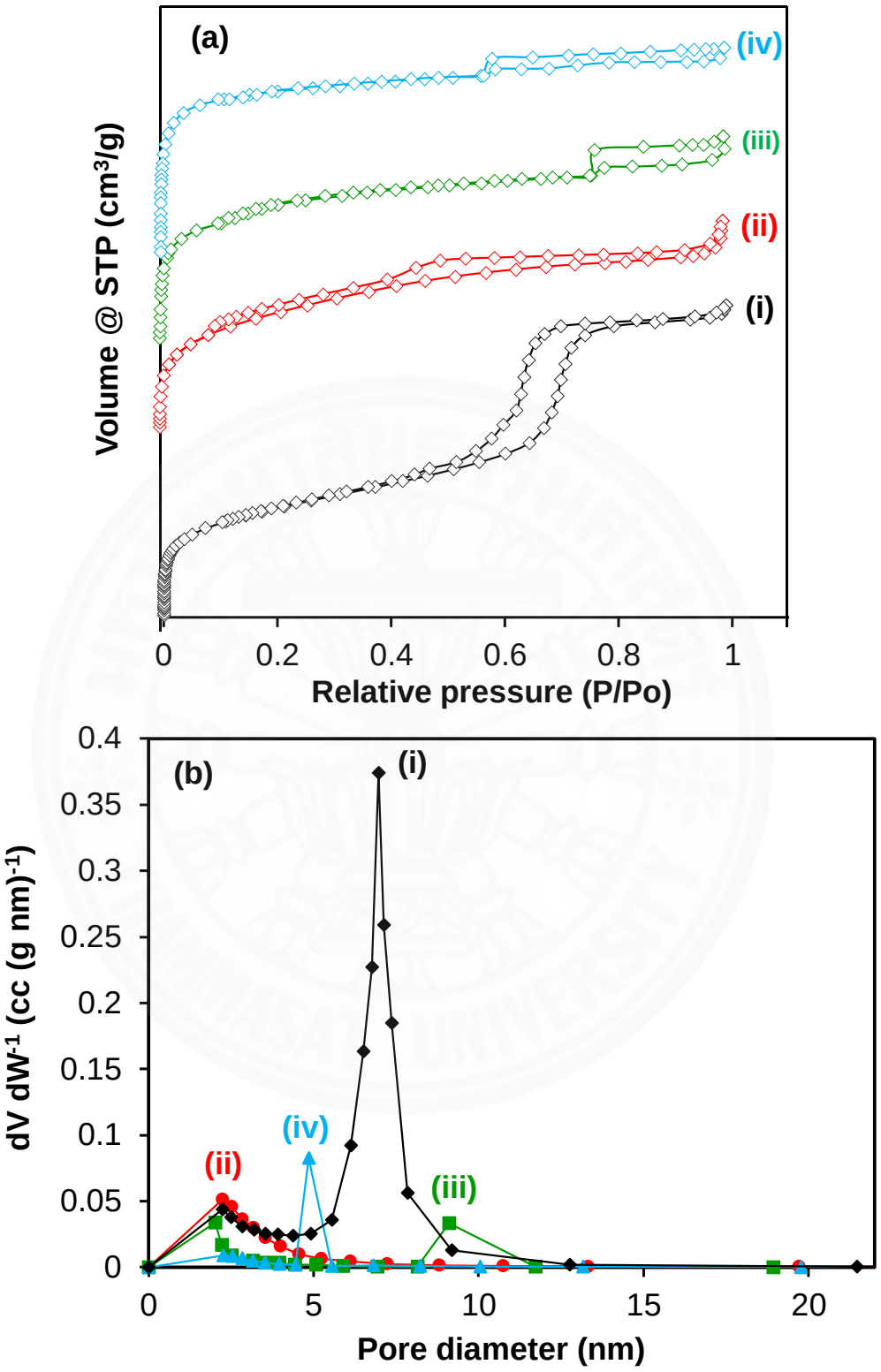

Figure 2.8 (a) Nitrogen sorption isotherms and (b) pore size distribution of (i) KIT-6, (ii) 0.1-KIT-6-SO_3H, (iii) 0.2-KIT-6-SO_3H and (iv) 0.3-KIT-6-SO_3H catalyst

Ref. code: 25625909320250YIN

2.5.1.3 X-ray photoelectron spectroscopy (XPS)

The surface chemical compositions of KIT-6 catalysts were investigated by X-ray photoelectron spectra of C1s, Si2p, S2p and O1s (**Figure 2.9**). The C1s peaks at binding energy 284.8 eV, 286 eV, and 289 eV were corresponded to C-C, C-O and –COO bonds, respectively. Furthermore, XPS spectra of Si2p showed sequential peaks of Si-O-Si and C-Si-O- at binding energy 103.3 eV and 101.4 eV attributed of SiO_2 on the KIT-6 structure. The peak of S2p at 168.8 eV assigned to sulfonic acid groups (-SO_3H) on KIT-6 structure (Moulder, 1995; Russo et al., 2014). This result revealed of the precursor thiol (-SH) group was successful oxidized to the sulfonic acid group.

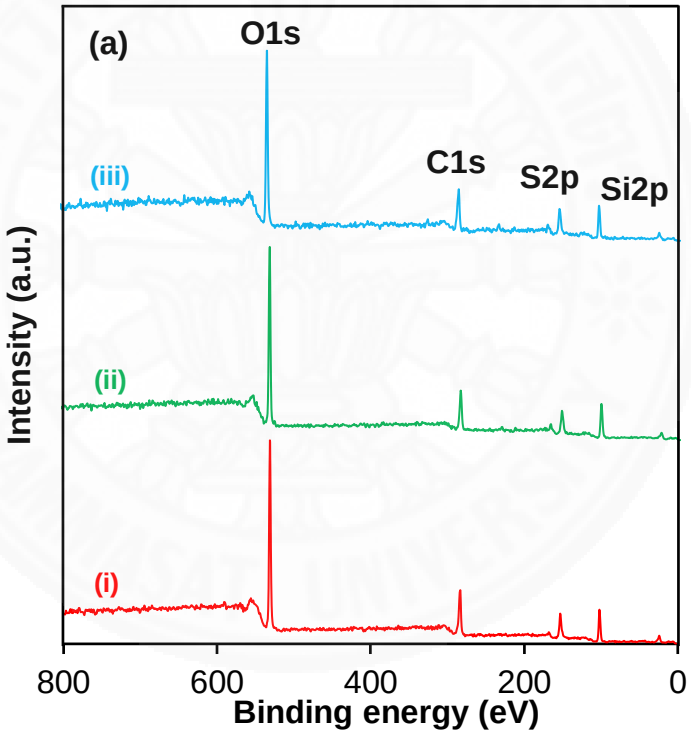

Figure 2.9 XPS spectra of (a) Wide scan, (b) C1s, (c) Si2p, (d) S2p and (e) O1s of (i) 0.1-KIT-6-SO_3H, (ii) 0.2-KIT-6-SO_3H and (iii) 0.3-KIT-6-SO_3H catalyst

Ref. code: 25625909320250YIN

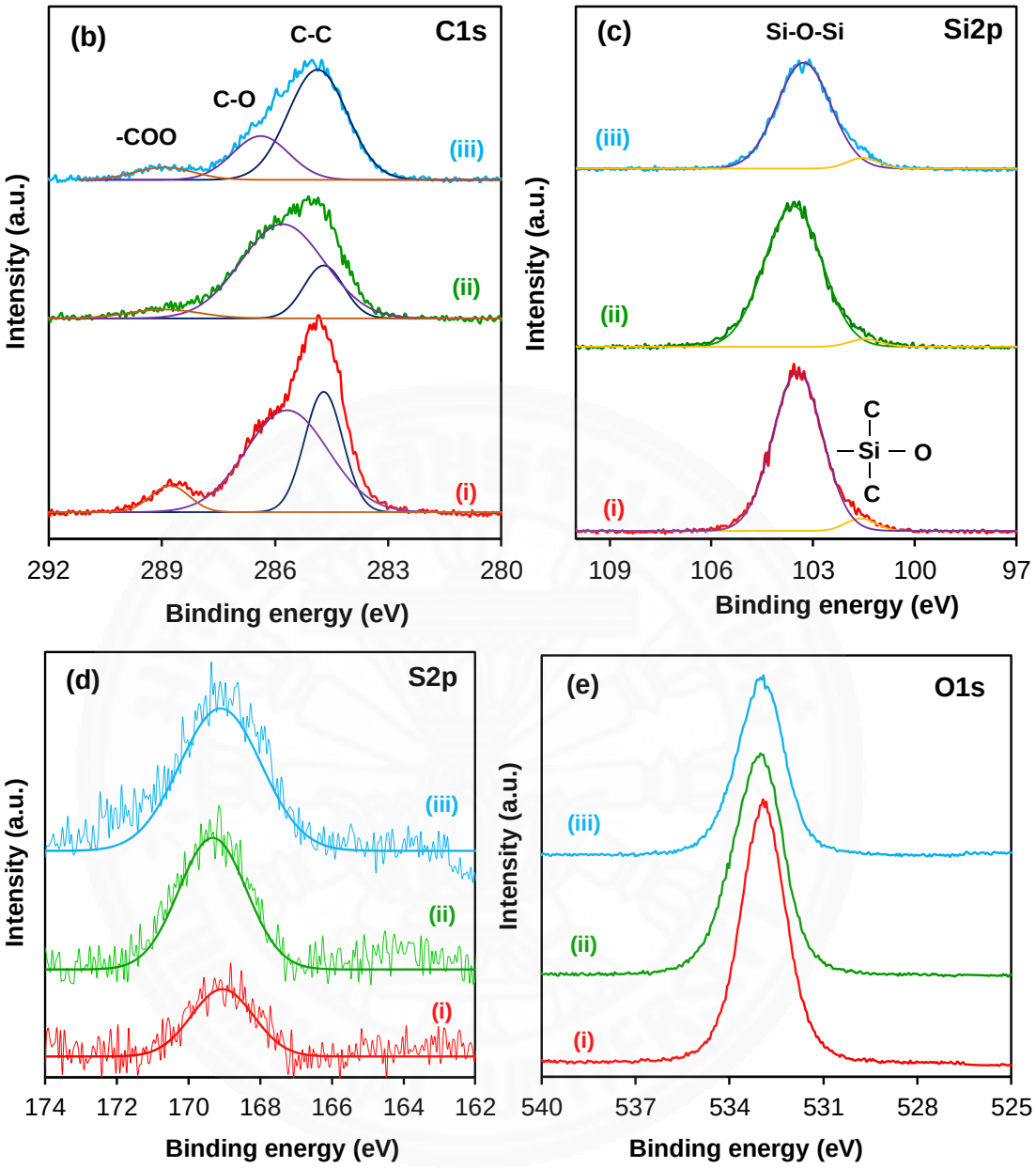

Figure 2.9 XPS spectra of (a) Wide scan, (b) C1s, (c) Si2p, (d) S2p and (e) O1s of (i) 0.1-KIT-6-SO_3H, (ii) 0.2-KIT-6-SO_3H and (iii) 0.3-KIT-6-SO_3H catalyst (cont.)

2.5.1.4 Ammonia temperature programmed desorption (NH_3-TPD)

The NH_3-TPD of catalysts presented two different acid sites as shown in **Figure 2.10** and **Table 2.3**. The low and high desorption temperature of ammonia corresponded weak and strong acid sites (Román Aguirre, Gochi, Sánchez, de la Torre, & Aguilar Elguezabal, 2008). The first peak as weak acid sites was observed at the temperature range of 130 – 150 ℃ that represent desorption of ammonia from

Ref. code: 25625909320250YIN

silanol group (Si-OH), Si-O-Si bridge, and O-H group. Meanwhile, the second peak presented at high temperature of 260 – 300 °C which ascribed to strong acid sites (-SO_3H group). The total acidity decreased from 1.53 to 0.69 mmol/g when the MPMDS:TEOS molar ratio decreasing from 0.3 to 0.1 because of the decreased number of sulfonic acid sites on KIT-6 structure.

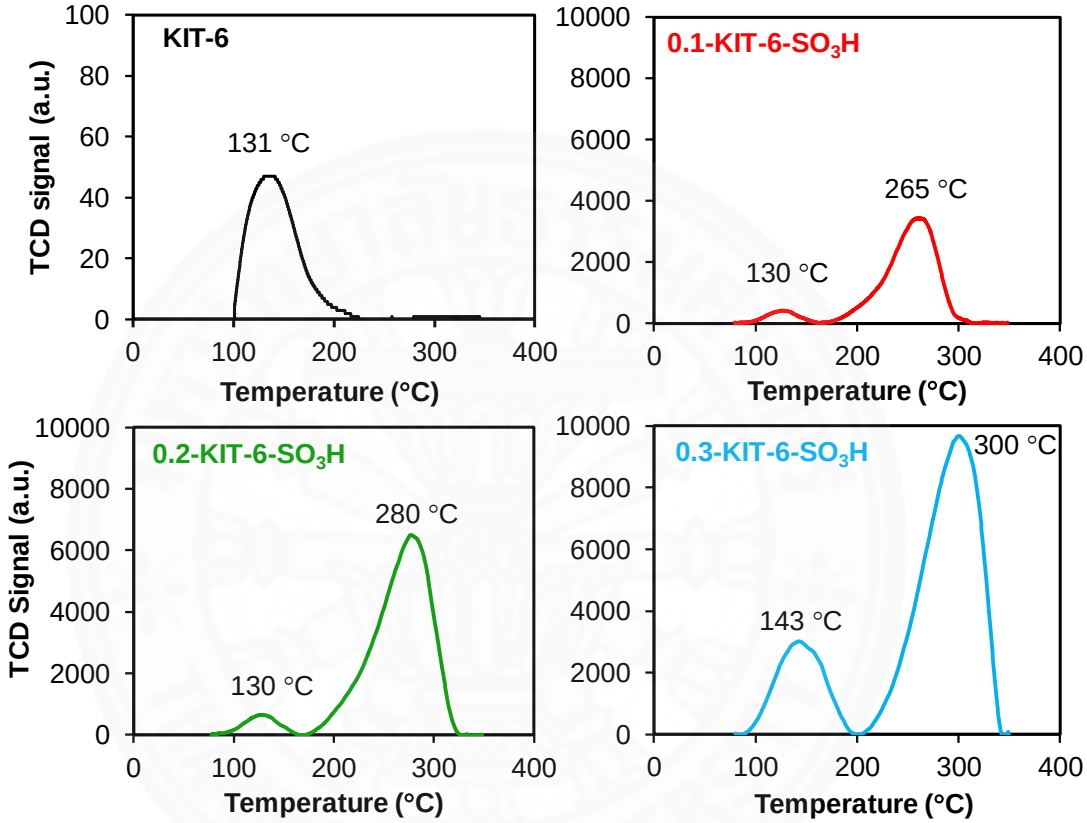

Figure 2.10 NH_3-TPD profile of KIT-6 and KIT-6-SO_3H catalysts

2.5.2 Catalytic activity in furfural production via xylose dehydration

The catalytic performance in xylose dehydration to furfural was studied by sulfonic acid-functionalized mesoporous silica (KIT-6-SO_3H) catalyst in the water/toluene bi-phasic system. In this part, the experiment was carried out at different reaction temperatures, reaction times, catalyst loadings. Besides, the effects of acid density of catalyst, MPMDS:TEOS molar ratio on the yield and selectivity of furfural were investigated.

Ref. code: 25625909320250YIN

2.5.2.1 Effect of catalytic activity and catalyst loading

The effects of catalytic activity and selectivity on xylose conversion at three different molar ratios of MPMDS:TEOS on catalyst are shown in **Table 2.4**. Among these, the difference in MPMDS:TEOS molar ratios had influenced the acidity and pore diameter of the catalyst. The 0.3-KIT-6-SO_3H catalyst gave the highest xylose conversion (98.01%) because of the highest acidity. The xylose conversion decreased with decreasing molar ratios of MPMDS:TEOS. Meanwhile, the turnover frequency (TOF) increased. Hence, the catalytic activity was affected by acidity and acid density as well. The 0.1-KIT-6-SO_3H catalyst presented low acid density but still gave high xylose conversion due to the fast reaction rate, the reactant good accessibility toward the catalyst sites than 0.2-KIT-6-SO_3H which was higher acid density. However, the 0.3-KIT-6-SO_3H catalyst presented high acidity but TOF was lowed owing to the disruption of the 3D catalyst structure. Besides that, (Cortés, Pineros-Castro, & Campos Rosario, 2013) reported the xylose dehydration carried out without catalyst at 170 °C for 4 h as shown in **Table 2.4**. The xylose conversion was reached to 86.20% but the furfural selectivity was low (17.10%) since many by-products were formed. Normally, side reactions, such as isomerization, condensation, and resinification could occur during the production of furfural from D-xylose resulting in the formation of organic acids as undesired by-products (Termvidchakorn et al., 2017).

Therefore, the 3D structure of KIT-6 catalyst could enhance the reaction rate and diffusion of reactant to the catalyst sites. In addition, the 0.2-KIT-6-SO_3H catalyst gave the highest furfural selectivity (94.65%) and furfural yield (92.29%) which was affected by the highest acid density. As mention above, the 0.2-KIT-6-SO_3H catalyst was not only shown the high conversion of xylose, but also high yield and selectivity of furfural which was selected as an optimized catalyst for the variation reaction conditions.

Ref. code: 25625909320250YIN

Table 2.4 The catalytic activity in the dehydration of xylose process under different x-KIT-6-SO_3H catalysts

Catalyst	Conversion (%)	Yield (%)	Selectivity (%)	TOF (h^{-1})
0.3-KIT-6-SO_3H	98.01	88.41	90.21	8.58
0.2-KIT-6-SO_3H	97.50	92.29	94.65	10.43
0.1-KIT-6-SO_3H	96.47	58.66	60.81	18.54
*No catalyst (Cortés et al., 2013)	86.20	n/d	17.10	n/d

*Reaction conditions: 170 ℃ – 4 h, D-xylose (0.75 g), and deionized water (25 mL) as a solvent

Figure 2.11 shows the effect of catalyst loading on xylose conversion, yield and selectivity of furfural. At catalyst loading 10 wt.%, the yield and selectivity of furfural were low due to the less amount of acid sites. Accordingly, the higher catalyst loading gave a higher amount of acid sites to give a high yield and selectivity of furfural. However, an excess amount of catalyst is not essential for this reaction to reduce furfural yield and furfural selectivity (Halilu et al., 2016). This may be due to poor mixing in the high viscosity of the reaction mixture, creating resistance to mass transfer in the multi-phase system. Therefore, the suitable catalyst loading was 25 wt.% to produce 97.50%, 92.50% and 93.90% of xylose conversion, furfural selectivity, and furfural yield, respectively.

Ref. code: 25625909320250YIN

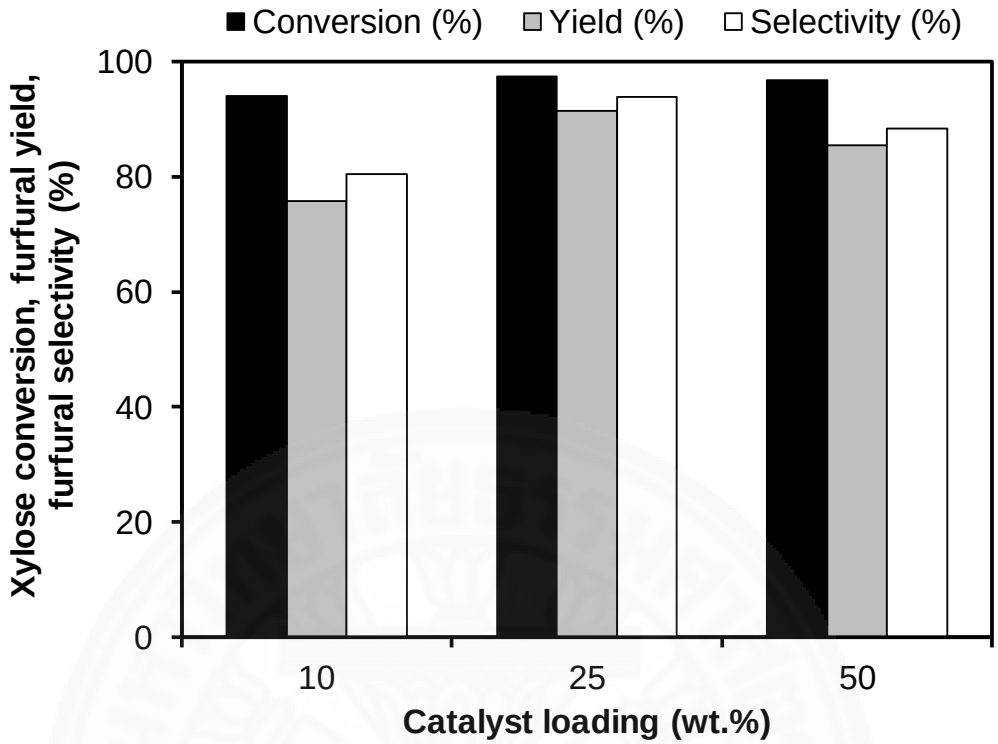

Figure 2.11 Catalytic activity of xylose dehydration at 170 ℃ for 2 h with different KIT-6-SO_3H catalyst loading

2.5.2.2 Effect of reaction temperature

The reaction temperature was studied at 130 ℃, 150 ℃ and 170 ℃. The xylose conversion, furfural selectivity and furfural yield were significantly affected by reaction temperature as shown in **Figure 2.12**. The xylose conversion increased from 83.10% to 97.50% when the temperature increased from 130 ℃ to 170 ℃, due to endothermic reaction (Huiling-Li et al., 2014; J. Zhang, Zhuang, Lin, Liu, & Zhang, 2012). A higher temperature also favored the furfural selectivity, which increased from ~43% at 130 ℃ to nearly 95.00% at 170 ℃. The highest furfural yield and furfural selectivity were 92.50% and ~ 95.00%, respectively at 170 ℃. Therefore, the optimal reaction temperature was 170 ℃.

Ref. code: 25625909320250YIN

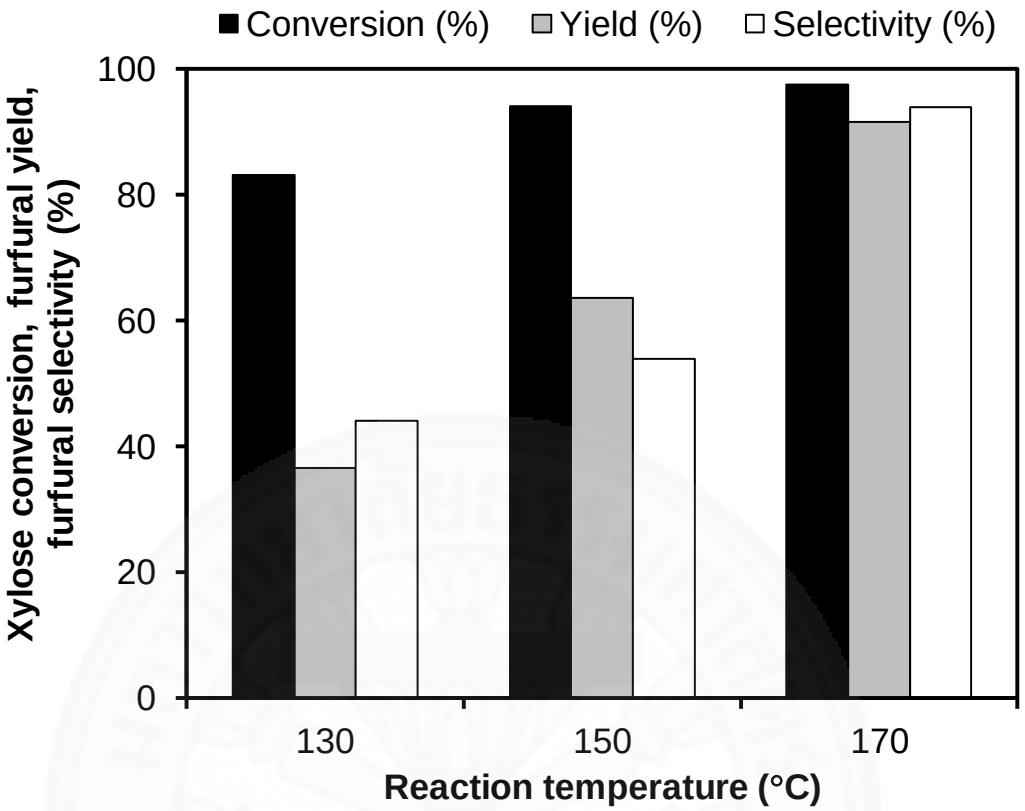

Figure 2.12 Catalytic activity of xylose dehydration at reaction time of 2 h with different reaction temperature under 25wt.% of 0.2-KIT-6-SO_3H catalyst

2.5.2.3 Effect of reaction time

The xylose conversion, furfural yield and furfural selectivity at different reaction time present in **Figure 2.13**. The reaction time slightly affected conversion of xylose because the chemical equilibrium was approached very fast (Tran et al., 2019; Tran et al., 2018). The xylose conversion could be achieved 97.70 % within 2 h, while the furfural selectivity initially increased from 80.90% to 94.70% after 2 h. As the results suggested that the reaction rate of xylose dehydration was fast due to the 3D structure of the catalyst, which could enhance the diffusion of reactant to the catalyst sites. However, the furfural selectivity decreased to 85.20% after 3 h. Hence, the longer reaction time could be going to further reactions including polymerization and oligomerization to furanic resins, a solid residue and formation of soluble degradation products (Huiling-Li et al., 2014). Besides, the yield of furfural was affected by reaction temperature and reaction time which obeyed a similar trend to the furfural selectivity. The optimal reaction time was 2 h.

Ref. code: 25625909320250YIN

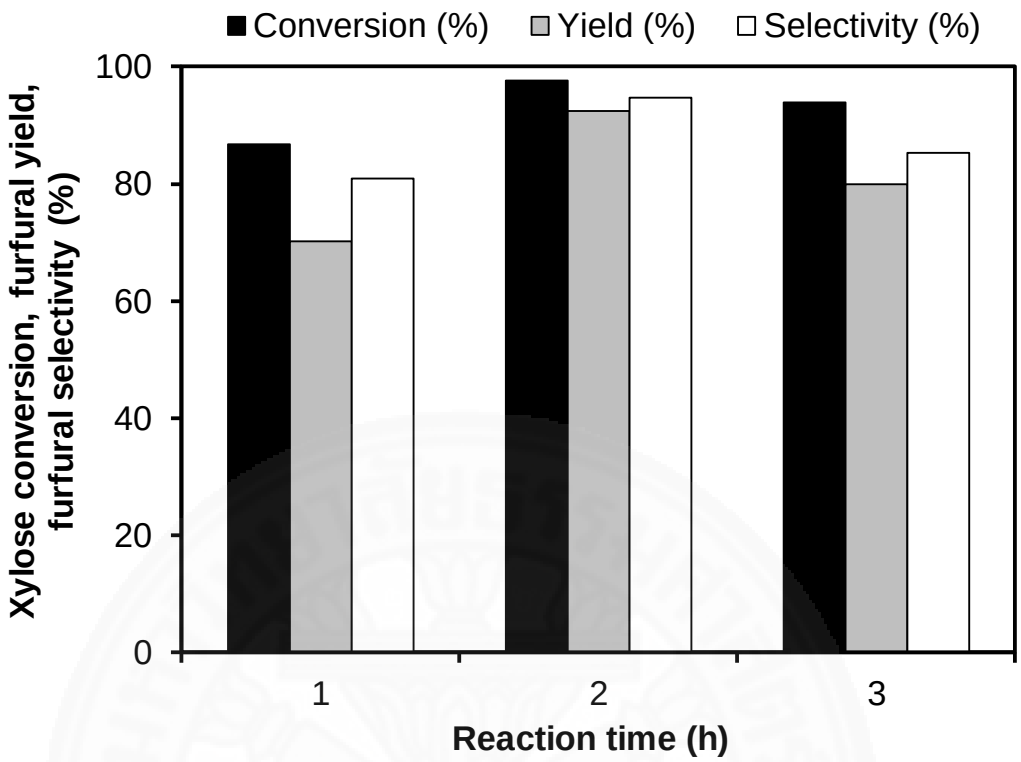

Figure 2.13 Catalytic activity of xylose dehydration at 170 °C with different reaction time under 25wt.% of 0.2-KIT-6-SO_3H catalyst

2.5.2.4 Reusability of catalyst

The stability of the KIT-6-SO_3H catalysts was carried out with 0.2-KIT-6-SO_3H over three cycles at optimize conditions (170 °C – 2 h – 25 wt.% catalyst loading) as shown in **Figure 2.14**. The xylose conversion was slightly decreased from 98.69 % to 93.02 % after 3rd cycle. Beside that the furfural selectivity decreased by 29 % after 3rd cycle. The reduction of the catalytic activity and the significantly decreased in furfural selectivity was resulted by the deactivation of catalyst (Kaiprommarat et al., 2016; Tran et al., 2019). Moreover, the loss of active site from further reaction was reached to the deposition of coke on the catalyst surface.

This deactivation of catalyst could be confirmed by the characteristic N_2 sorption and SEM micrographs of spent catalyst. The structures of the spent 0.2-KIT-6-SO_3H catalyst after 3 cycles presented H3 hysteresis loop with aggregates of plate-like particles forming slit-like pores. The low BET surface area (17 m^2/g) was given due to pore blocking, the pore size of spent catalyst decreased from

Ref. code: 25625909320250YIN

4.60 to 2.82 nm were reported in **Figure 2.15 and Table 2.3**. The surface area spent 0.2-KIT-6-SO_3H catalyst decreased due to the surface covered by reactants and/or products which could be observed by SEM as shown in **Figure 2.16**. In addition, the surface area of the spent KIT-6-SO_3H catalyst dramatically decreased owning to loss of internal surface area. The SEM micrographs of the spent 0.2-KIT-6-SO_3H catalyst presented the agglomeration of the covered by reacting and product compounds.

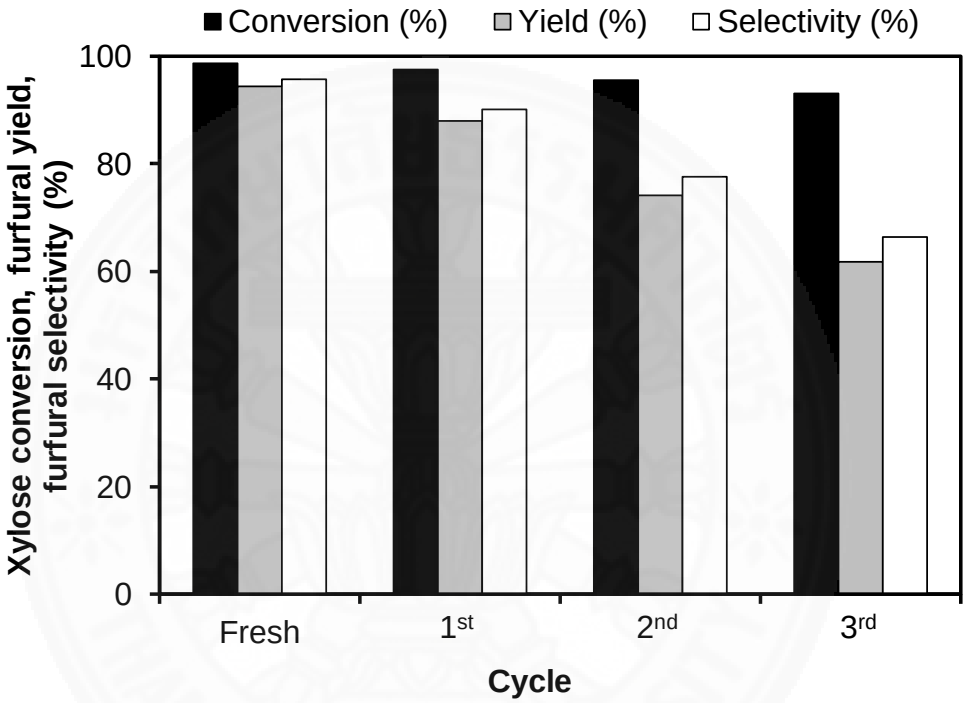

Figure 2.14 Catalytic activity of xylose dehydration of fresh and reused catalyst at 170 °C for 2 h under 25 wt.% 0.2-KIT-6-SO_3H catalyst loading

Ref. code: 25625909320250YIN

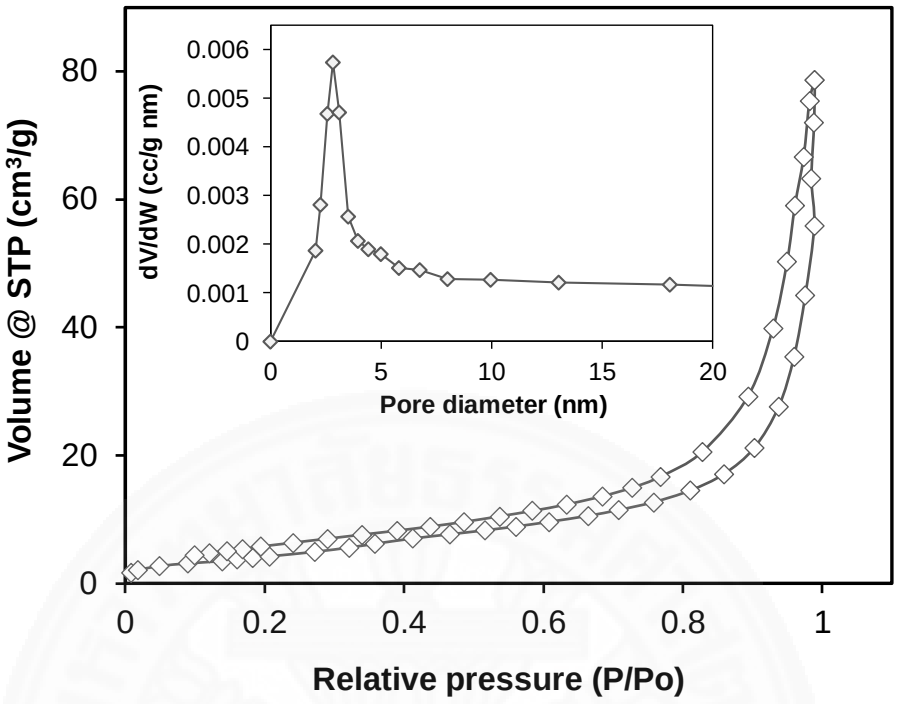

Figure 2.15 N_2 sorption and pore size distribution of 3rd used 0.2-KIT-6-SO_3H catalyst

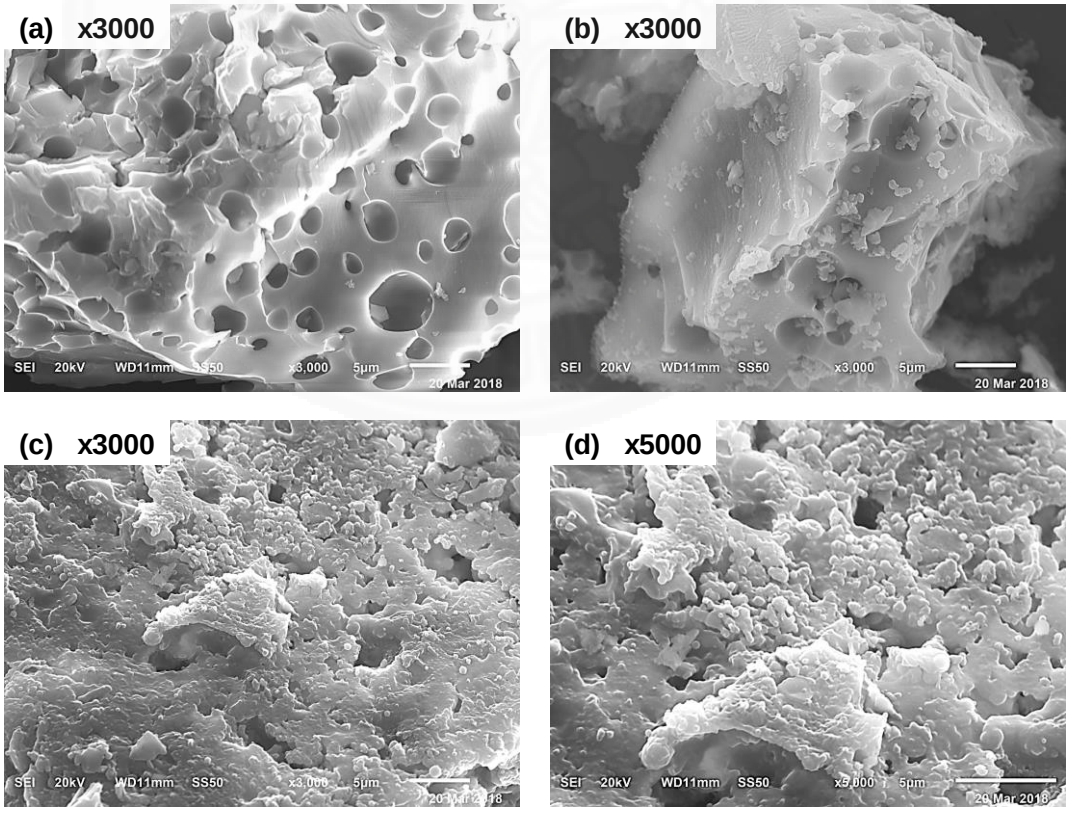

Figure 2.16 SEM micrograph of (a) fresh 0.2-KIT-6-SO_3H catalyst and (b) after 1st used and (c, d) after 3rd used catalyst at 170 °C for 2 h under 25 wt.% catalyst loading

Ref. code: 25625909320250YIN

2.6 Conclusions

The KIT-6-SO_3H catalyst could be prepared by sequential co-condensation and oxidation method with different molar ratios between MPMDS and TEOS. The pure KIT-6 and KIT-6-SO_3H catalysts were presented large surface area up to 872 m^2/g. The KIT-6 and KIT-6-SO_3H catalyst contained the mesopore structure. Besides that, SAXD has demonstrated the ordered structure with cubic Ia3d symmetry three-dimensional structure of both KIT-6 and KIT-6 catalyst. The 3D structure of the catalyst was discovered to be an important factor for enhanced the xylose conversion rate. The catalyst was tested the catalytic performance in dehydration of xylose to produce furfural. The highest furfural yield, furfural selectivity, and xylose conversion at optimized conditions were 92.5 %, 94.7 %, 97.7 %, respectively. The 0.2-KIT-6-SO_3H catalyst was the best catalyst in terms of xylose conversion, selectivity and yield of furfural, as well as the high TOF. The 0.2-KIT-6-SO_3H catalysts could be reused up to three cycles. The deactivation of catalyst was mainly caused by coke deposition to cover the active sites. In conclusion, the KIT-6-SO_3H catalyst can be a candidate the heterogeneous solid acid catalyst to perform the good performance in xylose dehydration.

Ref. code: 25625909320250YIN

2.7 References

Agirrezabal-Telleria, I., Gandarias, I., & Arias, P. L. (2014). Heterogeneous acid-catalysts for the production of furan-derived compounds (furfural and hydroxymethylfurfural) from renewable carbohydrates: A review. *Catalysis Today, 234*, 42-58. doi:https://doi.org/10.1016/j.cattod.2013.11.027

Agirrezabal Telleria, I., Gandarias, I., & Arias, P. L. (2014). Heterogeneous acid-catalysts for the production of furan-derived compounds (furfural and hydroxymethylfurfural) from renewable carbohydrates: A review. *Catalysis Today, 234*, 42-58. doi:https://doi.org/10.1016/j.cattod.2013.11.027

Agirrezabal Telleria, I., Larreategui, A., Requies, J., Güemez, M. B., & Arias, P. L. (2011). Furfural production from xylose using sulfonic ion-exchange resins (Amberlyst) and simultaneous stripping with nitrogen. *Bioresource Technology, 102* (16), 7478-7485. doi:https://doi.org/10.1016/j.biortech.2011.05.015

Agirrezabal Telleria, I., Requies, J., Güemez, M. B., & Arias, P. L. (2012). Pore size tuning of functionalized SBA-15 catalysts for the selective production of furfural from xylose. *Applied Catalysis B: Environmental, 115-116*, 169-178. doi:https://doi.org/10.1016/j.apcatb.2011.12.025

Alipour, S., Omidvarborna, H., & Kim, D. S. (2017). A review on synthesis of alkoxymethyl furfural, a biofuel candidate. *Renewable and Sustainable Energy Reviews, 71*, 908-926. doi:https://doi.org/10.1016/j.rser.2016.12.118

Antal, M. J., Leesomboon, T., Mok, W. S., & Richards, G. N. (1991). Mechanism of formation of 2-furaldehyde from d-xylose. *Carbohydrate Research, 217*, 71-85. doi:https://doi.org/10.1016/0008-6215(91)84118-X

Binder, J. B., Blank, J. J., Cefali, A. V., & Raines, R. T. (2010). Synthesis of furfural from xylose and xylan. *ChemSusChem, 3* (11), 1268-1272. doi:10.1002/cssc.201000181

Bozell, J. J., & Petersen, G. R. (2010). Technology development for the production of biobased products from biorefinery carbohydrates - the US Department of Energy's "Top 10" revisited. *Green Chemistry, 12* (4), 539-554. doi:10.1039/B922014C

Choudhary, V., Sandler, S. I., & Vlachos, D. G. (2012). Conversion of xylose to furfural using Lewis and Bronsted acid catalysts in aqueous media. *ACS Catalysis, 2* (9), 2022-2028. doi:10.1021/cs300265d

Ref. code: 25625909320250YIN

Cortés, W., Pineros-Castro, Y., & Campos Rosario, A. M. (2013). Conversion of D-xylose into furfural with aluminum and hafnium pillared clays as catalyst. *Dyna, 80* (180), 105-112. uri:https://repositorio.unal.edu.co/handle/unal/38508

Danon, B., Marcotullio, G., & de Jong, W. (2014). Mechanistic and kinetic aspects of pentose dehydration towards furfural in aqueous media employing homogeneous catalysis. *J Green Chemistry, 16* (1), 39-54.

Dias, A. S., Pillinger, M., & Valente, A. A. (2005a). Dehydration of xylose into furfural over micro-mesoporous sulfonic acid catalysts. *Journal of Catalysis, 229* (2), 414-423. doi:https://doi.org/10.1016/j.jcat.2004.11.016

Dias, A. S., Pillinger, M., & Valente, A. A. (2005b). Liquid phase dehydration of D-xylose in the presence of Keggin-type heteropolyacids. *Applied Catalysis A: General, 285* (1), 126-131. doi:https://doi.org/10.1016/j.apcata.2005.02.016

Gairola, K., & Smirnova, I. (2012). Hydrothermal pentose to furfural conversion and simultaneous extraction with SC-CO_2 – Kinetics and application to biomass hydrolysates. *Bioresource Technology, 123*, 592-598.
doi:https://doi.org/10.1016/j.biortech.2012.07.031

Galarneau, A., Cambon, H., Di Renzo, F., Ryoo, R., Choi, M., & Fajula, F. (2003). Microporosity and connections between pores in SBA-15 mesostructured silicas as a function of the temperature of synthesis. *New Journal of Chemistry, 27* (1), 73-79.

Halilu, A., Ali, T. H., Atta, A. Y., Sudarsanam, P., Bhargava, S. K., & Abd Hamid, S. B. (2016). Highly selective hydrogenation of biomass-derived furfural into furfuryl alcohol using a novel magnetic nanoparticles catalyst. *Energy & Fuels, 30* (3), 2216-2226.
doi:10.1021/acs.energyfuels.5b02826

Hoydonckx, H. E., Van Rhijn, W. M., Van Rhijn, W., De Vos, D. E., & Jacobs, P. A. (2007). *Furfural and Derivatives*. Weinheim, Wiley-VCH.

Isikgor, F. H., & Becer, C. R. (2015). Lignocellulosic biomass: a sustainable platform for the production of bio-based chemicals and polymers. *Polymer Chemistry, 6* (25), 4497-4559.

Jezak, S., Dzida, M., & Zorebski, M. (2016). High pressure physicochemical properties of 2-methylfuran and 2,5-dimethylfuran – second generation biofuels. *Fuel, 184*, 334-343.
doi:https://doi.org/10.1016/j.fuel.2016.07.025

Ref. code: 25625909320250YIN

Kaiprommarat, S., Kongparakul, S., Reubroycharoen, P., Guan, G., & Samart, C. (2016). Highly efficient sulfonic MCM-41 catalyst for furfural production: Furan-based biofuel agent. *Fuel, 174*, 189-196. doi:https://doi.org/10.1016/j.fuel.2016.02.011

Lam, E., Chong, J. H., Majid, E., Liu, Y., Hrapovic, S., Leung, A. C. W., & Luong, J. H. T. (2012). Carbocatalytic dehydration of xylose to furfural in water. *Carbon, 50* (3), 1033-1043. doi:https://doi.org/10.1016/j.carbon.2011.10.007

Li, H., Deng, A., Ren, J., Liu, C., Wang, W., Peng, F., & Sun, R. (2014). A modified biphasic system for the dehydration of D-xylose into furfural using $SO_4^{2-}/TiO^{2-}ZrO_2/La^{3+}$ as a solid catalyst. *Catalysis Today, 234*, 251-256.
doi:https://doi.org/10.1016/j.cattod.2013.12.043

Li, X. L., Pan, T., Deng, J., Fu, Y., & Xu, H. J. (2015). Catalytic dehydration of D-xylose to furfural over a tantalum-based catalyst in batch and continuous process. *RSC Advances, 5* (86), 70139-70146.

Li, Z., Assary, R. S., Atesin, A. C., Curtiss, L. A., & Marks, T. J. (2014). Rapid ether and alcohol C–O bond hydrogenolysis catalyzed by tandem high-valent metal triflate + supported Pd catalysts. *Journal of the American Chemical Society, 136* (1), 104-107.
doi:10.1021/ja411546r

Liu, S., Chen, J., Peng, Y., Hu, F., Li, K., Song, H., . . . Li, J. (2018). Studies on toluene adsorption performance and hydrophobic property in phenyl functionalized KIT-6. *Chemical Engineering Journal, 334*, 191-197.
doi:https://doi.org/10.1016/j.cej.2017.08.091

Lourvanij, K., & Rorrer, G. L. (1997). Reaction rates for the partial dehydration of glucose to organic acids in solid-acid, molecular-sieving catalyst powders. *Journal of Chemical Technology & Biotechnology, 69* (1), 35-44.
doi:10.1002/(SICI)1097-4660(199705)69:1<35::AID-JCTB685>3.0.CO;2-9

Marzialetti, T., Valenzuela Olarte, M. B., Sievers, C., Hoskins, T. J. C., Agrawal, P. K., & Jones, C. W. (2008). Dilute acid hydrolysis of loblolly pine: A comprehensive approach. *Industrial & Engineering Chemistry Research, 47* (19), 7131-7140. doi:10.1021/ie800455f

Montané, D., Salvadó, J., Torras, C., & Farriol, X. (2002). High-temperature dilute-acid hydrolysis of olive stones for furfural production. *Biomass and Bioenergy, 22* (4), 295-304. doi:https://doi.org/10.1016/S0961-9534(02)00007-7

Ref. code: 25625909320250YIN

Morais, A. R. C., Matuchaki, M. D. D. J., Andreaus, J., & Bogel Lukasik, R. (2016). A green and efficient approach to selective conversion of xylose and biomass hemicellulose into furfural in aqueous media using high-pressure CO_2 as a sustainable catalyst. *Green Chemistry, 18* (10), 2985-2994. doi:10.1039/C6GC00043F

Morales, G., Paniagua, M., Melero, J. A., & Iglesias, J. (2017). Efficient production of 5-ethoxymethylfurfural from fructose by sulfonic mesostructured silica using DMSO as co-solvent. *Catalysis Today, 279*, 305-316.
doi:https://doi.org/10.1016/j.cattod.2016.02.016

Moulder, J. F. (1995). Handbook of X-ray photoelectron spectroscopy. *Physical Electronics*, 230-232.

Ng, E. P., Mohd Subari, S. N., Marie, O., Mukti, R. R., & Juan, J.C. (2013). Sulfonic acid functionalized MCM-41 as solid acid catalyst for tert-butylation of hydroquinone enhanced by microwave heating. *Applied Catalysis A: General, 450*, 34-41.
doi:https://doi.org/10.1016/j.apcata.2012.09.055

Pirez, C., Caderon, J. M., Dacquin, J. P., Lee, A. F., & Wilson, K. (2012). Tunable KIT-6 mesoporous sulfonic acid catalysts for fatty acid esterification. *ACS Catalysis, 2* (8), 1607-1614. doi:10.1021/cs300161a

Rác, B., Molnár, Á., Forgo, P., Mohai, M., & Bertóti, I. (2006). A comparative study of solid sulfonic acid catalysts based on various ordered mesoporous silica materials. *Journal of Molecular Catalysis A: Chemical, 244* (1), 46-57.
doi:https://doi.org/10.1016/j.molcata.2005.08.043

Román Aguirre, M., Gochi, Y. P., Sánchez, A. R., de la Torre, L., & Aguilar Elguezabal, A. (2008). Synthesis of camphene from α-pinene using SO_3^{2-} functionalized MCM-41 as catalyst. *Applied Catalysis A: General, 334* (1), 59-64.
doi:https://doi.org/10.1016/j.apcata.2007.09.031

Rong, C., Ding, X., Zhu, Y., Li, Y., Wang, L., Qu, Y., . . . Wang, Z. (2012). Production of furfural from xylose at atmospheric pressure by dilute sulfuric acid and inorganic salts. *Carbohydrate Research, 350*, 77-80. doi:https://doi.org/10.1016/j.carres.2011.11.023

Russo, P., Antunes, M., Neves, P., Wiper, P., Fazio, E., Neri, F., . . . Pinna, N. (2014). Solid acids with SO_3H groups and tunable surface properties.

Ref. code: 25625909320250YIN

Suxia, R., Haiyan, X., Jinling, Z., Shunqing, L., Xiaofeng, H., & Tingzhou, L. (2012). Furfural production from rice husk using sulfuric acid and a solid acid catalyst through a two-stage process. *Carbohydrate Research, 359*, 1-6. doi:https://doi.org/10.1016/j.carres.2012.07.006

Termvidchakorn, C., Itthibenchapong, V., Songtawee, S., Chamnankid, B., Namuangruk, S., Faungnawakij, K., . . . Sano, N. (2017). Dehydration of D-xylose to furfural using acid-functionalized MWCNTs catalysts. *J Advances in Natural Sciences: Nanoscience Nanotechnology, 8* (3), 035006.

Titirici, M. M., White, R. J., Falco, C., & Sevilla, M. (2012). Black perspectives for a green future: hydrothermal carbons for environment protection and energy storage. *Energy & Environmental Science, 5* (5), 6796-6822. doi:10.1039/C2EE21166A

Tran, T. T. V., Kongparakul, S., Karnjanakom, S., Reubroycharoen, P., Guan, G., Chanlek, N., & Samart, C. (2019). Highly productive xylose dehydration using a sulfonic acid functionalized KIT-6 catalyst. *Fuel, 236*, 1156-1163. doi:https://doi.org/10.1016/j.fuel.2018.09.089

Tran, T. T. V., Kongparakul, S., Reubroycharoen, P., Guan, G., Nguyen, M. H., Chanlek, N., & Samart, C. (2018). Production of furan based biofuel with an environmental benign carbon catalyst. *Environmental Progress & Sustainable Energy, 37* (4), 1455-1461. doi:10.1002/ep.12796

Tuteja, J., Nishimura, S., & Ebitani, K. (2012). One-pot synthesis of furans from various saccharides using a combination of solid acid and base catalysts. *Bulletin of the Chemical Society of Japan, 85* (3), 275-281.

Wang, X., Lin, K. S. K., Chan, J. C. C., & Cheng, S. (2005). Direct synthesis and catalytic applications of ordered large pore aminopropyl-functionalized SBA-15 mesoporous materials. *The Journal of Physical Chemistry B, 109* (5), 1763-1769. doi:10.1021/jp045798d

Xu, Z., Li, W., Du, Z., Wu, H., Jameel, H., Chang, H.M., & Ma, L. (2015). Conversion of corn stalk into furfural using a novel heterogeneous strong acid catalyst in γ-valerolactone. *Bioresource Technology, 198*, 764-771. doi:https://doi.org/10.1016/j.biortech.2015.09.104

Ref. code: 25625909320250YIN

Yuan, Z., Zhang, Z., Zheng, J., & Lin, J. (2015). Efficient synthesis of promising liquid fuels 5-ethoxymethylfurfural from carbohydrates. *Fuel, 150*, 236-242. doi:https://doi.org/10.1016/j.fuel.2015.02.020

Zhang, J., Zhuang, J., Lin, L., Liu, S., & Zhang, Z. (2012). Conversion of D-xylose into furfural with mesoporous molecular sieve MCM-41 as catalyst and butanol as the extraction phase. *Biomass and Bioenergy, 39*, 73-77. doi:https://doi.org/10.1016/j.biombioe.2010.07.028

Zhang, L., Yu, H., Wang, P., Dong, H., & Peng, X. (2013). Conversion of xylan, d-xylose and lignocellulosic biomass into furfural using $AlCl_3$ as catalyst in ionic liquid. *Bioresource Technology, 130*, 110-116. doi:https://doi.org/10.1016/j.biortech.2012.12.018

Zhou, P., & Zhang, Z. (2016). One-pot catalytic conversion of carbohydrates into furfural and 5-hydroxymethylfurfural. *Catalysis Science & Technology, 6* (11), 3694-3712. doi:10.1039/C6CY00384B

Ref. code: 25625909320250YIN

CHAPTER 3
PRODUCTION OF ISOAMYL ACETATE FROM FUSEL OIL USING A SULFONIC ACID FUNCTIONALIZED KIT-6 CATALYST

3.1 Introduction

Nowadays, it is well known that the amount of fossil fuels all over the world is limited and non-renewable. The consumption of energy generated from fossil fuels tends to increase with the development of the economy and the growth of the global population. Moreover, the use of fossil fuels results in an increase of greenhouse gas which leads to global warming. (AlNouss, McKay, & Al-Ansari, 2019; Gebremariam & Marchetti, 2018) Therefore, the utilization of renewable resources for fossil fuel replacement has been interested. (Dasan, Lam, Yusup, Lim, & Lee, 2019; Janampelli & Darbha, 2018; Kakakhel et al., 2019; Wu, Wang, Zheng, Wang, & Han, 2019) Recently, gasohol, a mixture of gasoline and ethanol has been promoted and completely replaced conventional gasoline leading to the fast growth of bioethanol industry. As a result, fusel oil a by-product of bioethanol fermentation (C_3-C_5 alcohols mixture) was also concurrently produced during the production of bioethanol which is close to 0.25 vol.% of bioethanol. In Brazil, a main bioethanol production country, the amount of this by-product was reached more than 59 million gallons (Pereira et al., 2015). Hence, the value-added of fusel oil is an interesting topic for adding economic viability to bioethanol industry. It is interesting that isoamyl alcohol (C_5) is found as the main component in fusel oil which could be used to produce isoamyl acetate which is used in pharmaceutical manufactures, food and fragrance. This component could be obtained via both esterification routes: enzymatic catalyst and chemical catalyst. (Corregidor, Acosta, Gonzo, & Destéfanis, 2020; Zare, Golmakani, & Niakousari, 2019) The esterification reaction is both slow and reversible. Esterification is mainly the reaction between a carboxylic acid RCOOH and an alcohol R'OH (where R and R' can be the same or different) to form esters. The isoamyl alcohol esterification and mechanism of this process is shown in **Figure 3.1.** First, the acetic acid took a proton

Ref. code: 25625909320250YIN

of (hydrogen ion) from acid catalyst to form the protonation of the carboxyl group of the acetic acid and was attacked by the nucleophilic alcohol group on the carbonyl, presenting with a tetrahedral intermediate. (1,2) Then, this tetrahedral intermediate undertook transfer of the proton to produce a water molecule followed by loss of a proton and made easy the breakdown of the transition state. (3,4) Next, the carbonyl group regenerated and dehydrated the molecule of water results in isoamyl acetate product when protonation on the oxygen of the carbonyl group was captured by a water molecule and produced the H_3O^+ (5) (Feygroupchem, January 8, 2014; Teo & Saha, 2004).

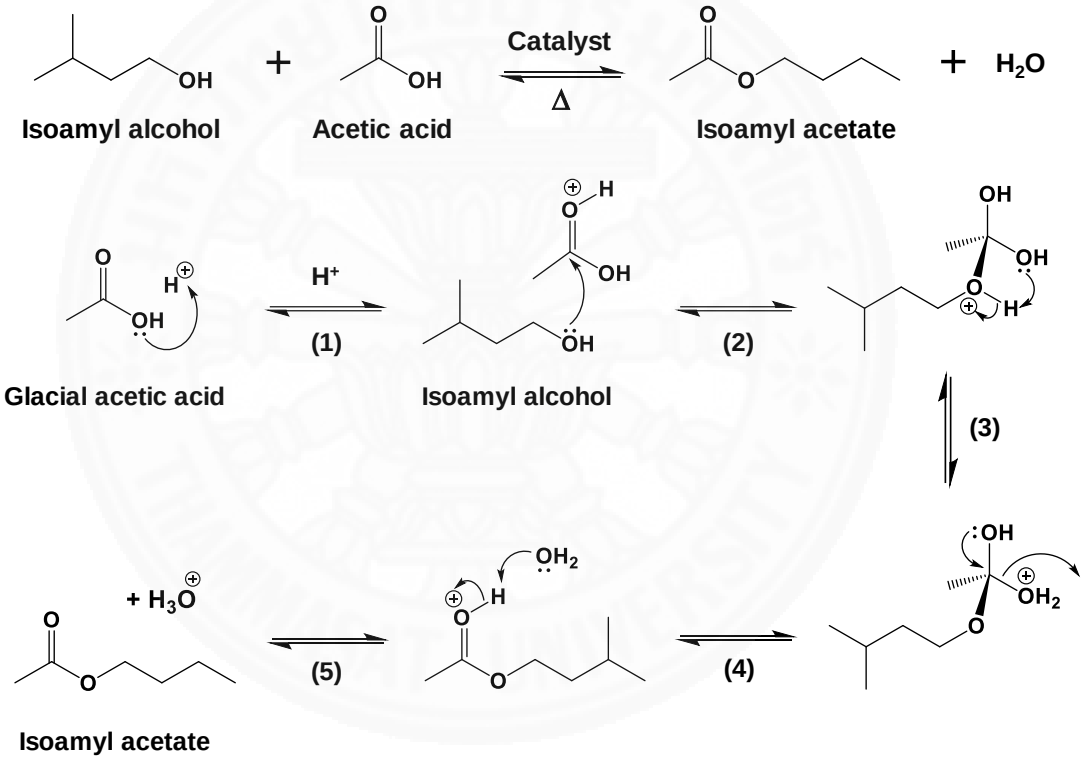

Figure 3.1 The fusel oil esterification to synthesis of isoamyl acetate (banana oil) under acid catalyst (Feygroupchem, January 8, 2014; Teo & Saha, 2004)

On the view of approaches, process improvement and development of catalyst have been focused on. Process improvement prefers to increase the purity of ester product with a separation process while development of catalyst focuses on the use of biocatalysts and chemical catalysts. Typical achievements in process improvement were distillation procedure which reduced operating cost up to 40% (Li,

Ref. code: 25625909320250YIN

Zhou, Sun, & Zhang, 2019). Furthermore, vapor-liquid equilibrium thermodynamics in binary mixture of ester product was investigated (Sánchez, Sánchez, Orjuela, Gil, & Rodríguez, 2017). On the other hand, the use of supported lipase-based enzyme in both batch and continuous system was studied in esterification process (Vilas-Bôas, Ceron, Bento, & de Castro, 2018). Conversion level at 95% of isoamyl butyrate was observed without any required organic solvent under microwave irradiation for 2 h (Bansode & Rathod, 2018). Moreover, the reaction time was six times reduction when applying ultrasonic to the esterification reaction system (Nyari et al., 2018). However, the purity of the product was low and large amount of waste from the reaction.

Meanwhile, a chemical catalyst performed high potential in commercial scale of fusel oil esterification. (Osorio-Viana, Duque-Bernal, Fontalvo, Dobrosz-Gómez, & Gómez-García, 2013) found that the reaction rate was strongly affected by the sorption affinity when investigating kinetic behavior in esterification reaction of amyl alcohol and acetic acid with Amberlite IR-120 catalyst. Nevertheless, (Wang, Liu, Yuan, & Guo, 2013) reported that the ion exchange resin catalyst performed the catalytic performance in isoamyl acetate synthesis as 95% of ester yield within reaction time of 2 h. However, those polymeric material catalysts were low thermal stability and surface area leading to the limitation in practical use. On the other hand, inorganic materials appeared a good candidate to take over the drawbacks of polymeric based catalyst. (Jiang, Xu, Zeng, Xue, & Li, 2018) investigated kinetic pathway of the esterification reaction of isoamyl alcohol and lactic acid using sodium hydrogen sulphate on silica gel support catalyst (silica gel-based catalyst). The author reported that the dynamic model Eley-Rideal (ER) was the most appropriate for this esterification reaction. The lactic acid conversion could be over 90% at 90 °C for 1500 minutes and lactic acid:alcohol molar ratio of 1:5. Isoamyl acetate yield could be reached 94% with sulfated TiO_2 at the reaction condition of temperature of 130 °C for 5 h with acetic acid:alcohol molar ratio of 1:7 (Afshar et al., 2015). Moreover, isoamyl alcohol conversion was reached to 98% when HZSM-5 zeolite catalyst was used in the reaction between isoamyl alcohol and vinyl acetate. However, the selectivity of isoamyl acetate competed with di-isoamyl alcohol acetal (Corregidor et al., 2020). In addition, iso-pentanol and acetic acid esterification was also conducted in a membrane reactor

Ref. code: 25625909320250YIN

(Xue et al., 2019). The formation of water was separated during the reaction leading to a remarkable increase in isoamyl acetate yield up to 98% for 160 h of operation. However, in order to archive higher yield of isoamyl acetate, high temperature of reaction and long reaction time were required. Moreover, reusability of the catalyst was poor due to water from the reaction. Low surface area and small pore size caused the limiting for accessibility of reaction site and leading to deactivation. Therefore, highly effective and selective catalyst would be developed. Sulfonated carbon and sulfonic acid functionalized mesoporous silica were solid catalyst to perform outstanding performance in catalyzing the organic reaction (Islam et al., 2019; Nowicki, Jaroszewska, Nowakowska-Bogdan, Szmatoła, & Iłowska, 2018). (Karnjanakom, Maneechakr, Samart, & Guan, 2019; Ramdani et al., 2019) studied the carbohydrate glycosylation and sugar transformation. The author found that sulfonated carbon gave the excellent catalytic performance with high reusability. In addition, (Ponnuru et al., 2018) studied enantioselective nitroaldol reaction using sulfonic functionalized mesoporous silica SBA-15. The author found that the catalyst showing high catalytic performance and high product selectivity.

In this chapter, the author proposed a new mesoporous silica KIT-6 functionalized with sulfonic acid catalyst for esterification reaction between acetic acid and fusel oil. This catalyst was expected to improve diffusion effect of intra-particle (Karnjanakom et al., 2016) due to its three dimensional porous structure. The catalyst would be synthesized by hydrothermal process and characterized its physical properties including NH_3-TPD, XPS, SAXS, N_2 sorption. The fusel oil, without purification was collected from a KTIS bioethanol company. The study would be investigated the effect of reaction condition on the catalytic performance. The catalytic performance of the catalyst was benchmarked with conventional catalyst under optimized conditions. Furthermore, catalyst reusability was also investigated.

3.2 Review of literature

(Bi et al., 2008) studied preparation of isopentyl acetate from esterification of acetic acid and isoamyl alcohol by immobilized Cadida Antarctica Lipase. At the

Ref. code: 25625909320250YIN

optimized conditions of 9% enzyme loading with reaction temperature 40 °C for 6 h and molar ratio of acid:alcohol was 1:2, 92% yield of ester could be achieved. In addition, this enzyme could be reused up to six times.

(Krishna et al., 2001) synthesized isopentyl acetate using Rhizomucor miehei lipase catalyst. The author investigated the effect of reaction parameters including molar ratio of substrate (acid): nucleophile (alcohol) and enzyme concentration. At the optimizing conditions of 10 g/L enzyme content with reaction temperature 40 °C for 72 h and molar ratio of acid:alcohol was 1:2, the yield of product could be reached above 80% with reusability of catalyst up to ten times.

(Zare et al., 2019) synthesized isoamyl acetate with different acyl donors (acetic acid, acetic anhydride, and ethyl acetate) using lipase catalyst under microwave irradiation. This research also compared different reactor systems including microwave, ohmic, ultrasound, and incubator. The author suggested that the microwave technique gave the highest isoamyl acetate yield up to 100% at the optimize conditions of reaction time 1 h, 1% Novozyme 435, acetic anhydride: isoamyl alcohol ratio of 1:1, agitation speed of 120 rpm and microwave power 100W. The catalyst could be reused up to seven times.

The application of biocatalyst for isoamyl acetate production could be carried out at low reaction temperature and gave high purity of product. Furthermore, the enzyme could be reused. However, the rate of the reaction was low to take long reaction time. Hence, many researchers have focused on the heterogeneous catalyst to improve the catalytic activity.

(Pang et al., 2008) studied the isoamyl alcohol esterification using an expandable graphite catalyst. At the optimizing conditions, the yield of isoamyl acetate could be obtained 96.0%.

(Teo & Saha, 2004) examined the esterification of isoamyl alcohol esterification using cation-exchange resin (Purolite CT-175) catalyst in batch reactor. The kinetics of heterogeneous catalyzed esterification was studied. At the optimizing conditions of 85 °C for 6 h, molar ratio of isoamyl alcohol to acetic acid of 2:1 and 10 wt.% catalyst loading resulted in the equilibrium conversion of acetic acid about 80%. This catalyst studied reusability up to three times. The author reported that the

Ref. code: 25625909320250YIN

Langmuir–Hinshelwood–Hougen–Watson (LHHW) kinetic model was the most appropriate for this esterification reaction.

As mentioned above, the sulfonated functionalized group has attracted a lot of interests and has been selected as a functional group for KIT-6 catalyst to be used in fusel oil esterification reaction. This catalyst was expected to improve the diffusion effect of intra-particle (Karnjanakom et al., 2016) due to its three dimensional porous structure.

3.3 Materials

All chemicals and equipment used in this research were shown in **Table 3.1** and **Table 3.2**, respectively.

3.3.1 Chemicals

Table 3.1 List of the chemicals used in this research

Chemicals	Manufacturer	Country
Acetone, commercial grade	RCI Labscan	USA
Acetic acid, AR grade	QReC	New Zealand
n-Butanol, AR grade	RCI Labscan	USA
Ethanol Absolute, 99%	QReC	New Zealand
Fusel oil	KTIS	Thailand
Hexane, AR grade, 99%	QReC	New Zealand
Hydrogen peroxide, AR grade, 30%	QReC	New Zealand
Hydrochloric acid, AR grade, 37%	QReC	New Zealand
3-Mercaptopropyl methyldimethoxysilane, AR grade, 95%	Sigma-Aldrich	USA
Methyl heptadecanoate, 99.99%	Sigma-Aldrich	USA
Pluronic P123 triblock copolymer, poly (ethylene glycol)-block-poly (propylene glycol)-block-poly (ethylene glycol), Mw = 5800, AR grade	Sigma-Aldrich	USA

Ref. code: 25625909320250YIN

Table 3.1 List of the chemicals used in this research (cont.)

Tetraethyl orthosilicate, AR grade, 98%	Sigma-Aldrich	USA
Sodium bicarbonate anhydrous ($NaHCO_3$)	Ajax Finechem	Australia
Sodium carbonate anhydrous (Na_2CO_3)	Ajax Finechem	Australia
Sodium sulfate anhydrous (Na_2SO_4)	Ajax Finechem	Australia
Sulfuric acid, 98%	QReC	New Zealand

3.3.2 Equipment

Table 3.2 List of the instrument used in this research

	Company
Autoclave reactor, 50ml	Parr, model 4744, USA
Gas Chromatography-Mass Spectrometry (GC-MS)	Shimadzu, GCMS-QP 2010, Japan
High Performance Liquid Chromatograph (HPLC)	Shimadzu, Japan, LC-20AT (pump), SPD-20A (UV dectector)
Oven	Memmert UF 110
Surface area & Porosimetry analyzer	Gold App Instrument, V-sorb 2800P
Scanning Electron Microscope (SEM)	JEOL, Japan, JSM-6510LV
Temperature Programed Desorption of amonia (NH_3-TPD)	BET-CAT (BEL, Japan)
X-ray diffraction (SAXD)	Rigaku, TTRAX III and Bruker, D8 advance
X-ray photoelectron Spectroscopy (XPS)	ULVAC-PHI, PHI 500 VersaProbe II, Japan

3.4 Methods

3.4.1 x-KIT-6-SO_3H catalyst synthesis

Co-condensation method was used for the preparation of the KIT-6-SO_3H catalyst, in generally, with a molar compositions mixture of 195 H_2O: 1.31 n-butanol: 0.017 Pluronic triblock copolymer (P123): 1.83 HCl: x 3-mercaptopropyl(methyl)dimethoxysilane (MPMDS): (1-x) tetraethoxysilane (TEOS), where x was from 0.1-0.3 (Tran et al., 2019).

Ref. code: 25625909320250YIN

The synthesis method was as follow: using a mixture of 1.88 g HCl (37%) and 37.0 g DI water completely dissolve 1.0 g of P123 (P123 acts as structure-directing agent). After that, under vigorous stirring, 1.0 g n-butanol was added with continuous stirring for 1 h at temperature of 35 °C. Then, a solution of 2.15 g of TEOS and a g MPMDS follow the ratio as mentioned before was dropped wisely to the mixture and stirring for 24 h with the temperature of 35 °C before treating the mixture in autoclave for hydrothermal at the condition of 100 °C for 24 h. After hydrothermal treating step, the solid particle was collected and dried for 12 h at temperature of 80 °C. In the following step, Soxhlet extraction was used to remove remained surfactant with the solvent mixture of HCl: ethanol volume ratio at 1:10 to obtain sulfhydryl functionalized KIT-6 mesoporous silica (KIT-6-SH). At final step, the collected solid was oxidized with 30% H_2O_2 at ambient temperature for 24 h, the sulfonic acid-functionalized KIT-6 catalyst was finally obtained. This catalyst was designated as x-KIT-6-SO_3H catalyst (x: molar content of MPMDS).

3.4.2 Characterization of synthesized catalyst

Small-angle X-ray diffraction (SAXD) was used to characterize pore arrangement of catalyst within 2θ range of 0.5° to 5°, a resolution of 0.02° and scan speed 0.1 second per step using radiation of Cu Kα on a Rigaku TTRAX III X-ray diffractometer.

Nitrogen (N_2) sorption technique was used to measure BET surface area and pore properties, pore diameter was calculated by Barrett-Joyner-Halenda (BJH) using the data of N_2 desorption region of the isotherm. The nitrogen (N_2) sorption was conducted by a V-sorb 2800 P (Gold APP Instruments Corporation) with the condition of -196 °C.

X-ray photoelectron spectroscopy (XPS) was applied to analyze elemental composition and chemical state of catalyst. The XPS carried out with Al Kα X-ray radiation on a ULVAC-PHI, PHI500 VersaProbe II. C1s peak at 284.5 eV was used to correct other peaks. To prove the present of sulfonic acid functional group on KIT-6 surface, S2p spectra was fitted with Gaussian/Lorentzian peak shape for the confirmation.

Ammonia-temperature programmed desorption (NH_3-TPD) was employed to measure acidity of the catalyst obtained by using a BELCAT (BEL

Ref. code: 25625909320250YIN

instrument). In a measurement, u-shaped quartz cell was used to pack the catalyst inside. Then the cell was preheated under 50 cm^3/min He for 1 h at 750 °C to remove moisture remaining in the structure of catalyst. In the following step, a mixture of 5 %NH_3/95 %He was flown to the cell for saturating environment surrounding of catalyst in the cell at ambient temperature for 1 h. When the system inside the cell was stable, NH_3 desorption process was conducted by heating the cell to 400 °C under He flow at heating rate 5 °C/min. The amount of desorbed NH_3 was detected by TCD detector.

3.4.3 Catalytic activity in isoamyl acetate production via fusel oil and acetic acid esterification

3.4.3.1 Fusel oil esterification

Isoamyl alcohol was determined as the main chemical composition of fusel oil used for this work as listed in **Table 3.3**. Esterification of fusel oil and acetic acid formed isoamyl acetate as a desired product. First, the mixture of the reactants and catalysts was stirred at 800 rpm in a small glass bottle. The conditions of the reaction, such as reaction time, reaction temperature, catalyst loading was set according to the investigation requirement. After reaction finished, the reaction mixture was cooled and separated catalyst from the mixture. The liquid product was collected and washed with cold water several times. The remain acetic acid was neutralized by 5 wt.% solution of $NaHCO_3$ prior to obtain the final product. The moisture in organic phase was removed by anhydrous sodium sulfate. For the reusability study of catalyst, the used catalyst was washed by acetone, then dried at 70 °C and re-oxidized by H_2O_2 (Hua et al., 2013). The catalytic activity of used catalyst with and without re-oxidation were compared under the same reaction condition.

Ref. code: 25625909320250YIN

Table 3.3 Chemical composition of fusel oil

Component	Concentration (%)
Isopropyl alcohol	3.32
Butanol (n, t, i-BuOH)	9.95
3-Methyl-2-butanol	1.42
Isoamyl alcohol	71.83
3-Methyl-2-pentanol	0.54
1-Hexanol	0.44
2-Heptanol	0.31
Acetyl furan	0.77
Acetic acid	0.84
Other	10.58

3.4.3.2 Product analysis

The isoamyl acetate yield was determined by gas chromatography (Shimadzu GC-17A, flame ionization detector). The capillary column was DB-WAX (30.0 m length, 0.25 mm internal diameter and 0.25 mm film thickness). The injection was split mode with 27 mL/min of split rate. The temperature program was heated to 50 ℃, hold equilibration for 3 min, heated to 100 ℃ at heating rate of 30 ℃/min and hold for 2 min, followed by increasing to 220 ℃ at heating rate of 25 ℃/min, hold for 3 min and the temperature of injector and detector was 250 ℃. The isoamyl acetate yield was calculated by integration area of the peak of methyl heptadecanoate (C17) as an internal standard by **Equation 3.1**.

$$\text{Isoamyl acetate yield} = \frac{A_{\text{Isoamyl acetate}}}{A_{EI}} \times \frac{C_{EI} \times V_{EI}}{m} \times 100 \qquad (3.1)$$

$A_{\text{Isoamyl acetate}}$ is the peak area of isoamyl acetate production

A_{EI} is the peak area of internal standard (methyl heptadecanoate)

C_{EI} is the concentration of the internal standard (mg/mL)

V_{EI} is the volume of the internal standard solution (mL)

m is the mass of the sample (mg)

Ref. code: 25625909320250YIN

3.5 Results and discussion

3.5.1 Physicochemical properties of catalyst

3.5.1.1 N_2 sorption analysis

N_2 sorption isotherms confirmed porous structures of KIT-6 and the KIT-6-SO_3H catalysts as shown in **Figure 3.2**. Isotherms of either KIT-6 or KIT-6-SO_3H catalysts approached IUPAC type IV isotherms. The isotherm of KIT-6 presented H1 hysteresis which indicated a well-defined cylindrical mesoporous structure meanwhile, the isotherms of KIT-6-SO_3H catalysts presented H4 hysteresis which indicated a narrow-slit like mesoporous structure. The presence of mercaptoalkyl silane affected the formation of ordered structure which remained distribution of pore size evenly. **Table 3.4** presented the textural properties of the KIT-6 and KIT-6-SO_3H catalysts. Comparing to the KIT-6, the surface area of the KIT-6-SO_3H catalysts was significantly decreased over 80 % due to loss of ordered porous structure. It was also found that an increase in sulfonic acid concentration resulted in a decrease in pore diameter. Pore formation was hindered by the existence of sulfhydryl group during porous formation. However, the porous structure was derived from space of inter-particle of uniformly particle size (Nowicki et al., 2018). It was interesting to observe that the surface area and pore size were larger when the ratio of MPMDS:TEOS increased from 0.2 to 0.3 (0.3-KIT-6-SO_3H) indicating the generation of hierarchical mesoporous structure. Hence, the pore structure of the catalyst could be obtained by adjusting the ratio between MPMDS:TEOS. However, the excessing amount of MPMDS could result in the change in the structure of KIT-6. Therefore, in this research, the maximum ratio of MPMDS:TEOS would be limited at 0.3.

Ref. code: 25625909320250YIN

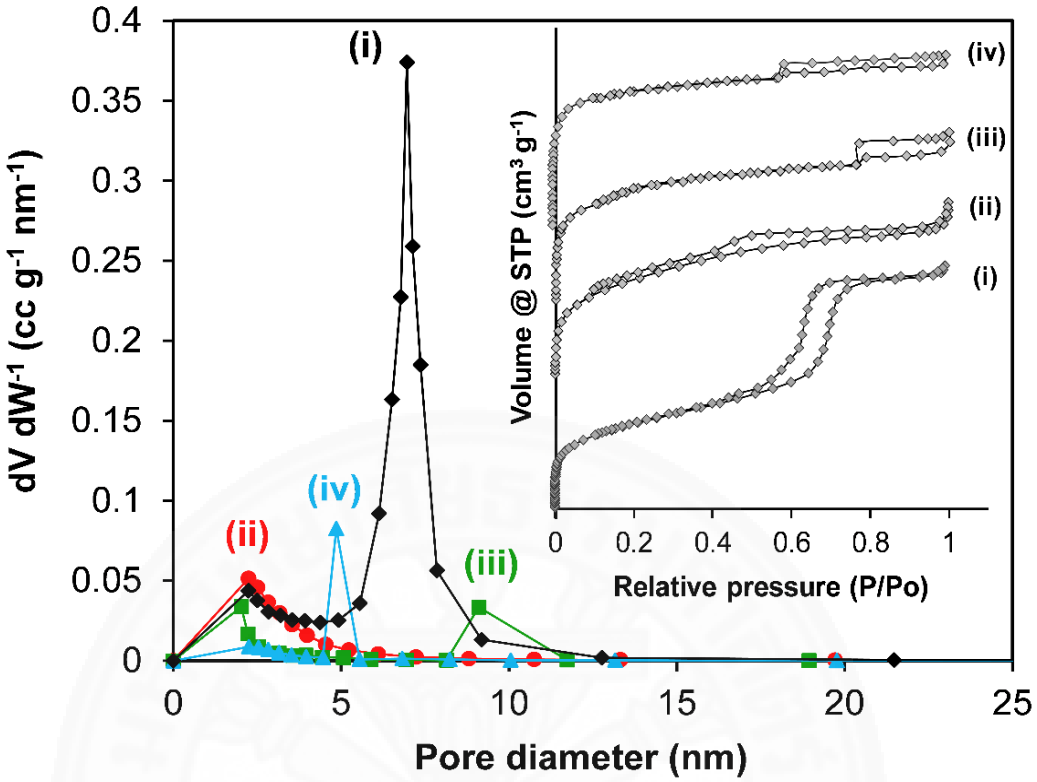

Figure 3.2 Nitrogen sorption isotherms and pore size distribution of (i) KIT-6, (ii) 0.1-KIT-6-SO_3H catalyst, (iii) 0.2-KIT-6-SO_3H catalyst, and (iv) 0.3-KIT-6-SO_3H catalyst

Table 3.4 Textural properties and acidity of KIT-6 and x-KIT-6-SO_3H catalysts

Catalyst	Surface area (m^2/g)	Pore size (nm)	BJH pore volume (cm^3/g)	Acidity (mmol/g)	Acid density ($mmol/m^2$)
KIT-6	872	6.2	0.88	0.02	n/d
0.1-KIT-6-SO_3H	269	4.7	0.21	0.69	0.003
0.2-KIT-6-SO_3H	157	4.6	0.13	1.25	0.008
0.3-KIT-6-SO_3H	225	4.5	0.10	1.53	0.007

3.5.1.2 Small angle X-ray diffraction (SAXD)

Figure 3.3 shows the porous structure from SAXD pattern. Three-dimensional (3D) ordered porous structure was observed on KIT-6 with the evidence at 2θ of 0.76°, 0.89°, and 1.53° which ascribed to scattering plane of (2 1 1), (2 2 0), (3 3 2), respectively. Partially collapse of 3D structure was observed by the

Ref. code: 25625909320250YIN

disappearance of (3 3 2) scattering plane and broader peaks of (2 1 1) and (2 2 0) due to the presence of sulfonic acid functional group. However, the ordered structure of catalyst was remained even though its 3D structure was lost.

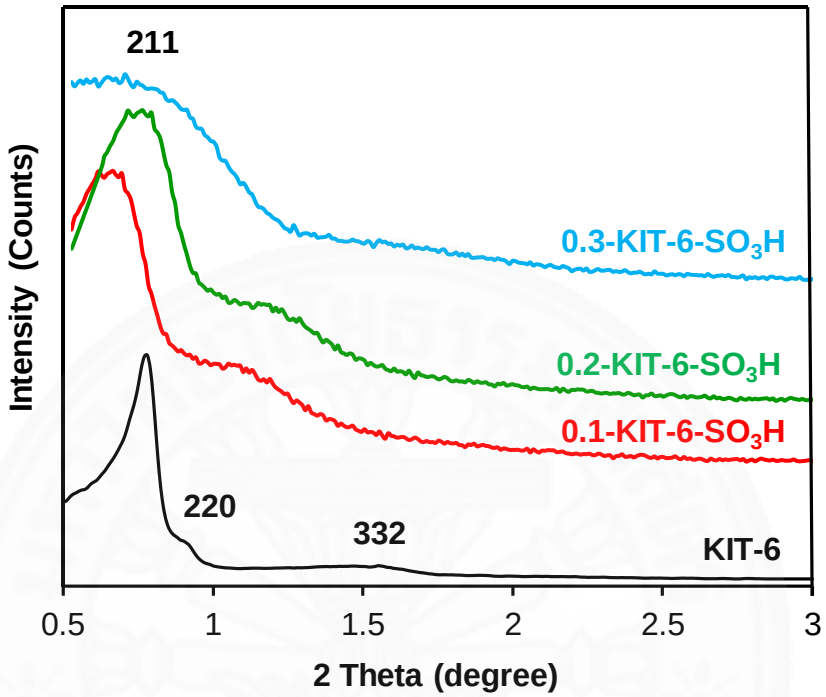

Figure 3.3 Small angle XRD patterns of KIT-6 and x-KIT-6-SO_3H catalyst

3.5.1.3 X-ray photoelectron spectroscopy (XPS)

With XPS analysis, shown in **Figure 3.4**, the surface functional groups of the KIT-6-SO_3H catalyst were determined. Besides, spectral of Si2p and C1s at BE of 103.5 eV and 284.8 eV were observed in the wide scan. In **Figure 3.4 (b),** the presence of SiO_2 in the framework of mesoporous silica (Si-O-Si) and sulfonic acid (S-O-H) was reflected by the peak of O1s with a broad spectrum at BE range of 530 eV to 535 eV (Kumar & Srivastava, 2019). Furthermore, in the S2p spectrum, the presence of alkyl sulfonic structure has been detected by the peak at 168.9 eV, as shown in **Figure 3.4 (c)**. Moreover, the conversion of sulfhydryl (-SH) groups to the sulfonic acid (-SO_3H) group was completed as represented by single peak of S2p spectra. However, the active sites lost and/or contaminated by impurities from fusel oil could be probably caused by the decreasing in intensity of S2p spectra of spent catalyst (iv). Also, there is a peak at BE 103.5 eV indicating the presence of an SiO_2 framework (**Figure 3.4 (d))**

Ref. code: 25625909320250YIN

while C1s spectra confirms the presence of functionalized sulfonic acid on the surface of KIT-6 as shown in **Figure 3.4 (e)** including three separated peaks: BE equal 284 eV (C-C bonds in alkyl sulfonic molecules), 285 eV (C-O bonds) and 289 eV (O-C=O bonds) (Song, An, Lu, Guo, & Leng, 2015; Y. Wang et al., 2015).

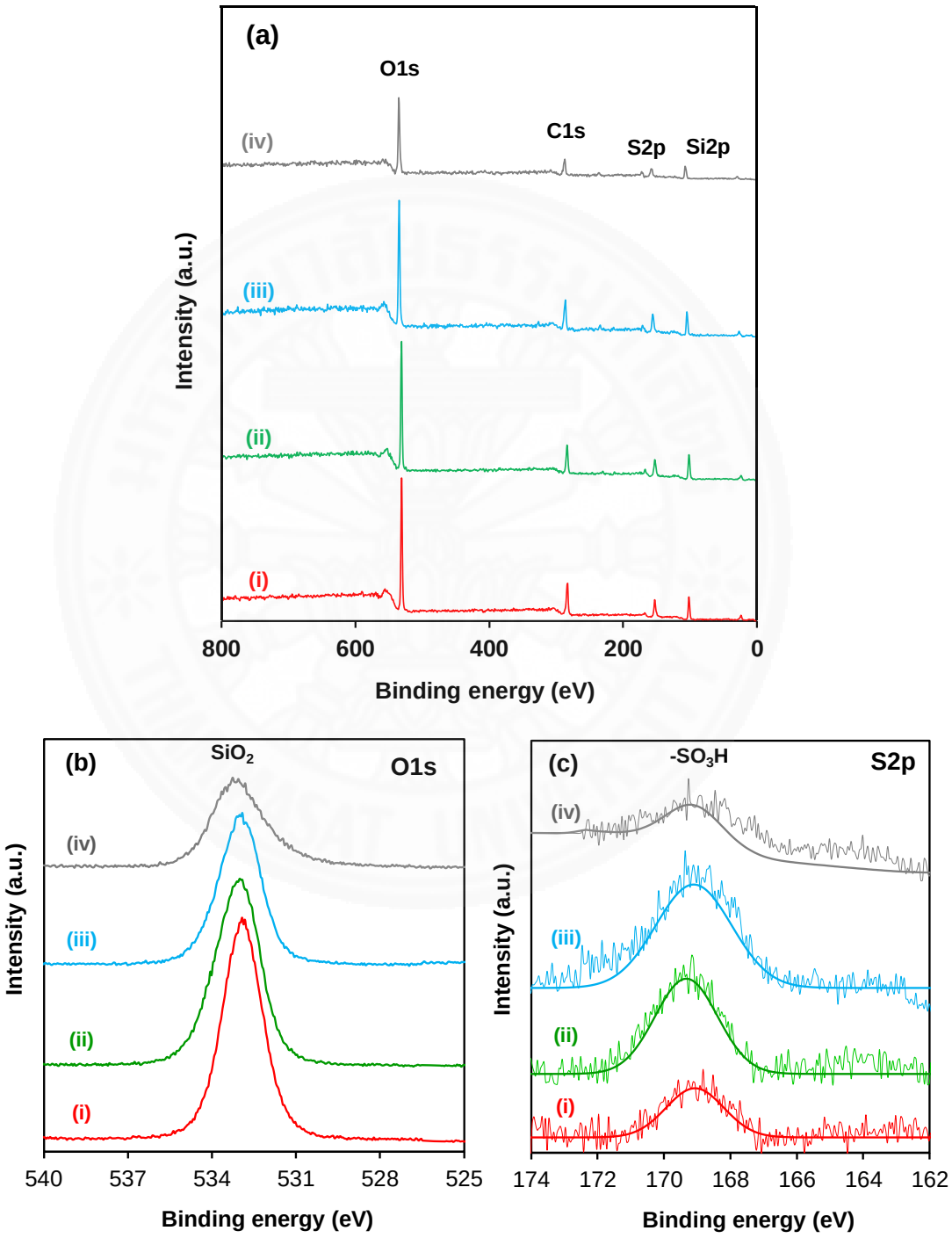

Ref. code: 25625909320250YIN

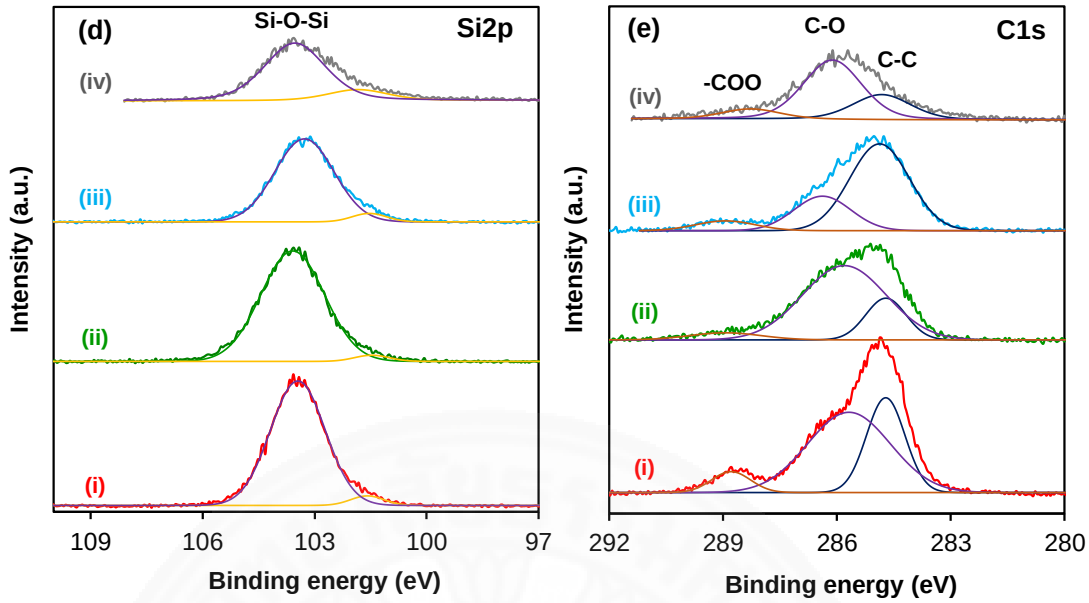

Figure 3.4 XPS spectral of (a) Wide scan, (b) O1s, (c) S2p, (d) Si2p and (e) C1s of (i) 0.1-KIT-6-SO_3H, (ii) 0.2-KIT-6-SO_3H, (iii) 0.3-KIT-6-SO_3H catalyst and (iv) used 0.3-KIT-6-SO_3H catalysts after 3rd cycle.

3.5.1.4 Ammonia temperature programmed desorption (NH_3-TPD)

NH_3-TPD profiles shows in **Figure 3.5**. In order to prevent the decomposition of sulfonic acid functionalized molecules, the measurement of NH_3 desorption was limited at 400 °C (Hafizi, Najafi-Chermahini, Saraji, & Mohammadnezhad, 2016). The decomposition of the functionalized group was proved by thermogravimetric analysis as shown in **Figure 3.6**. From NH_3-TPD profiles, an individual peak appeared at 130 °C in the KIT-6 indicating the weak acid sites of silanol group (Si-OH) while two distinct peaks were observed on KIT-6-SO_3H catalysts. The first peak was similar to the KIT-6 but this peak on 0.3-KIT-6-SO_3H has appeared at higher temperature of 143 °C due to the effect of sulfonic acid (Román-Aguirre, Gochi, Sánchez, de la Torre, & Aguilar-Elguezabal, 2008). The second peak was presented at higher temperature of 260 – 300 °C indicating the sulfonic acid sites. When the concentration of sulfonic acid increased, the position of NH_3-TPD peaks was shifted to higher temperatures because of strong charge-charge interaction between the sulfonic acid site and NH_3 molecule. The integration area of desorption peaks was related with the acidity as shown in **Table 3.4**. The acidity increased with increasing the sulfonic acid concentration. An increase

Ref. code: 25625909320250YIN

of MPMDS:TEOS molar ratio from 0.1 to 0.3 had resulted in an increase the acidity from 0.69 mmol/g to 1.53 mmol/g. In this study, it is well known that the performance of catalysts, as well as the accessibility of the reactant, has been affected by acidity (Tran et al., 2019).

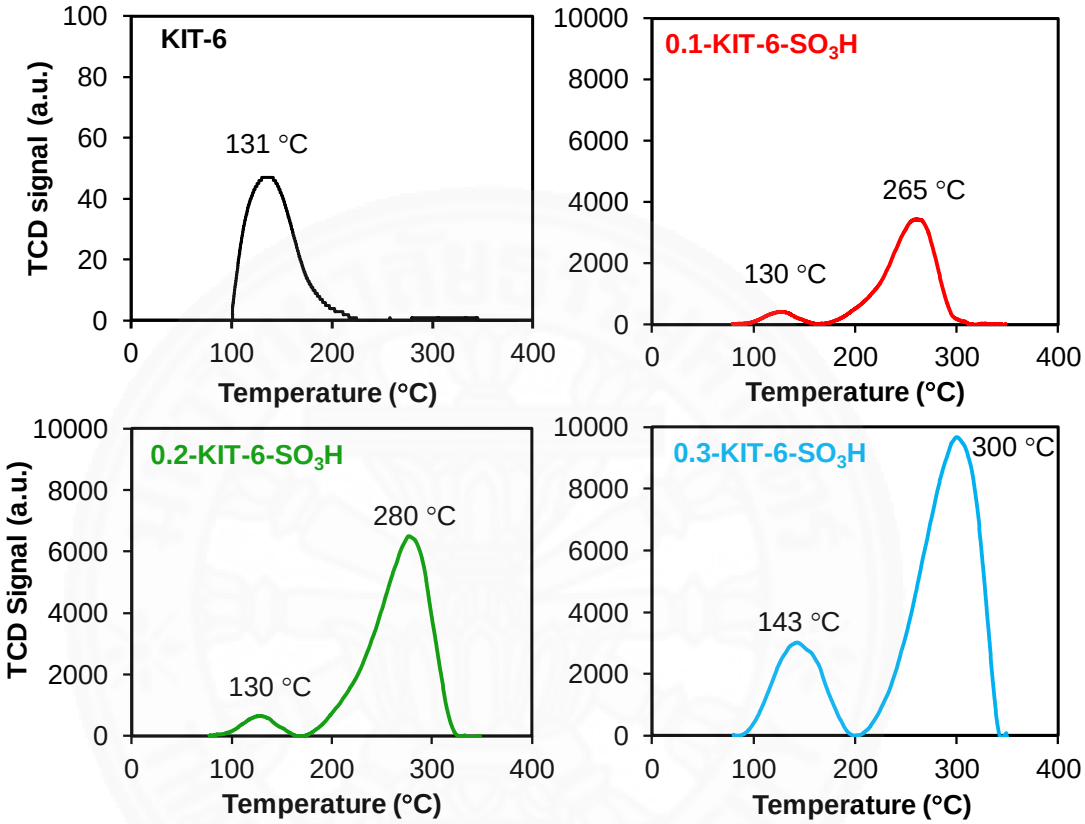

Figure 3.5 NH_3-TPD profile of KIT-6 and x-KIT-6-SO_3H catalysts

Ref. code: 25625909320250YIN

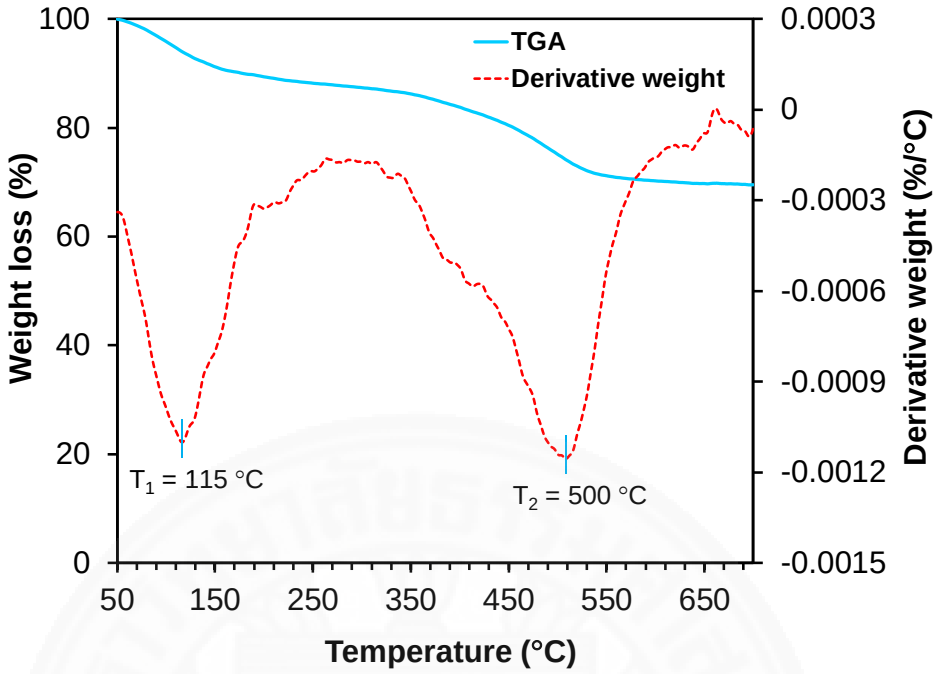

Figure 3.6 Thermogravimetric analysis of 0.3-KIT-6-SO_3H catalysts

3.5.2 Catalytic activity in the esterification of fusel oil

3.5.2.1 Effect of MPMDS:TEOS molar ratio

The catalytic activities of the catalysts in term of isoamyl acetate yield and turnover frequency (TOF) were investigated as shown in **Figure 3.7**. The isoamyl acetate yield was depended on the ratio of MPMDS:TEOS. When the ratio was increased from 0.1 to 0.3, the increase in the isoamyl acetate yield was observed from 86.64% to 95.27% and the mechanism of acid-catalyzed isoamyl acetate is well investigated (Corregidor et al., 2020). The isoamyl acetate yield was strongly depended on the number of acid sites because these sites initiated the formation of electrophilic carbonyl carbon to react with nucleophilic isoamyl alcohol yielding isoamyl acetate. Therefore, the 0.3-KIT-6-SO_3H gave the highest isoamyl acetate yield because of the highest acidity. Whereas, the highest TOF was presented in 0.1-KIT-6-SO_3H catalyst. The increase in ratio of MPMDS:TEOS reduced the TOF number. The higher TOF indicates that more isoamyl acetate could be produced per active site (Trejda, Nurwita, & Kryszak, 2019). The higher ratio of MPMDS:TEOS containing higher acid density resulted as a barrier against the approach of reactant to the active site from neighboring active

Ref. code: 25625909320250YIN

site. As mention above, the 0.3-KIT-6-SO_3H catalyst performed the highest yield of isoamyl acetate which was selected as an optimized catalyst for further study.

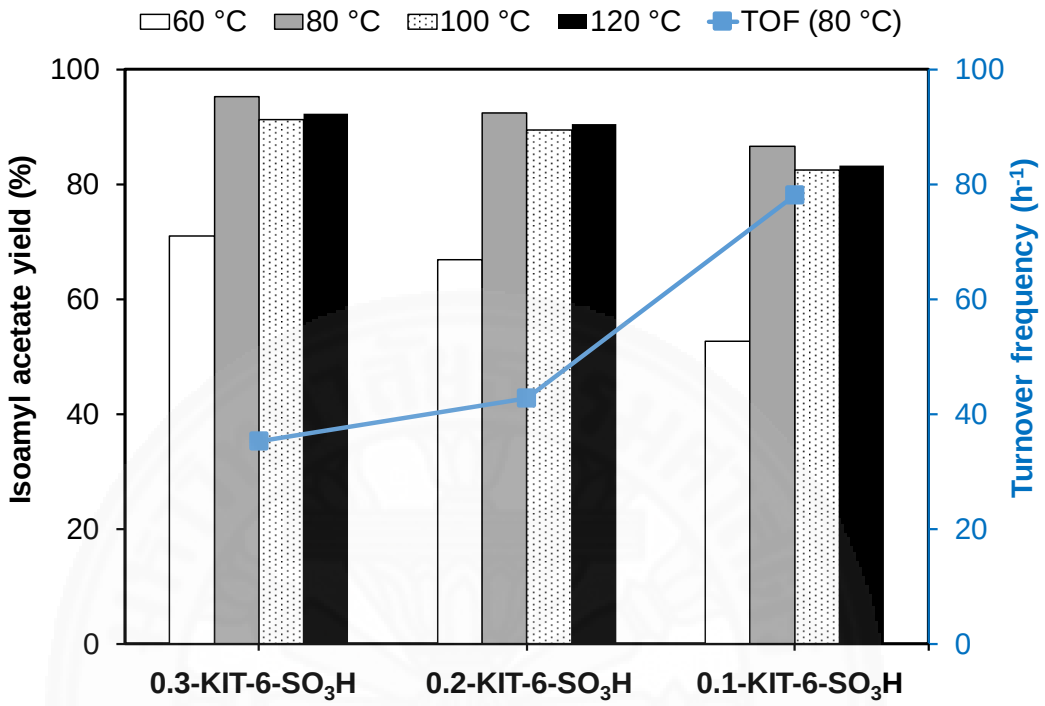

Figure 3.7 Catalytic activity in the fusel oil esterification process under different x-KIT-6-SO_3H catalysts for 3 h and 5 wt.% of catalyst loading

3.5.2.2 Effect of reaction time and reaction temperature

The 0.3-KIT-6-SO_3H catalyst was chosen to study the effect of reaction time and reaction temperature. The isoamyl acetate yield was increased continuously with increasing reaction temperature. The highest isoamyl acetate yield was observed at the reaction temperature of 80 °C. The isoamyl acetate yield would be decreased at the reaction temperature over 80 °C due to the vaporization of acetic acid leading (Ni, Li, Wang, Wang, & Gao, 2019). The result shows in **Figure 3.8**. As reaction time increase, the yield of isoamyl acetate was initial increase and reach equilibrium at 3 h. At longer reaction time the isoamyl acetate yield was slightly decreased due to the accessibility of reactant to active site was controlled by diffusion effect and the number of unoccupied sites. In this investigation, the optimized reaction condition using the catalyst was identified at 80 °C in 3 h.

Ref. code: 25625909320250YIN

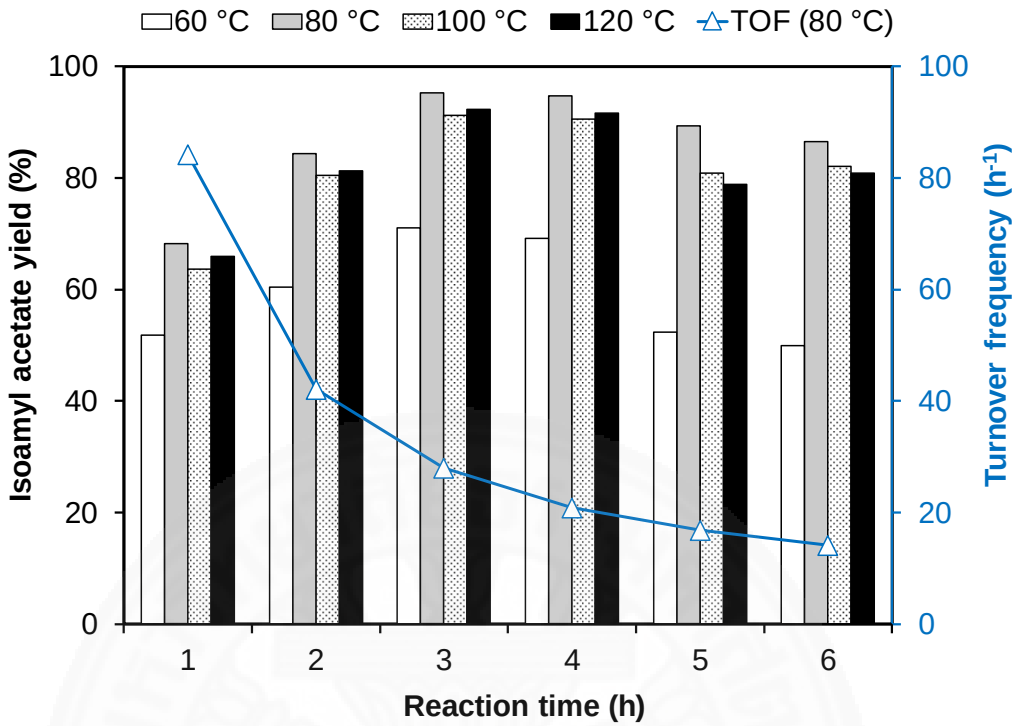

Figure 3.8 Catalytic activity of fusel oil esterification of different reaction temperatures and reaction times at 5 wt.% of catalyst loading and 2:1 molar ratio between acetic acid/fusel oil

3.5.2.3 Effect of acetic acid:fusel oil molar ratio

Isoamyl acetate yield remarkable increased when the acetic acid:fusel oil ratio was increased from 1:1 to 2:1 as shown in **Figure 3.9 (a)**. However, the stoichiometry number of esterification reaction requires a 1:1. According reversible reaction, the reaction favor to produce isoamyl acetate with excess of acetic acid. Hence, the unreacted acetic acid was remained in the reaction mixture at the end of reaction which could be recovered by evaporation for economic reasons. At the ratio was greater than 2:1, the isoamyl acetate yield gradually decreased because of the mixing problem. Therefore, the optimal molar ratio for the esterification reaction between acetic acid and fusel oil was 2:1.

3.5.2.4 Effect of catalyst loading

The effect of catalyst loading on isoamyl acetate yield was shown in **Figure 3.9 (b).** The yield of isoamyl acetate also increased with increasing the catalyst loading indicating that more available active sites to enhance the efficiency

Ref. code: 25625909320250YIN

of esterification reaction. However, the isoamyl acetate yield decreased with increase catalyst loading to 7 wt.% due to the non-homogeneity of reaction mixture (Ni et al., 2019). Poorly mixing at highly viscous slurries reduced the mass transfer between solid-liquid phases in the system. Moreover, at high catalyst loading level, acetic anhydride was produced from some acetic acid which suppressed the isoamyl acetate formation (Yang, Zhou, Zhang, Li, & Chen, 2010). Nevertheless, under highly acidic conditions, the formation of water also increased leading to catalyst deactivation. The optimal catalyst loading for esterification reaction between acetic acid and fusel oil was 5 wt.%. Besides, the mechanism of the synthesis reaction of isoamyl acetate by the esterification route was proposed (Yang et al., 2010). At the initial stage, the protonated C=O group of acetic acid was formed by acid catalyst. In the next state, this protonated group reacted with the isoamyl alcohol leading to the tetrahedral intermediate formation. Also, in this stage, the second intermediate is formed from a proton loss of one oxygen atom and a protonated ester formed by the removing of water. A final stage, isoamyl acetate product was formed by proton transfer to a molecule of acetic or water. (**Figure 3.1**)

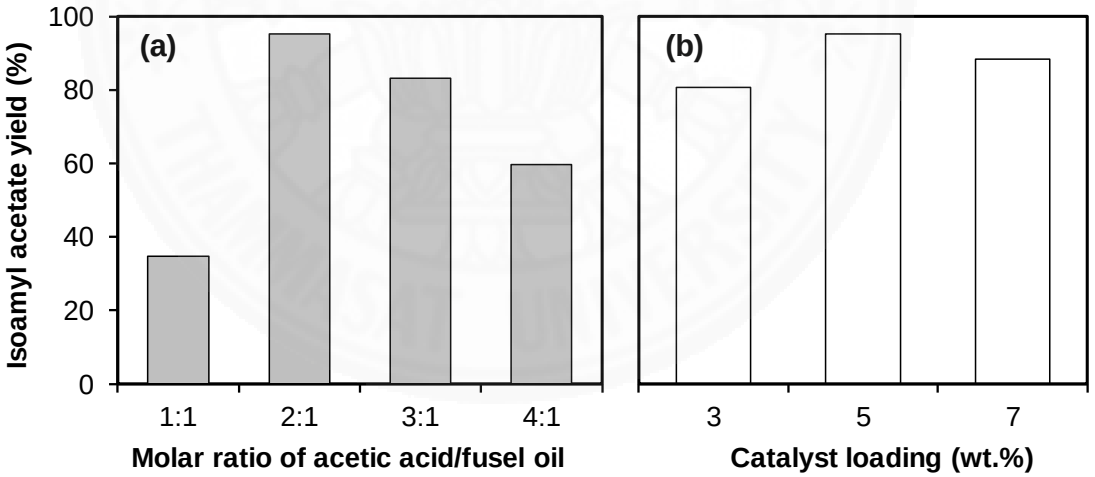

Figure 3.9 Catalytic activity of fusel oil esterification of different (a) molar ratio (acetic acid/fusel oil) and (b) catalyst loading at 80 °C - 3 h

3.5.2.5 Catalyst reusability and comparison with commercial catalysts

The reusability of the catalyst, 0.3-KIT-6-SO_3H was carried out under the optimized conditions at 80 °C in 3 h, with the molar ratio of acetic acid:fusel oil was 2:1 and 5 wt.% of catalyst loading. Besides, the catalyst was regenerated by re-oxidized with H_2O_2 after washed by acetone and dried at 70 °C. The reusability of

Ref. code: 25625909320250YIN

catalyst with and without regeneration were compared as shown in **Figure 3.10**. In the reusability study of catalyst without regeneration, the isoamyl acetate yield decreased by 7%, 9% and 11% over 1st, 2nd and 3rd cycles, respectively and the yield were remarkably decreased by 24% as further cycles due to the impurities in fusel oil. This deduction of active sites was verified by XPS spectra (**Figure 3.4**). On the other hand, the catalyst with re-oxidized was not significant reduction of the isoamyl acetate yield over the three-cycle as shown in **Figure 3.10 (b)**. The isoamyl acetate yield always was obtained over 92.0%. After reaction, the white color of the fresh catalyst was turned to brown and turned to white again after re-oxidation (**Figure 3.11**). The catalyst used in this study demonstrates an excellent activity at the mild condition with the reaction temperature of 80 ℃ for 3 h to obtain 95.25% isoamyl acetate yield. The catalyst showing a very good performance even though the fusel oil did not treat prior to use. Therefore, the KIT-6-SO_3H catalyst was a promising candidate for isoamyl acetate production through esterification reaction of fusel oil with acetic acid.

In comparison with the commercial catalyst, a homogeneous catalyst of H_2SO_4 and a heterogeneous catalyst of Amberlyst-35, the performance of KIT-6-SO_3H catalyst was conducted at 80 ℃ for 3 h as summarized in **Figure 3.10 (a)**. The KIT-6-SO_3H catalyst gave the highest yield of isoamyl acetate because of its large surface area and high acidity. Moreover, the 3D structure of the catalyst enhances a reaction rate leading to the fast equilibrium of the reaction within 3 h. Despite higher in acidity, the conventional heterogeneous catalyst such as Amberlyst-35 (with acidity >5.00 mmol/g) demonstrated a lower catalytic activity compare to the KIT-6-SO_3H catalyst at the same reaction condition. The high acidity of Amberyst-35 had promoted the side-product formation and the strong hydrophilic structure to attract hydrophilic molecules like water and absorb onto its surface leading to blocking active site as well as the deactivation by leaching of active site. The excellent performance of KIT-6-SO_3H catalyst could be explained by the presence of both methyl and sulfonic group. The polar molecules like H_2O were well repelled by methyl groups leading to the adsorption of these molecules was partially inhibited to active sites and catalyst stability enhancement (Teo & Saha, 2004).

Ref. code: 25625909320250YIN

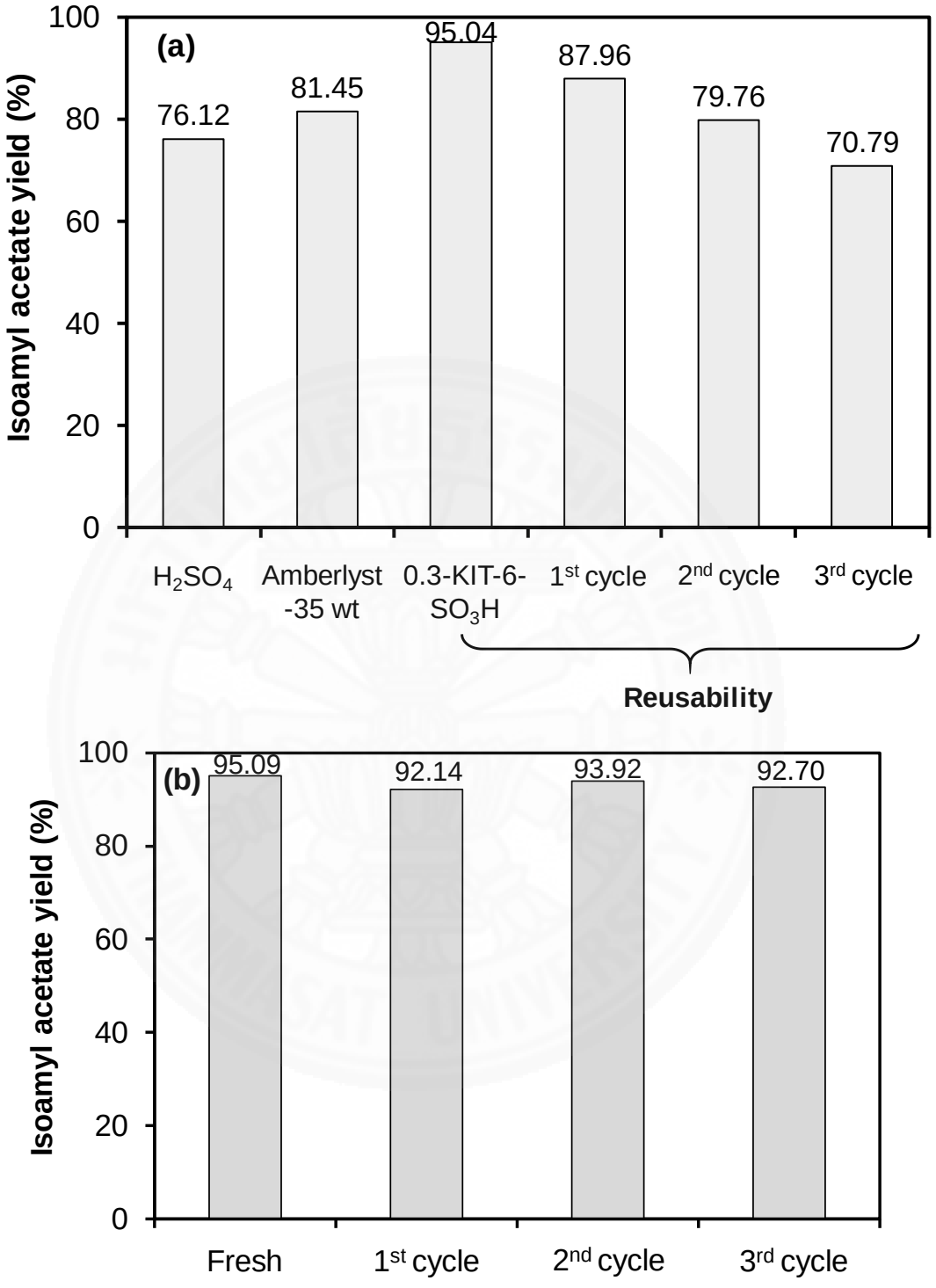

Figure 3.10 Catalytic activity of fusel oil esterification at 80 °C – 3 h – 5 wt.% catalyst loading, 2:1 molar ratio of acetic acid to fusel oil of (a) commercial catalyst (H_2SO_4, Amberlyst-35) and reused of 0.3-KIT-6-SO_3H catalyst without regeneration and (b) reused of 0.3-KIT-6-SO_3H catalyst was regenerated with H_2O_2

Ref. code: 25625909320250YIN

0.3-KIT-6-SO_3H (Fresh) **After reaction** **After treatment with H_2O_2**

Figure 3.11 0.3-KIT-6-SO_3H catalyst before and after regeneration

3.6 Conclusions

The isoamyl acetate production from fusel oil and acetic acid via the esterification route was acquired with high conversion using the KIT-6-SO_3H catalyst. The catalyst was prepared by the co-condensation method with the difference molar ratio of MPMDS:TEOS. The number of acid site, as well as the accessibility of reactants strongly affected the catalyst performance. In conclusion, the 0.3-KIT-6-SO_3H catalyst performed the highest isoamyl acetate yield, while 0.1-KIT-6-SO_3H gave the highest TOF number. The accessibility of reactant to active site was hindered by increasing the number of acid sites. The optimal reaction condition was reaction temperature at 80 ℃ for 3 h, 5 wt.% of catalyst loading and molar ratio of acetic acid:fusel oil as 2:1. In comparison to commercial catalysts, the KIT-6-SO_3H catalyst showed higher efficiency than Amberlyst-35 catalyst.

Ref. code: 25625909320250YIN

3.7 References

Afshar, S., Sadehvand, M., Azad, A., Dekamin, M. G., Jalali-Heravi, M., Mollahosseini, A., . . . Tadjarodi, A. (2015). Optimization of catalytic activity of sulfated titania for efficient synthesis of isoamyl acetate by response surface methodology. *Monatshefte für Chemie - Chemical Monthly, 146* (12), 1949-1957. doi:10.1007/s00706-015-1533-5

AlNouss, A., McKay, G., & Al-Ansari, T. (2019). A techno-economic-environmental study evaluating the potential of oxygen-steam biomass gasification for the generation of value-added products. *Energy Conversion and Management, 196*, 664-676. doi:https://doi.org/10.1016/j.enconman.2019.06.019

Bansode, S. R., & Rathod, V. K. (2018). Enzymatic sythesis of Isoamyl butyrate under microwave irradiation. *Chemical Engineering and Processing - Process Intensification, 129*, 71-76. doi:https://doi.org/10.1016/j.cep.2018.04.015

Bi, F., Ali, A., Iqbal, S., Arman, M., & Ul-Hassan, M. J. J. C. S. P. (2008). Chemical Esterification of Fusel Oil Alcohol for the Production of Flavor and Fragrance Esters. *30*, 919-923.

Corregidor, P. F., Acosta, D. E., Gonzo, E. E., & Destéfanis, H. A. (2020). Isoamyl acetate preparation from reaction of vinyl acetate and isoamyl alcohol catalyzed by H-ZSM-5 zeolite: a kinetic study. *Molecular Catalysis, 481*, 100611. doi:https://doi.org/10.1016/j.mcat.2018.06.009

Dasan, Y. K., Lam, M. K., Yusup, S., Lim, J. W., & Lee, K. T. (2019). Life cycle evaluation of microalgae biofuels production: Effect of cultivation system on energy, carbon emission and cost balance analysis. *Science of The Total Environment, 688*, 112-128. doi:https://doi.org/10.1016/j.scitotenv.2019.06.181

Feygroupchem. (January 8, 2014). Banana (Musa acuminata, Musa balbisiana). Retrieved from website: https://chempics.wordpress.com/2014/01/08/banana-musa-acuminata-musa-balbisiana/

Gebremariam, S. N., & Marchetti, J. M. (2018). Economics of biodiesel production: Review. *Energy Conversion and Management, 168*, 74-84. doi:https://doi.org/10.1016/j.enconman.2018.05.002

Hafizi, H., Najafi Chermahini, A., Saraji, M., & Mohammadnezhad, G. (2016). The catalytic conversion of fructose into 5-hydroxymethylfurfural over acid-functionalized KIT-6, an ordered mesoporous silica. *Chemical Engineering Journal, 294*, 380-388.

Ref. code: 25625909320250YIN

doi:https://doi.org/10.1016/j.cej.2016.02.082

Hari Krishna, S., Divakar, S., Prapulla, S. G., & Karanth, N. G. (2001). Enzymatic synthesis of isoamyl acetate using immobilized lipase from Rhizomucor miehei. *Journal of Biotechnology, 87* (3), 193-201. doi:https://doi.org/10.1016/S0168-1656(00)00432-6

Hua, D., Li, P., Wu, Y., Chen, Y., Yang, M., Dang, J., . . . Sun, X. Y. (2013). Preparation of solid acid catalyst packing AAO/SBA-15-SO_3H and application for dehydration of xylose to furfural. *Journal of Industrial and Engineering Chemistry, 19* (4), 1395-1399. doi:https://doi.org/10.1016/j.jiec.2013.01.002

Islam, M. M., Bhanja, P., Halder, M., Das, A., Bhaumik, A., & Islam, S. M. (2019). Chiral Cr(III)-salen complex embedded over sulfonic acid functionalized mesoporous SBA-15 material as an efficient catalyst for the asymmetric Henry reaction. *Molecular Catalysis, 475*, 110489. doi:https://doi.org/10.1016/j.mcat.2019.110489

Janampelli, S., & Darbha, S. (2018). Effect of support on the catalytic activity of WO_x promoted Pt in green diesel production. *Molecular Catalysis, 451*, 125-134. doi:https://doi.org/10.1016/j.mcat.2017.11.029

Jiang, Z., Xu, J., Zeng, Z., Xue, W., & Li, S. (2018). Kinetics of the esterification between lactic acid and isoamyl alcohol in the presence of silica gel-supported sodium hydrogen sulphate. *The Canadian Journal of Chemical Engineering, 96* (9), 1972-1978. doi:10.1002/cjce.23127

Kaka khel, T., Mäki-Arvela, P., Azkaar, M., Vajglová, Z., Aho, A., Hemming, J., . . . Murzin, D. Y. (2019). Hexadecane hydrocracking for production of jet fuels from renewable diesel over proton and metal modified H-Beta zeolites. *Molecular Catalysis, 476*, 110515. doi:https://doi.org/10.1016/j.mcat.2019.110515

Karnjanakom, S., Guan, G., Asep, B., Hao, X., Kongparakul, S., Samart, C., & Abudula, A. (2016). Catalytic upgrading of bio-oil over Cu/MCM-41 and Cu/KIT-6 prepared by β-cyclodextrin-assisted coimpregnation method. *The Journal of Physical Chemistry C, 120* (6), 3396-3407. doi:10.1021/acs.jpcc.5b11840

Karnjanakom, S., Maneechakr, P., Samart, C., & Guan, G. (2019). A facile way for sugar transformation catalyzed by carbon-based Lewis-Brønsted solid acid. *Molecular Catalysis, 479*, 110632. doi:https://doi.org/10.1016/j.mcat.2019.110632

Ref. code: 25625909320250YIN

Kumar, A., & Srivastava, R. (2019). $FeVO_4$ decorated $-SO_3H$ functionalized polyaniline for direct conversion of sucrose to 2,5-diformylfuran & 5-ethoxymethylfurfural and selective oxidation reaction. *Molecular Catalysis, 465*, 68-79. doi:https://doi.org/10.1016/j.mcat.2018.12.017

Li, J., Zhou, H., Sun, L., & Zhang, N. (2019). Design and control of different pressure thermally coupled reactive distillation for synthesis of isoamyl acetate. *Chemical Engineering and Processing - Process Intensification, 139*, 51-67. doi:https://doi.org/10.1016/j.cep.2019.03.014

Ni, Z.H., Li, F.S., Wang, H., Wang, S., & Gao, S.Y. (2019). Catalytic esterification, kinetics, and cold flow properties of isobutyl palmitate. *Fuel, 254*, 115368. doi:https://doi.org/10.1016/j.fuel.2019.04.125

Nowicki, J., Jaroszewska, K., Nowakowska-Bogdan, E., Szmatoła, M., & Iłowska, J. (2018). Synthesis of 2,2,4-trimethyl-1,2-H-dihydroquinoline (TMQ) over selected organosulfonic acid silica catalysts: Selectivity aspects. *Molecular Catalysis, 454*, 94-103. doi:https://doi.org/10.1016/j.mcat.2018.05.016

Nyari, N., Paulazzi, A., Zamadei, R., Steffens, C., Zabot, G. L., Tres, M. V., . . . Dallago, R. M. (2018). Synthesis of isoamyl acetate by ultrasonic system using Candida antarctica lipase B immobilized in polyurethane. *Journal of Food Process Engineering, 41* (6), e12812. doi:10.1111/jfpe.12812

Osorio-Viana, W., Duque-Bernal, M., Fontalvo, J., Dobrosz-Gómez, I., & Gómez-García, M. Á. (2013). Kinetic study on the catalytic esterification of acetic acid with isoamyl alcohol over Amberlite IR-120. *Chemical Engineering Science, 101*, 755-763. doi:https://doi.org/10.1016/j.ces.2013.07.009

Pang, X.Y., Lv, P., Yang, Y.S., Ren, H.L., & Gong, F. J. J. O. C. (2008). Estrification of acetic acid with isoamyl alcohol over expandable graphite catalyst. *5* (1), 149-154.

Pereira, F. S., Pereira, L. J., Crédito, D. F. A., Girão, L. H. V., Idehara, A. H. S., & González, E. R. P. (2015). Cycling of waste fusel alcohols from sugar cane industries using supercritical carbon dioxide. *RSC Advances, 5* (99), 81515-81522. doi:10.1039/C5RA16346C

Ponnuru, K., Manayil, J. C., Cho, H. J., Osatiashtiani, A., Fan, W., Wilson, K., & Jentoft, F. C. (2018). Tuning solid catalysts to control regioselectivity in cross aldol condensations

Ref. code: 25625909320250YIN

with unsymmetrical ketones for biomass conversion. *Molecular Catalysis, 458*, 247-260. doi:https://doi.org/10.1016/j.mcat.2017.11.005

Ramdani, W. G., Karam, A., De Oliveira Vigier, K., Rio, S., Ponchel, A., & Jérôme, F. (2019). Catalytic glycosylation of glucose with alkyl alcohols over sulfonated mesoporous carbons. *Molecular Catalysis, 468*, 125-129. doi:https://doi.org/10.1016/j.mcat.2019.02.016

Román-Aguirre, M., Gochi, Y. P., Sánchez, A. R., de la Torre, L., & Aguilar-Elguezabal, A. (2008). Synthesis of camphene from α-pinene using SO_3^{2-} functionalized MCM-41 as catalyst. *Applied Catalysis A: General, 334* (1), 59-64. doi:https://doi.org/10.1016/j.apcata.2007.09.031

Sánchez, C. A., Sánchez, O. A., Orjuela, A., Gil, I. D., & Rodríguez, G. (2017). Vapor–liquid equilibrium for binary mixtures of acetates in the direct esterification of fusel oil. *Journal of Chemical & Engineering Data, 62* (1), 11-19. doi:10.1021/acs.jced.6b00221

Song, D., An, S., Lu, B., Guo, Y., & Leng, J. (2015). Arylsulfonic acid functionalized hollow mesoporous carbon spheres for efficient conversion of levulinic acid or furfuryl alcohol to ethyl levulinate. *Applied Catalysis B: Environmental, 179*, 445-457. doi:https://doi.org/10.1016/j.apcatb.2015.05.047

Teo, H. T. R., & Saha, B. (2004). Heterogeneous catalysed esterification of acetic acid with isoamyl alcohol: kinetic studies. *Journal of Catalysis, 228* (1), 174-182. doi:https://doi.org/10.1016/j.jcat.2004.08.018

Tran, T. T. V., Kongparakul, S., Karnjanakom, S., Reubroycharoen, P., Guan, G., Chanlek, N., & Samart, C. (2019). Highly productive xylose dehydration using a sulfonic acid functionalized KIT-6 catalyst. *Fuel, 236*, 1156-1163. doi:https://doi.org/10.1016/j.fuel.2018.09.089

Trejda, M., Nurwita, A., & Kryszak, D. (2019). Synthesis of solid acid catalysts for esterification with the assistance of elevated pressure. *Microporous and Mesoporous Materials, 278*, 115-120. doi:https://doi.org/10.1016/j.micromeso.2018.11.009

Vilas Bôas, R. N., Ceron, A. A., Bento, H. B. S., & de Castro, H. F. (2018). Application of an immobilized Rhizopus oryzae lipase to batch and continuous ester synthesis with a mixture of a lauric acid and fusel oil. *Biomass and Bioenergy, 119*, 61-68. doi:https://doi.org/10.1016/j.biombioe.2018.09.011

Ref. code: 25625909320250YIN

Wang, L. X., Liu, S. H., Yuan, H., & Guo, L. L. (2013). Catalytic synthesis of isoamyl acetate by ion exchange resin-supported $(NH_4)_6[MnMo_9O_{32}].8H_2O$ with Waugh structure. *Paper presented at the Advanced Materials Research*.

Wang, Y., Wang, D., Tan, M., Jiang, B., Zheng, J., Tsubaki, N., & Wu, M. (2015). Monodispersed hollow SO_3H-functionalized carbon/silica as efficient solid acid catalyst for esterification of oleic acid *ACS Applied Materials & Interfaces, 7* (48), 26767-26775. doi:10.1021/acsami.5b08797

Wu, L., Wang, Y., Zheng, L., Wang, P., & Han, X. (2019). Techno-economic analysis of bio-oil co-processing with vacuum gas oil to transportation fuels in an existing fluid catalytic cracker. *Energy Conversion and Management, 197*, 111901. doi:https://doi.org/10.1016/j.enconman.2019.111901

Xue, M., Zhu, M.H., Zhong, C.J., Li, Y.Q., Hu, N., Kumakiri, I., . . . Kita, H. (2019). Preparation of Isoamyl Acetate by High Performance ZSM-5 Zeolite Membrane. *Journal of Chemical Engineering of Japan, 52* (1), 69-74. doi:10.1252/jcej.17we352

Yang, Z., Zhou, C., Zhang, W., Li, H., & Chen, M. (2010). β-MnO_2 nanorods: A new and efficient catalyst for isoamyl acetate synthesis. *Colloids and Surfaces A: Physicochemical and Engineering Aspects, 356* (1), 134-139. doi:https://doi.org/10.1016/j.colsurfa.2010.01.007

Zare, M., Golmakani, M.T., & Niakousari, M. (2019). Lipase synthesis of isoamyl acetate using different acyl donors: Comparison of novel esterification techniques. *LWT, 101*, 214-219. doi:https://doi.org/10.1016/j.lwt.2018.10.098

CHAPTER 4
GLYCEROL ETHERIFICATION USING A SULFONIC ACID FUNCTIONALIZED KIT-6 CATALYST FOR FUEL ADDITIVE

4.1 Introduction

Currently, it is well known that as economic growth, the demand for energy is also in the same trend rising concerns about environmental problems such as global warming and environmental pollution. However, traditional energy or non-renewable energy resources are limited. In this circumstance, the development of bioenergy is accelerated with sustainable technologies that are based on renewable resources. In various bioenergy technologies, biodiesel is one of the most used liquid fuels in the market (Cornejo, Barrio, Campoy, Lázaro, & Navarrete, 2017). Biodiesel is synthesized from animal fats, vegetable oils and waste cooking oil which are non-toxic, biodegradable and renewable resources (Bozbas, 2008; Dominguez, Romero, & Santos, 2019). However, a byproduct of biodiesel production, glycerol, is increased as the demand of biodiesel. It is about 11kg of glycerol is produced with 100kg of biodiesel in a typical transesterification reaction (Agency & Laboratory, 2009; Byrnett et al., 2009; Cornejo et al., 2017). Glycerol could not present in biodiesel due to its characteristics of poor thermal stability, high viscosity and low solubility. Thus, it would be interesting to create value-added to the glycerol which could enhance the economy of the process and avoid the abundance of glycerol in the market (Cornejo et al., 2017). There are several industrial processes use glycerol as raw material such as catalytic oxidation, dehydration, acetylation and ammoxidation to produce citric acid, lactic acid, acrolein, hydrogen, ethanol, etc. (Kong, Aroua, & Daud, 2016; Luo, Ge, Cui, & Li, 2016). The glycerol carbonate, green solvent for cosmetics and medicine could be produced using the catalytic oxidative carbonylation of glycerol (Gabriele et al., 2011). One of a process of increasing value of glycerol that stands out from other glycerol valorization serving for energy industry, etherification is converting of glycerol to glycerol ether for higher value fuel-oxygenates (Melero, Vicente, Paniagua, Morales, & Muñoz, 2012) which is considered

Ref. code: 25625909320250YIN

as additives in liquid fuels (Demirbas, 2007; Pico, Romero, Rodríguez, & Santos, 2012). The product of glycerol etherification as fuel additive could enhance the combustion efficiency leading to the reduction of pollutant emission including particulate matter, hydrocarbons, carbon monoxide and unregulated aldehydes (Frusteri et al., 2009). Furthermore, the ethers can also act as cold flow improver (Melero et al., 2008). The etherification of glycerol could be obtained by acid catalyst either homogeneous or heterogeneous systems (Lee, Seung, Filimonov, & Kim, 2011; Lee, Seung, Jung, Kim, & Filimonov, 2010; Pico et al., 2012). However, in the concerning environmental pollutions, heterogeneous catalysts are preferable. Solid catalysts have been studied such as Amberlyst-15 (Frusteri et al., 2009; Klepáþová, Mravec, Hajekova, & Bajus, 2003), Amberlyst-35 (Klepáčová, Mravec, Kaszonyi, & Bajus, 2007), Nafion®, H-Y & H-β zeolite (Klepáčová et al., 2007; Samoilov, Ramazanov, Nekhaev, & Maksimov, 2016), propyl sulfonic acid functionalized SBA-15 mesoporous catalyst (Hermida, Abdullah, & Mohamed, 2011), sulfonic acid-modified mesostructured silicas (Di Serio, Casale, Tesser, & Santacesaria, 2010). (Gu, Azzouzi, Pouilloux, Jérôme, & Barrault, 2008) studied the etherification reaction between glycerol and different alcohols (alkyl alcohols, olefins and dibenzyl alcohol) under acid-functionalized silica catalyst. The yields of mono and di glycerol ethers were reached 61 and 96%, respectively due to highly acidity. (Melero et al., 2008) studied the etherification of glycerol and isobutylene using propyl sulfonic acid functionalized mesoporous silica (Pr-SO_3H-SBA-15) catalyst at 75 °C, 5 wt.% catalyst loading and reaction time for 4 h. The catalyst presented highly selective toward di- and tri- glycerol tert-butyl ethers (GTBE) up to 92%. The acid strength, acidity, surface area and porosity of catalyst were the key factors which affected the glycerol conversion (Nandiwale, Patil, & Bokade, 2014). Hence, the more attractive in sulfonic acid mesoporous silica and its rapid development because it is not only high surface area, high acid property, adjustable in porosity but high thermal and chemical stabilities also present.

On the other hand, the etherification reactions of glycerol could be conducted with various reactants such as olefins (mainly isobutylene) and alcohol (mainly tert-butyl alcohol). The tert-butyl alcohol could be also used as reaction solvent. Hence, the reactive phase could be a single phase but the disadvantage is

Ref. code: 25625909320250YIN

low conversion of glycerol (Pico et al., 2012). However, even that tert-butyl alcohol is mainly used alcohol in etherification of glycerol, n-butanol has recently found to be an alternative due to the similar performance of both alcohols (Nandiwale et al., 2014). n-butanol could act as a dual function of both reactant and solvent in the reaction system which simplified the technology problem and avoids the drawbacks of a complex three-phase system like mass transfer phenomena (Frusteri et al., 2009; Klepáčová, Mravec, & Bajus, 2005). The glycerol etherification with n-butanol and mechanism of this process is shown in **Figure 4.1.**

In this chapter, the mesoporous silica KIT-6 functionalized with methyl propyl sulfonic acid catalyst would be prepared and applied for etherification reaction between n-butanol and glycerol. This catalyst was expected to improve reaction rate due to its three-dimensional porous structure and high acidity. The effect of reaction condition on the catalytic performance was investigated.

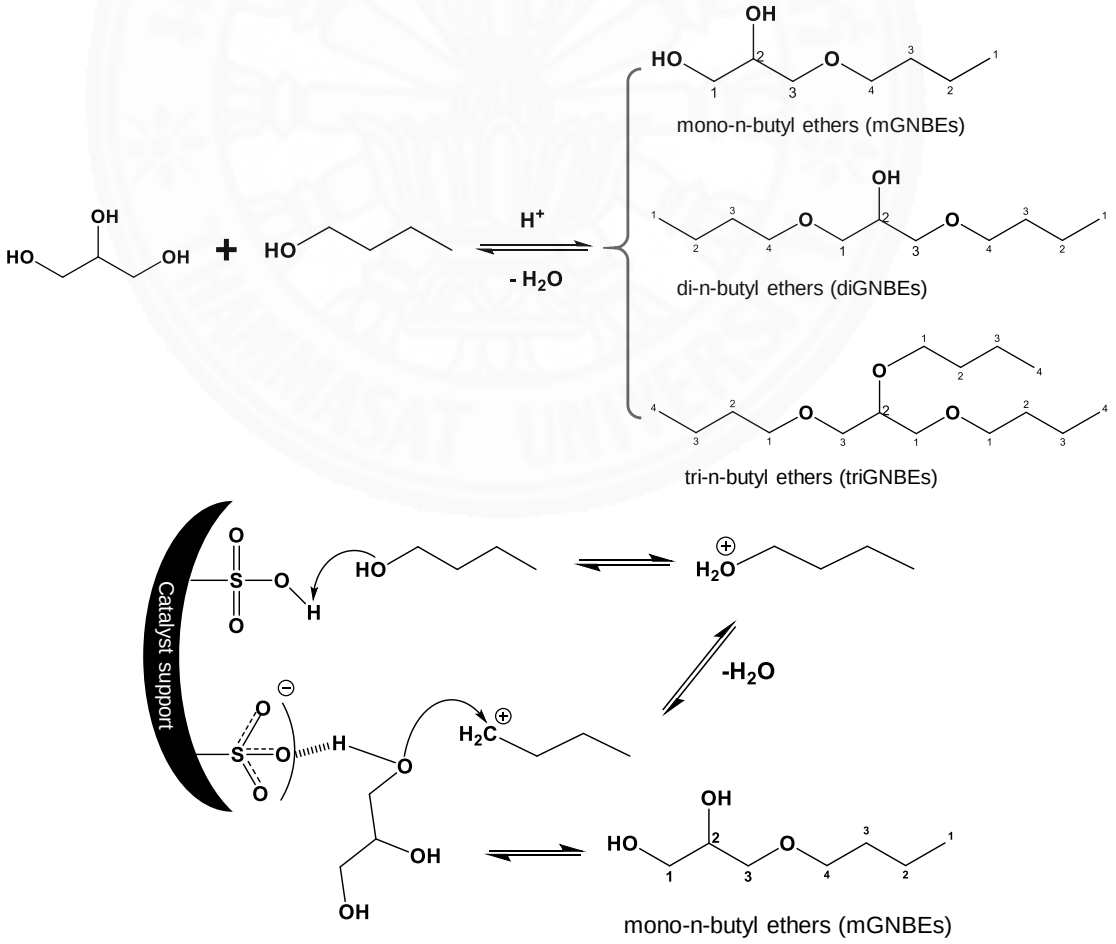

Figure 4.1 Rection mechanism of glycerol etherification with acid catalyst

Ref. code: 25625909320250YIN

4.2 Review of literature

(Liu et al., 2013) reported the use of the homogeneous catalyst including Lewis acid and Brønsted acid for glycerol etherification with n-butanol. As the results in **Table 4.1**, the Lewis acids catalyst especially $Bi(OTf)_3$ catalyst showed the highest both glycerol conversion and mono-ethers yield of 30% and 70%, respectively. The Brønsted acid catalyst could convert glycerol to ethers but it is still less activity and selectivity to mono-ether than Lewis acid catalyst.

Table 4.1 Catalytic etherification of glycerol with n-butanol in the presence of Lewis acids and Brønsted acids catalyst at 150 °C for 24 h, 1:4 molar ratio of glycerol to n-butanol and 6.5 mol% of catalyst

	Catalyst	Glycerol conversion (%)	Butanol conversion (%)	Mono-ethers (B1G1) yield (%)	Di-ethers (B2G1) yield (%)
Lewis acid catalyst	$Bi(OTf)_3$	30	91	70	7
	$Ga(OTf)_3$	23	80	62	2
	$Al(OTf)_3$	18	65	48	0
	$In(OTf)_3$	17	70	45	0
	$Al(TFSI)_3$	10	55	32	0
	$Sc(OTf)_3$	12	31	28	0
	$Fe(OTf)_3$	5	30	19	0
	$Fe(TFSI)_3$	6	52	17	0
	$Nd(OTf)_3$	4	20	12	0
Brønsted acid catalyst	DBSA	22	63	46	0
	MSA	45	90	56	0
	H_2SO_4	46	89	46	0
	Bet.HCl	8	6	2	0
	$Bet.H_2SO_4$	0	0	0	0
	TFSI	20	71	56	6

Ref. code: 25625909320250YIN

(Nandiwale et al., 2014) studied the etherification of glycerol with n-butanol as an alkylating agent under different solid acid catalysts including H-beta zeolite, DTPA/K-10, HZSM-5, and K-10. The glycerol conversion was 55% under the H-beta zeolite catalyst which was the highest activity. The catalytic performance was affected by the surface area and acidity of the catalyst. In addition, the H-beta zeolite catalyst could be reused up to four cycles under optimized condition at 140 °C for 4h, 15 wt.% catalyst loading.

(Samoilov et al., 2016) examined the glycerol etherification with n-butyl alcohol under sulfonated cation exchange resins and various zeolite catalysts. The sulfonated cation exchange resins catalyst including Amberlyst-36, and Amberlyst-70 selective to glycerol mono-n-butyl ethers (mGNBEs) up to 88 mol% with 98 mol% of glycerol conversion. Besides, the Y zeolite and β zeolite catalyst preferred glycerol di-n-butyl ethers (diGNBEs) production with 28 mol% selectivity of diGNBEs and 25 mol% of glycerol conversion at the same reaction condition.

(Srinivas et al., 2014) studied glycerol etherification with tert-butyl alcohol using Tungstophosphoric acid catalysts supported on Y-zeolite (TPA/Y-zeolite). The effect of reaction parameters including the molar ratio of t-butanol to glycerol and catalyst concentration were investigated. The results show that the catalytic activity was affected by the acidity of catalyst. The 20%TPA/Y-zeolite catalyst containing the highest acidity gave the highest glycerol conversion and mono-ether selectivity up to 84% and 85%, respectively. In addition, the 20%TPA/Y-zeolite catalyst could be reused up to four times.

(Frusteri et al., 2009) synthesized the glycerol etherification with tert-butyl alcohol took place on various solid acid catalysts including silica supported acid catalyst (Nafion® ionomer (N-17) and tungstophosphoric heteropoly acid (HPW-17)), commercial ion-exchange resins (Nafion® on amorphous silica (SAC-13), and Amberlyst®15 dry (A-15)). The author investigated the effects of reaction temperature in the range of 30 – 90 °C, reaction times, catalyst loading and molar ratio of alcohol/glycerol on glycerol conversion and selectivity of di-ether products. The Amberlyst®15 dry catalyst containing the highest acidity (4.7 mmol/g) and large pore diameter (300 A°) showed the highest glycerol conversion up to 95% and selectivity of

Ref. code: 25625909320250YIN

di-ether of 29.7% at 90 °C for 6 h under the pressure of 0.1 MPa, 4:1 molar ratio of alcohol/glycerol molar ratio and 7.5 wt.% catalyst loading. The catalytic performance and reaction rate were affected by acidity and pore size distribution. The large pore size distribution enhanced the turnover frequency due to the accessibility of reactant to an active site. In addition, the increasing of reaction temperature enhanced the formation of di-ether products.

(Melero et al., 2008) synthesized glycerol tert-butyl ethers (GTBE) over glycerol etherification with isobutylene in the presence of propyl sulfonated mesoporous silica (Pr-SO_3H-SBA-15) and arenesulfonic acid functionalized mesostructured silica (Ar-SBA-15) catalysts. The results indicated that the Ar-SO_3H-SBA-15 catalyst containing the higher acidity (1.24 H^+ meq/g) showed higher selective toward di-GTBE (54%) and tri-GTBE (41%) than Pr-SO_3H-SBA-15 catalyst containing acidity (1.20 H^+ meq/g) showed di-GTBE (56%) and tri-GTBE (35%) at 75 °C for 4 h, 4:1 molar ratio of isobutylene to glycerol, and 5 wt.% catalyst loading. Therefore, the effect of acidity on catalytic performance was observed.

The sulfonated mesoporous silica catalyst with large surface area, high acidity and high selective to di-GNBEs production. Hence, this catalyst has attracted a lot of interests and has been selected in glycerol etherification reaction.

4.3 Materials

All chemicals and equipment used in this research are listed in **Table 4.2** and **Table 4.3**, respectively

4.3.1 Chemicals

Table 4.2 List of the chemicals used in this research

Chemicals	Manufacturer	Country
Acetone, commercial grade	RCI Labscan	USA
n-butanol, AR grade	QReC	New Zealand
Ethanol Absolute, 99%	QReC	New Zealand
Glycerol, AR grade	QReC	New Zealand

Ref. code: 25625909320250YIN

Table 4.2 List of the chemicals used in this research (cont.)

Hydrogen peroxide, AR grade, 30%	QReC	New Zealand
Hydrochloric acid, AR grade, 37%	QReC	New Zealand
Methanol, HPLC grade	RCI Labscan	USA
Methyl heptadecanote, AR grade, 99%	Sigma-Aldrich	USA
3-Mercaptopropyl methyldimethoxysilane, AR grade, 95%	Sigma-Aldrich	USA
Pluronic P123 triblock copolymer, poly (ethylene glycol)-block-poly (propylene glycol)-block-poly (ethylene glycol), Mw = 5800, AR grade	Sigma-Aldrich	USA
Tetraethyl orthosilicate, AR grade, 98%	Sigma-Aldrich	USA
Sodium sulfate anhydrous (Na_2SO_4)	Ajax Finechem	Australia
Sulfuric acid, 98%	QReC	New Zealand

4.3.2 Equipment

Table 4.3 List of the instrument used in this research

	Company
Autoclave reactor, 50ml	Parr, model 4744, USA
Gas Chromatography-Mass Spectrometry (GC-MS)	GC-Agilent 7890A, MS-Agilent 5975C
Oven	Memmert UF 110
Surface area & Porosimetry analyzer	Gold App Instrument, V-sorb 2800P
Temperature Programed Desorption of amonia (NH_3-TPD)	BET-CAT (BEL, Japan)
Thermogravimetric analysis (TGA)	Mettler Toledo, TGA/DSC, STAR system, USA
Thermo scientific stirrer reactor	Japan
X-ray diffraction (SAXD)	Rigaku, TTRAX III and Bruker, D8 advance
X-ray photoelectron Spectroscopy (XPS)	ULVAC-PHI, PHI 500 VersaProbe II, Japan

Ref. code: 25625909320250YIN

4.4 Methods

4.4.1 Preparation of KIT-6-SO_3H catalyst

The sulfonic acid functionalized KIT-6 catalyst was prepared by co-condensation method, with a molar composition mixture of 0.017 Pluronic P123:1.83 HCl:1.31 n-butanol:195 H_2O: (1-x) (TEOS):x MPMDS, where an x was molar content of MPMDS. The sample was designate as x-KIT-6-SO_3H (x: 0.1 - 0.3)

First, the mixture of 4.0 g of Pluronic P123 triblock co-polymer, 7.5 g of HCl and 145.0 mL of de-ionized water was dissolved at room temperature. After that, 4.0 g of n-butanol was added dropwise and stirred for 1 h at 35 ℃. Then, a solution of 8.6 g of TEOS and a g MPMDS base on the different ratios was dropped to the previous solution and kept the mixture for 24 h with the temperature at 35 ℃ with stirring. Thereafter, the mixture was hydrothermally treated in autoclave at temperature 100 ℃ for 24 h with autogenous pressure. After hydrothermal treatment, the white solid powder was collected and dried at 80 ℃ for 12 h. In the following step, the as-synthesized sample was removed the remaining of organic template by Soxhlet extraction with the mixture solvent of ethanol/HCl at 70 ℃ for 24 h in order to obtain sulfhydryl functionalized KIT-6 mesoporous silica. Finally, the sulfhydryl group was oxidized by 30% H_2O_2 solution for 24 h to obtain the methyl-propyl sulfonic acid functionalized KIT-6 catalyst (KIT-6-MPr-SO_3H). The catalyst was filtered, washed with DI water, and dried at 60 ℃ for 16 h.

4.4.2 Characterization of KIT-6 and KIT-6-SO_3H catalyst

The structure of KIT-6 and KIT-6-SO_3H catalyst were investigated by small angle X-ray diffraction pattern (SAXD) on Rigaku TTRAX III X-Ray diffractometer using Cu Kα (λ = 0.154 nm) radiation, a 40kV beam voltage and a 40 mA beam current in the 2θ angle of 0.5 – 5° with a resolution of 0.02° and scan speed 0.1 second per step.

The surface area, pore volume, and pore size distribution of KIT-6 and KIT-6-SO_3H catalysts were derived by N_2 sorption isotherms using a volumetric V-Sorb 2800P, Gold APP Instruments. Before analysis, the samples were consequently degassed at 50 ℃ for 60 minutes and 60 ℃ for 960 minutes, respectively. The surface area was calculated by Brunauer–Emmett–Teller (BET) equation. The desorption isotherm was used to get the pore size distribution by Barrett-Joiner-Halender (BHJ)

Ref. code: 25625909320250YIN

method. The total pore volume of the sample depended on the adsorbed N_2 volume at a relative pressure of approximately 0.99.

X-ray photoelectron spectroscopy (XPS) was used to analyze surface chemical composition of catalyst. The characterization was carried out with AlKα X-ray radiation on a ULVAC-PHI, PHI500 VersaProbe II. The binding energy (BE) of C1s peak at 284.5 eV was used to correct other peaks. To prove the present of the sulfonic functional group on KIT-6 surface, S2p spectra was fitted with Gaussian/Lorentzian peak shape.

The acidity and acid strength of KIT-6 and KIT-6 catalysts were studied by temperature programed desorption of ammonia (NH_3-TPD), BETCAT (BEL). In a typical acidity measurement, the catalyst was charged in an u-shaped quartz cell and preheated at 750 ℃ for 1 h under He flow in order to remove moisture remain in the structure of catalyst. Subsequently, the catalyst was saturated with a mixed gas of 5 % NH_3 and 95 % He at room temperature for 1 h with the flow rate of 50 cm^3/min. After stabilization, NH_3 desorption was carried out from 50 ℃ to 400 ℃ at a heating rate of 5 ℃/min under He flow. Thermal conductivity detector (TCD) was used to detect the desorbed NH_3 and the amount of NH_3 absorbed on the catalyst was determined from peak area based on standard gas.

4.4.3 Catalytic activity in glycerol n-butyl ethers (GNBEs) production via glycerol etherification with n-butanol

4.4.3.1 Glycerol etherification

First, the mixture of glycerol, n-butanol and catalysts was transferred in a small glass bottle and stirred at 1000 rpm. The reaction conditions including reaction time (120 ℃, 140 ℃ and 160 ℃), reaction temperature (2 – 10 h), catalyst loading (5, 10, 15 wt.%) was investigated. After reaction finish, the catalyst was separated by filtration. The liquid product was collected and dehydrated with anhydrous sodium sulfate. The methyl heptadecanoate was used as an internal standard diluted on methanol in the concentration of 5 mg/ml before analysis with GC-MS.

4.4.3.2 Product analysis

The composition of liquid product was identified by GC–MS (GC-Agilent 7890A, MS-Agilent 5975C) equipped with a HP-Innowax column (0.25 mm

Ref. code: 25625909320250YIN

ID, 30 m length, 0.25 mm film thickness) using He carrier gas at a flow rate of 1 mL/min. Then 1 μL of this solution was injected into the GC-MS with a split ratio of 40:1. The initial oven temperature was held at 70 °C for 3 min, then raised to 250 °C at 10 °C/min and held for 10 min. The injector and detector temperature were maintained at 260 °C. The composition of the product was identified based on the NIST Mass Spectral Library. The product yield, selectivity of each compound and glycerol conversion was calculated by normalization with the total peak area in the GC–MS follow **Equation 4.1**, **4.2**, and **4.3,** respectively.

$$\text{Product yield} = \frac{\text{Moles of produced product}}{\text{Moles of initial glycerol}} \times 100 \quad (4.1)$$

$$\text{Product selectivity} = \frac{\text{Moles of obtained product}}{\text{Total moles of product}} \times 100 \quad (4.2)$$

$$\text{Glycerol conversion} = \frac{\text{Moles of reacted glycerol}}{\text{Moles of initial glycerol}} \times 100 \quad (4.3)$$

4.5 Results and discussion

4.5.1 Characterization of KIT-6 and KIT-6-SO_3H catalyst

4.5.1.1 Small angle X-ray diffraction (SAXD)

The three-dimensional porous structure (3D) of KIT-6 and KIT-6-SO_3H catalysts were confirmed by SAXD patterns as shown in **Figure 4.2**. Both KIT-6 and KIT-6-SO_3H catalysts presented a distinct-peak, and two weak broad peaks at 2θ of 0.76°, 0.89° and 1.53° which were corresponded to scattering plane of (211), (220), and (332), respectively (Liu et al., 2018; Pirez, Caderon, Dacquin, Lee, & Wilson, 2012). However, the intensity of SAXD peak decreased with increasing molar ratio of MPMDS:TEOS resulting that the structure of KIT-6-SO_3H catalyst became disordered. The decreasing in order of porous structure caused from hindrance of the mercaptoalkoxide (Si-O-R-SH) molecules to the formation of ordered porous structure (Ng, Mohd Subari, Marie, Mukti, & Juan, 2013; Wang, Lin, Chan, & Cheng, 2005). Besides, the reflection peak KIT-6-SO_3H catalyst was shifted to higher 2θ indicating the reduction

Ref. code: 25625909320250YIN

of pore size. Therefore, all x-KIT-6-SO_3H catalyst presented smaller pore size than pristine KIT-6.

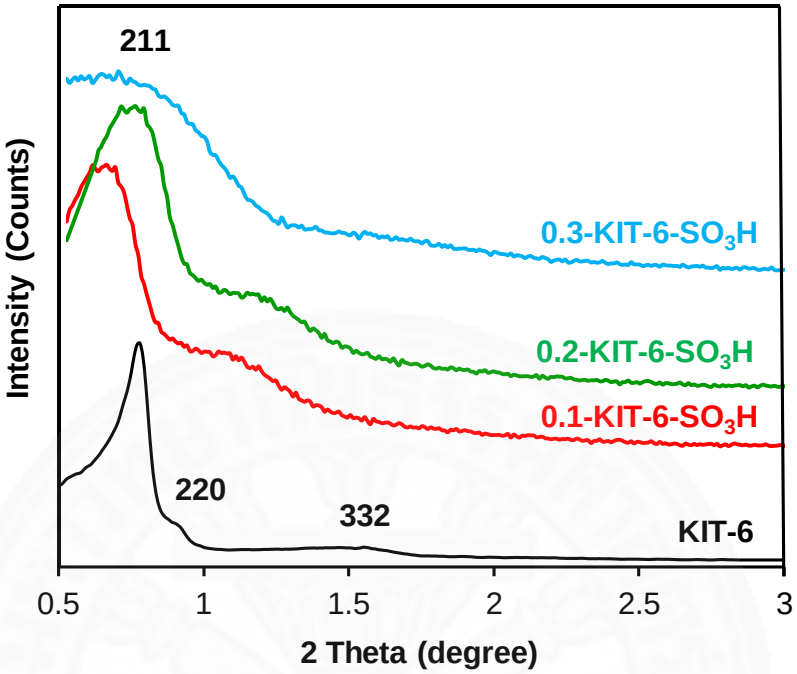

Figure 4.2 SAXD patterns of KIT-6 and KIT-6-SO_3H catalysts

4.5.1.2 N_2 sorption analysis

Figure 4.3 presented the N_2 sorption isotherm of KIT-6 and KIT-6-SO_3H catalysts. Both isotherms of KIT-6 and KIT-6-SO_3H catalysts revealed an IUPAC type IV isotherms indicating mesoporous structure. The H1 hysteresis was observed in the KIT-6 which indicated a well-defined open cylindrical pore structure and facile pore connectivity. Meanwhile, the isotherms of KIT-6-SO_3H catalysts presented H4 hysteresis which corresponded to a narrow-slit pore, particles with internal voids of regular shape. An increase of MPMDS:TEOS ratio decreased the order of mesoporous structure because of the steric effect and close packing of the alkyl-sulfonic chain to prevent the pore arrangement (Rác, Molnár, Forgo, Mohai, & Bertóti, 2006; Wang et al., 2005). The increasing of MPMDS:TEOS molar ratio decreased the BET surface area and pore size as shown in **Figure 4.3 (b)** and **Table 4.4**. The KIT-6 presented a large surface area (S_{BET} = 872 m^2/g) which was higher than the 0.3-KIT-6-SO_3H mesoporous silica catalyst (S_{BET} = 225 m^2/g). In addition, pore size of KIT-6-SO_3H catalyst decreased from 4.70 nm to 4.50 nm with increased MPMDS:TEOS molar ratio

Ref. code: 25625909320250YIN

from 0.1 to 0.3. The excess MPMDS destroy mesoporous structure that reflected to continuously enlarge the pore size of KIT-6-SO_3H catalyst. (Rác et al., 2006). Therefore, in this research, the maximum ratio of MPMDS:TEOS was 0.3.

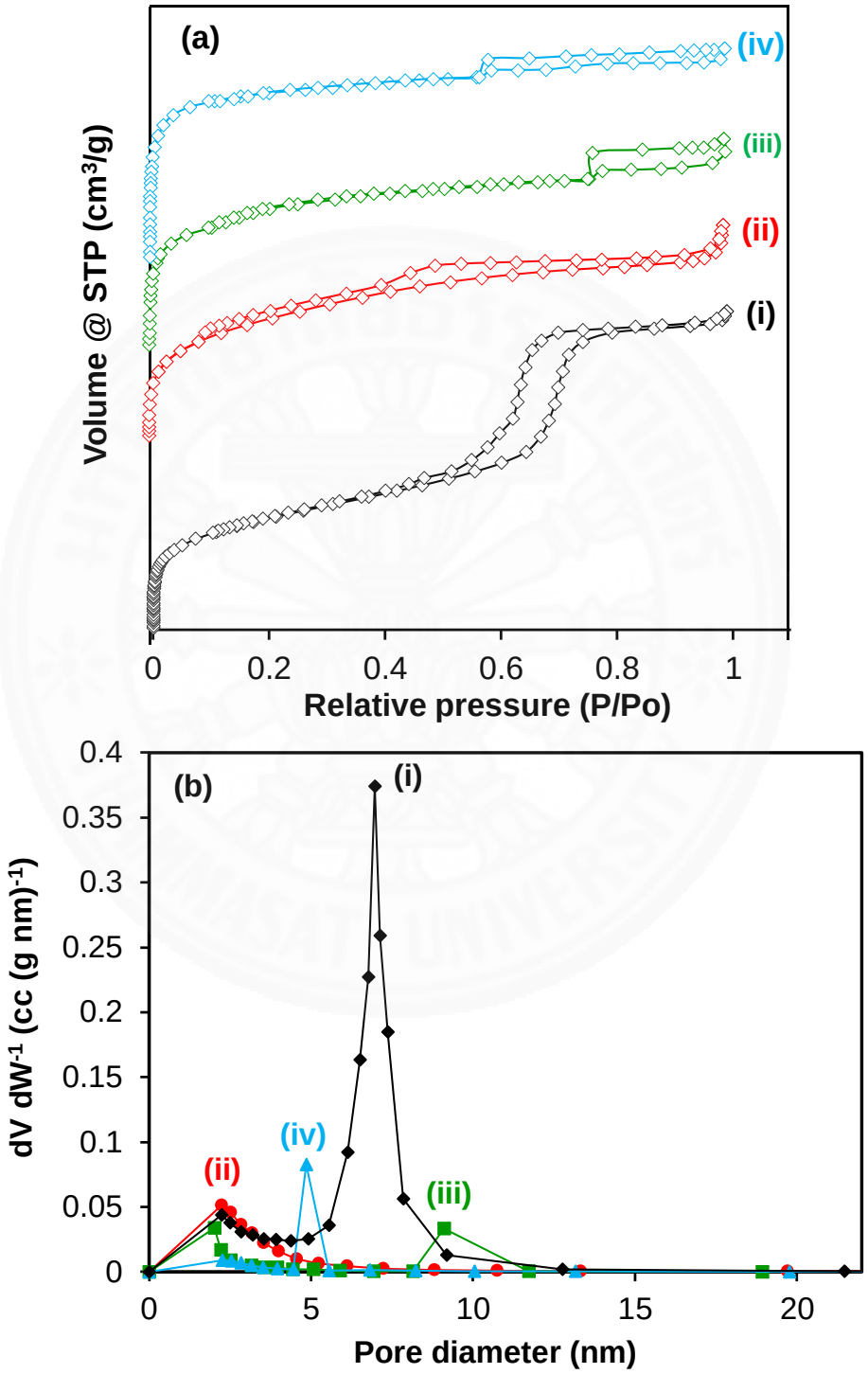

Figure 4.3 (a) Nitrogen sorption isotherms and (b) pore size distribution of (i) KIT-6, (ii) 0.1-KIT-6-SO_3H, (iii) 0.2-KIT-6-SO_3H and (iv) 0.3-KIT-6-SO_3H catalyst

Ref. code: 25625909320250YIN

Table 4.4 A comparison of the physical and chemical properties, along with the catalytic performance in glycerol etherification reaction of the different KIT-6-SO_3H catalysts with other reported acid catalysts

Catalyst	Surface area (m^2/g)	Pore size (nm)	BJH pore volume (cm^3/g)	Acidity (mmol/g)	Acid density ($mmol/m^2$)	Glycerol conversion (%)	di-GNBEs yield (%)	di-GNBEs selectivity (%)	TOF (h-1)	References
KIT-6	872	6.2	0.88	0.02	0.00002	n/d	n/d	n/d	n/d	This work
0.1-KIT-6-SO_3H	269	4.7	0.21	0.69	0.003	48.64	10.74	22.09	12.77	This work
0.2-KIT-6-SO_3H	157	4.6	0.13	1.25	0.008	53.28	21.49	40.34	7.51	This work
0.3-KIT-6-SO_3H	225	4.5	0.10	1.53	0.007	59.09	30.43	51.50	7.08	This work
3rd used of 0.3-KIT-6-SO_3H	19	29.0	0.14	n/d	n/d	43.62	15.51	35.56	n/d	This work
Amberlyst-35 (140 °C – 5 h)	50	24.0	0.20	5.3	0.106	91	14	4	1.87	(Samoilov et al., 2016)
Amberlyst-36 (140 °C – 5 h)	33	24.0	0.20	5.4	0.164	94	20	6	1.89	(Samoilov et al., 2016)
H-Beta Zeolite (180 °C – 4 h)	560	n/d	0.38	0.54	0.001	72	n/d	32.60	24.15	(Nandiwale et al., 2014)
HZSM-5 (140 °C – 4 h)	390	n/d	0.22	0.51	0.001	10	n/d	n/d	3.56	(Nandiwale et al., 2014)

Ref. code: 25625909320250YIN

4.5.1.3 X-ray photoelectron spectroscopy (XPS)

The surface chemical compositions of KIT-6-SO_3H catalysts were determined by X-ray photoelectron spectroscopy. The C1s, Si2p, S2p and O1s spectral were observed as shown in **Figure 4.4**. The presence of C-C bonding, C-O and –COO functional groups were reflected by the peak of C1s with a broad spectrum at binding energy 284.8 eV, 286 eV, and 289 eV, respectively (Song, An, Lu, Guo, & Leng, 2015; Wang et al., 2015). Furthermore, the presence of SiO_2 in the framework of mesoporous KIT-6 structure (Si-O-Si, C-Si-O-) has been detected by the peak of Si2p and O1s at binding energy 103.3 eV and 101.4 eV, respectively (Kumar & Srivastava, 2019). In addition, the single spectrum of S2p at 169 eV assigned to sulfonic acid groups (-SO_3H) on KIT-6 structure. (Moulder, 1995; Russo et al., 2014) This result demonstrated the complete conversion of sulfhydryl (-SH) group to the sulfonic acid (SO_3H) group.

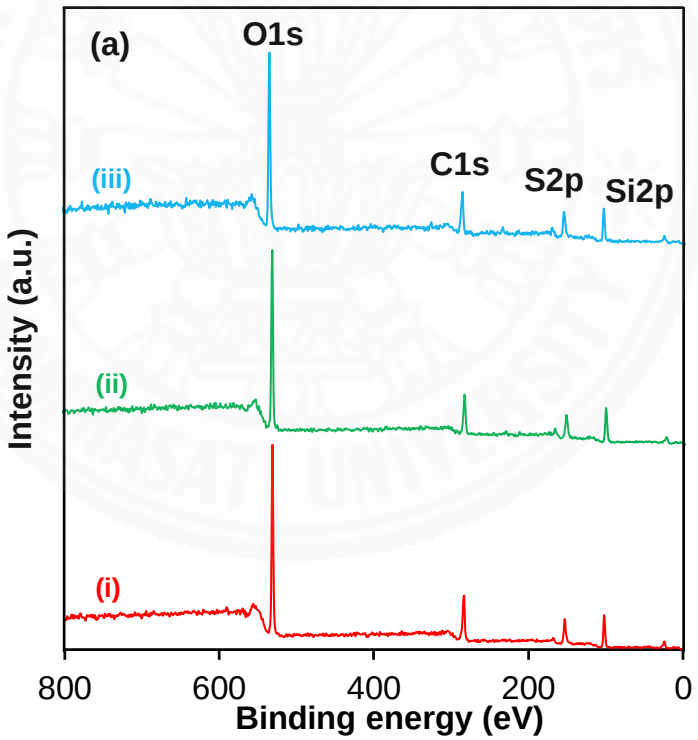

Figure 4.4 XPS spectra of (a) Wide scan, (b) C1s, (c) Si2p, (d) S2p and (e) O1s of (i) 0.1-KIT-6-SO_3H, (ii) 0.2-KIT-6-SO_3H and (iii) 0.3-KIT-6-SO_3H catalyst

Ref. code: 25625909320250YIN

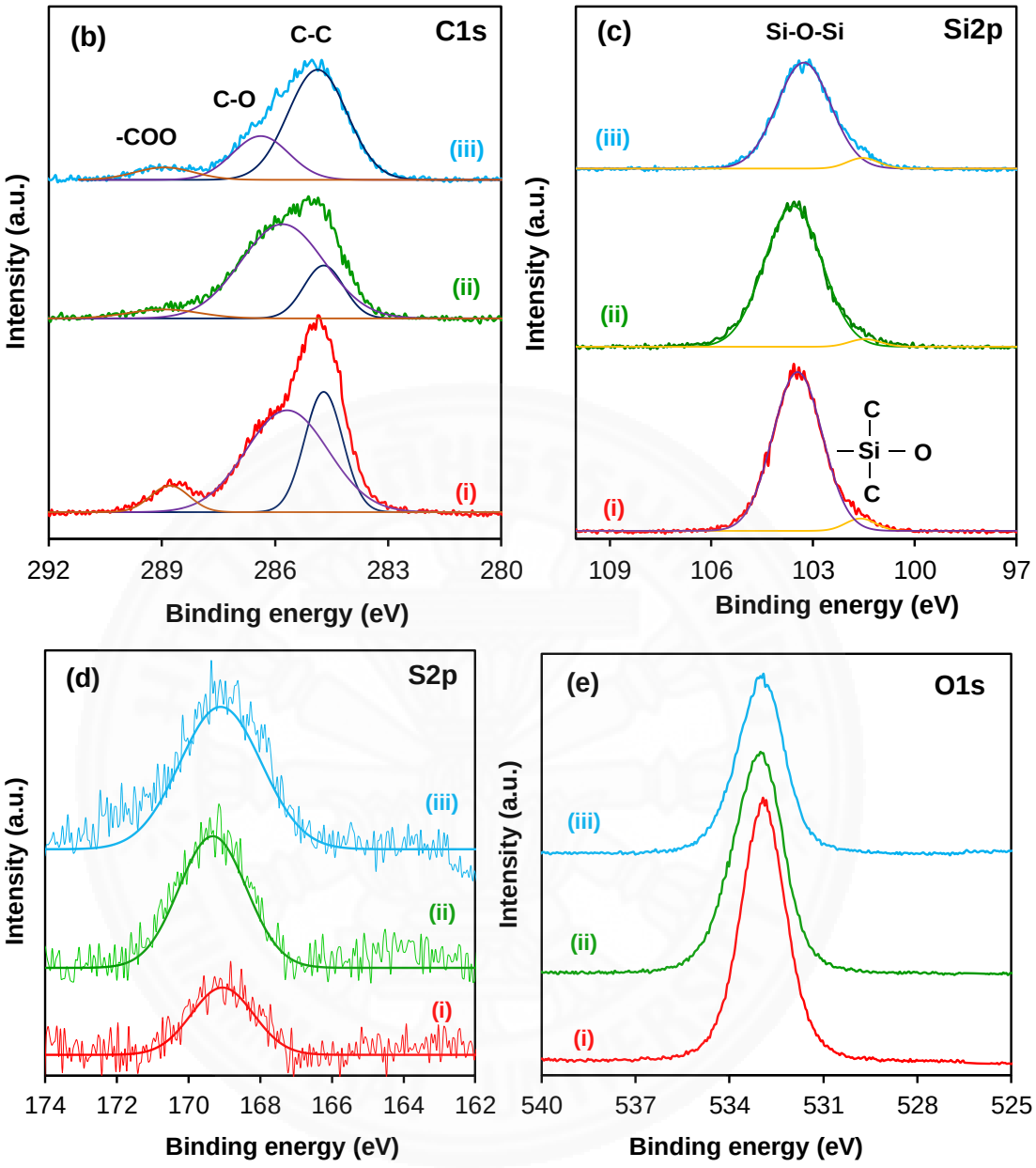

Figure 4.4 XPS spectra of (a) Wide scan, (b) C1s, (c) Si2p, (d) S2p and (e) O1s of (i) 0.1-KIT-6-SO_3H, (ii) 0.2-KIT-6-SO_3H and (iii) 0.3-KIT-6-SO_3H catalyst (cont.)

4.5.1.4 Ammonia temperature programmed desorption (NH_3-TPD)

The NH_3-TPD profiles presented the acid properties of the KIT-6 and KIT-6-SO_3H catalysts as shown in **Figure 4.5**. The NH_3-TPD profile of KIT-6 presented an individual peak appears at 130 °C indicating the weak acid sites of silanol group (Si-OH). Meanwhile, the two distinct desorption peaks were observed on KIT-6-SO_3H catalysts corresponded to weak and strong acid sites (Román-Aguirre, Gochi,

Ref. code: 25625909320250YIN

Sánchez, de la Torre, & Aguilar-Elguezabal, 2008). The first peak was similar to the KIT-6 as belonging to acid sites of silanol group (Si-OH). In the case of 0.3-KIT-6-SO_3H, this desorption peak was shifted to higher temperatures because of large interaction between the sulfonic acid site and NH_3 molecule (Román-Aguirre et al., 2008). The second peak was appeared at the temperature range of 260 – 300 °C indicating the sulfonic acid. The total acidity increased from 0.69 to 1.53 mmol/g with increasing MPMDS:TEOS molar ratio from 0.1 to 0.3 due to the increasing number of sulfonic acid sites on KIT-6 structure (**Table 4.4**).

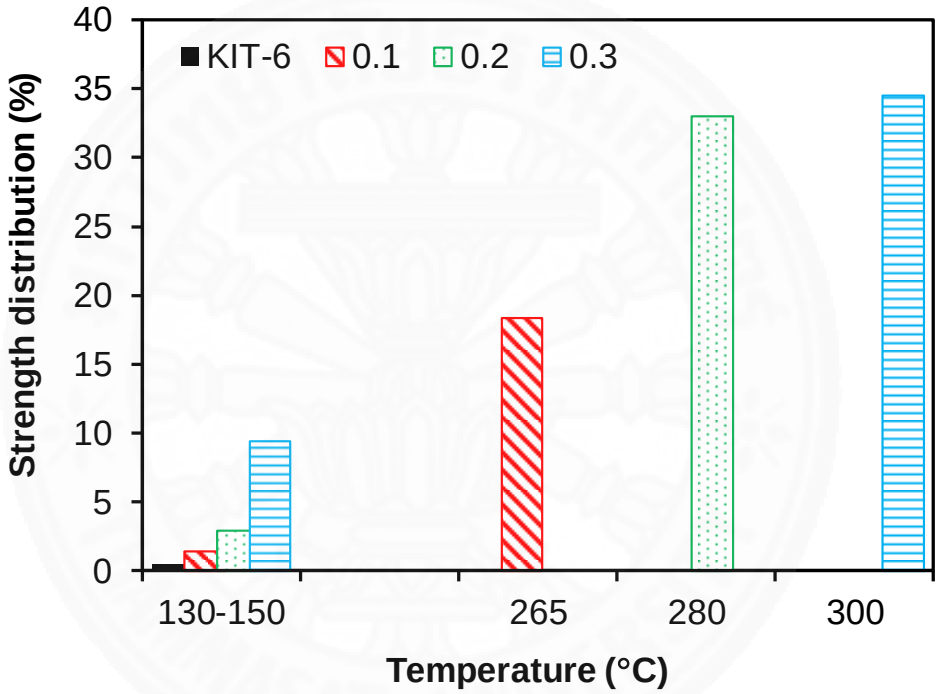

Figure 4.5 NH_3-TPD profile of KIT-6 and KIT-6-SO_3H catalysts

4.5.2 Catalytic activity in glycerol n-butyl ethers (GNBEs) production via glycerol etherification

4.5.2.1 Effect of reaction temperature

The effects of reaction temperature on catalytic activity including glycerol conversion, yield of di-GNBEs, and selectivity of di-glycerol n-butyl ethers (di-GNBEs) are shown in **Figure 4.6**. The glycerol conversion increased from 48.19% to 58.39% with increased reaction temperature from 120 °C to 140 °C and then the catalytic activity slightly increased at 160 °C (59.97%) due to approaching thermodynamic equilibrium. Otherwise, at the high reaction temperature, glycerol

Ref. code: 25625909320250YIN

could not convert to di-GNBEs production due to the occurrence of de-etherification (dehydrative etherification) reactions (Frusteri et al., 2009; Huang & Kim, 2015). Besides, the di-GNBEs selectivity was also slightly decreased at higher reaction temperature since the undesired side reaction and further reaction of product occurred. Therefore, the optimized reaction temperature was selected at 140 °C.

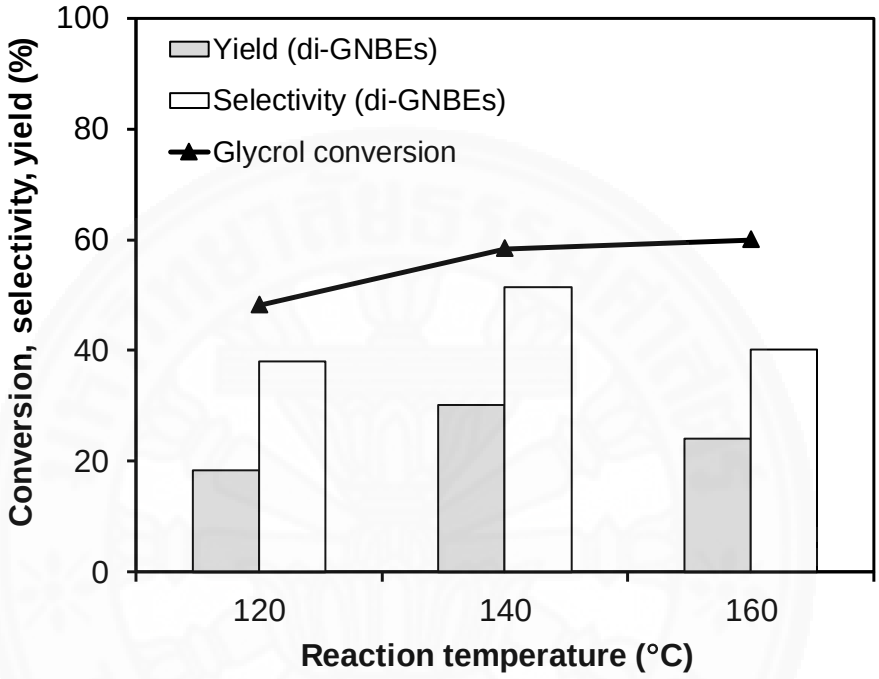

Figure 4.6 Catalytic activity of glycerol etherification at different reaction temperature for 6 h under 10 wt.% of 0.3-KIT-6-SO_3H catalyst

4.5.2.2 Effect of reaction time

The glycerol conversion, di-GNBEs yield and di-GNBEs selectivity at different reaction times were presented in **Figure 4.7**. The glycerol conversion increased with time and reached to 50.09% after 6 h. At the longer reaction time, the di-GNBEs was preferred due to the reaction between mono-GNBEs and available n-butanol (Nandiwale et al., 2014). However, after 6 h the selectivity of di-GNBEs was decreased due to the side-product formation and/or the formation of water absorb onto its surface leading to blocking active site of catalyst. The di-GNBEs selectivity was increased from 22.85% at 2 h to 51.50% at 6 h and then it decreased to 37.75% after 10 h. According, the di-GNBEs and tri-GNBEs are considered as good additives for diesel fuels (diesel, biodiesel and their mixtures) compare with mono-

Ref. code: 25625909320250YIN

GNBEs due to the low solubility of mono-GNBEs in diesel fuel (Lee et al., 2010; Melero et al., 2008; Pico et al., 2012). Meanwhile, the tri-GNBEs was not formed as a result of steric hindrance (Dominguez et al., 2019). Therefore, di-GNBEs was a desire product in the application of diesel fuel additive. From the study, the optimized reaction condition at 140 ℃ for 6 h was obtained and used for further study.

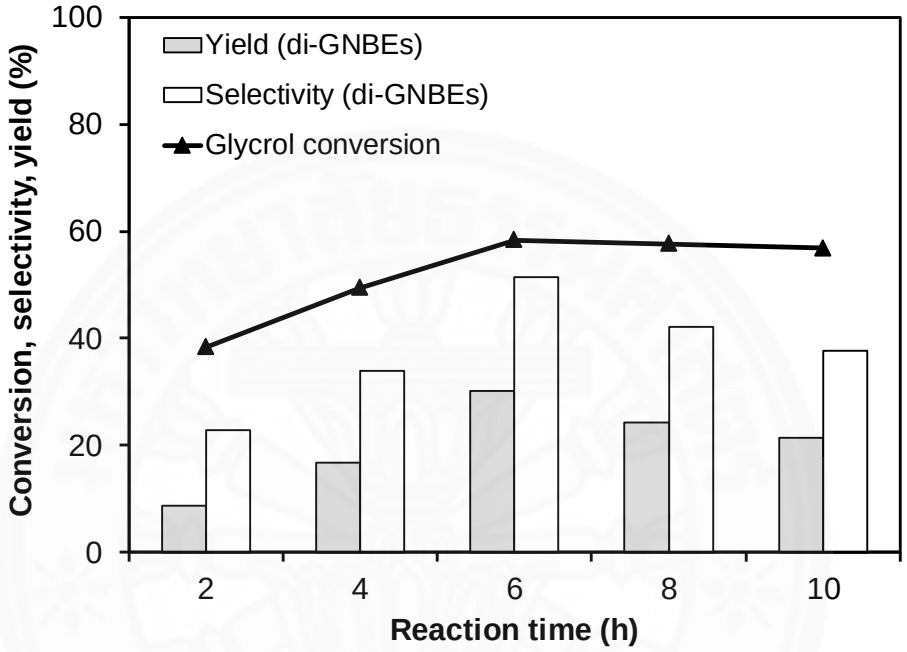

Figure 4.7 Catalytic activity of glycerol etherification at 140 ℃ with different reaction time under 10 wt.% of 0.3-KIT-6-SO_3H catalyst

4.5.2.3 Effect of catalyst loading and molar ratio of n-butanol to glycerol

The effect of catalyst loading on di-GNBEs selectivity, GNBEs yield and glycerol conversion was shown in **Figure 4.8 (a)**. At catalyst loading 5 wt.%, the yield and selectivity of di-GBNEs were low due to the less amount of acid sites. The yield of di-GNBEs also increased from 15.33% to 30.42% with increasing the catalyst loading from 5 wt.% to 10 wt.% indicating that more available active sites to enhance the etherification reaction. However, the di-GBNEs yield and di-GBNEs selectivity decreased with increasing catalyst loading up to 15 wt.% due to a poorly diffusional of the reactant at highly catalyst loadings reduced the mass transfer between solid-liquid phases in the system (Nandiwale et al., 2014). Moreover, at high catalyst loading level was affected the etherification of glycerol with n-butanol toward

Ref. code: 25625909320250YIN

side reactions such as glycerol oligomerization or dehydration for instance. Hence, the optimal catalyst loading for glycerol etherification reaction was 10 wt.%

The effect of n-butanol to glycerol molar ratio on the etherification reaction was shown in **Figure 4.8 (b)**. The etherification reaction is a reversible reaction, the increasing amount of n-butanol could enhance the conversion of glycerol and favor to produce di-GNBEs production (Srinivas et al., 2014; Dominguez et al., 2019). For further increases in the molar ratio above 9:1, the glycerol conversion was unchanged (48.30%). Besides that, the di-GNBEs selectivity was slightly decreased from 37.93% to 34.53%. This may be due to more n-butanol is available on the active catalyst surface, which hinders its activity and more side reaction occurs such as dehydration or oligomerization, etc. (Karinen & Krause, 2006). Thus, the optimized n-butanol/glycerol molar ratio for etherification was 9:1.

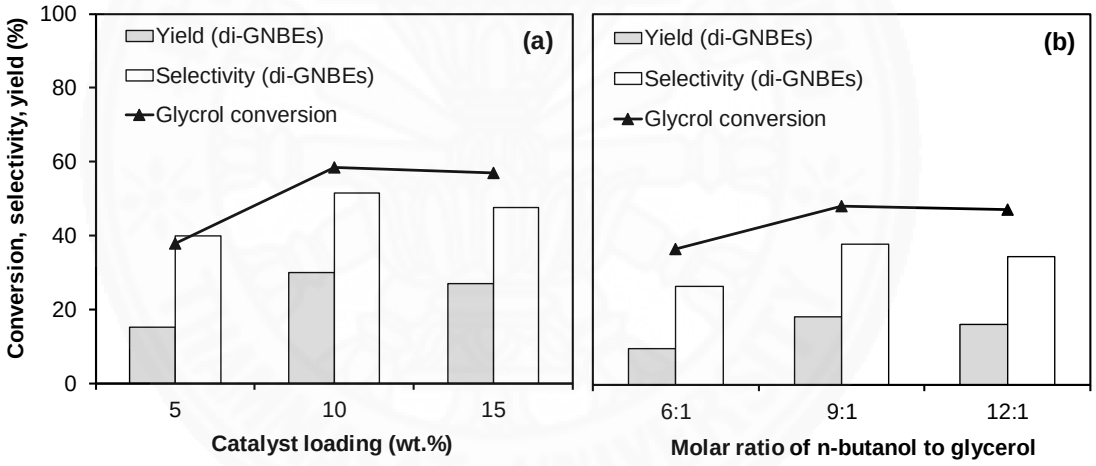

Figure 4.8 Catalytic activity of glycerol etherification of different (a) catalyst loading at 140 °C - 6 h and (b) molar ratio (n-butanol/glycerol) at 120 °C for 6 h, 10 wt.% of 0.3-KIT-6-SO_3H catalyst

4.5.2.4 Effect of MPMDS:TEOS molar ratio and catalyst reusability

The catalytic activity and selectivity of KIT-6-SO_3H catalyst with three different molar ratios of MPMDS:TEOS are shown in **Figure 4.9** and **Table 4.4**. The 0.3-KIT-6-SO_3H catalyst gave the highest glycerol conversion (59.09%) and di-GNBEs selectivity (51.50%) due to the highest acidity. The glycerol conversion increased with increasing molar ratios of MPMDS:TEOS. Hence, the di-GNBEs selectivity, di-GNBEs yield, and glycerol conversion was strongly dependent on the number of acid sites.

Ref. code: 25625909320250YIN

Meanwhile, the highest TOF was presented in 0.1-KIT-6-SO_3H catalyst because of the effect of 3D structure, the reactant has good accessibility toward the catalyst sites. The increase in the ratio of MPMDS:TEOS reduced the TOF number due to the decreased 3D ordered structure of the catalyst. The 0.3-KIT-6-SO_3H catalyst was not only shown the high glycerol conversion, but also high yield and selectivity of di-GNBEs which was selected as an optimized catalyst for the various reaction conditions.

(Zhao, Yang, Yi, Lei, & Xu, 2010) reported that the di- and tri-GNBEs production are miscible with diesel fuels and contain high oxygen contents of 23.5% (di-GNBEs) and 18.5% (tri-GNBEs). Moreover, the high-octane numbers of 112-128 (blending research octane number, BRON) and 91-99 (blending motor octane number, BMON) could be enhanced the combustion efficiency in internal combustion engines and reduced pollution. In comparison with previously reported acid catalysts including Amberlyst-35, Amberlyst-36, H-Beta Zeolite and HZSM-5 catalysts, the performance of the KIT-6-SO_3H catalyst was conducted at 140 °C for 6 h as summarized in **Table 4.4.** The KIT-6-SO_3H catalyst gave the highest di-GBNEs selectivity because of its large surface area and high acidity. Moreover, the 3D structure of catalyst enhances the reaction rate. Besides, the methyl group in anti-adsorption of product or water at active site, which improves the di-GBNES selectivity.

The reusability of the 0.3-KIT-6-SO_3H catalyst was carried out over three cycles at the optimum conditions at 140 °C in 6 h, with the molar ratio of n-butanol/glycerol was 9:1 as shown in **Figure 4.9**. The glycerol conversion was decreased from 59.09% to 43.92% after 3rd cycle. The di-GBNEs selectivity also decreased 16% after 3rd cycle. The reduction of glycerol conversion and di-GBNEs selectivity and di-GBNEs yield could be explained by deactivation of catalyst. Moreover, the loss of active site and disordered 3D structure of catalyst from side products was cover the surface of catalyst.

The deactivation of catalyst could be confirmed by the characteristic N_2 sorption were reported in **Figure 4.10** and **Table 4.4**. The structure of the spent 0.3-KIT-6-SO_3H catalyst after 3rd used presented type II isotherm represented non-porous structure. The low BET surface area of spent 0.3-KIT-6-SO_3H catalyst decreased from 225 to 19 m^2/g due to the surface coverage with reactants and/or products.

Ref. code: 25625909320250YIN

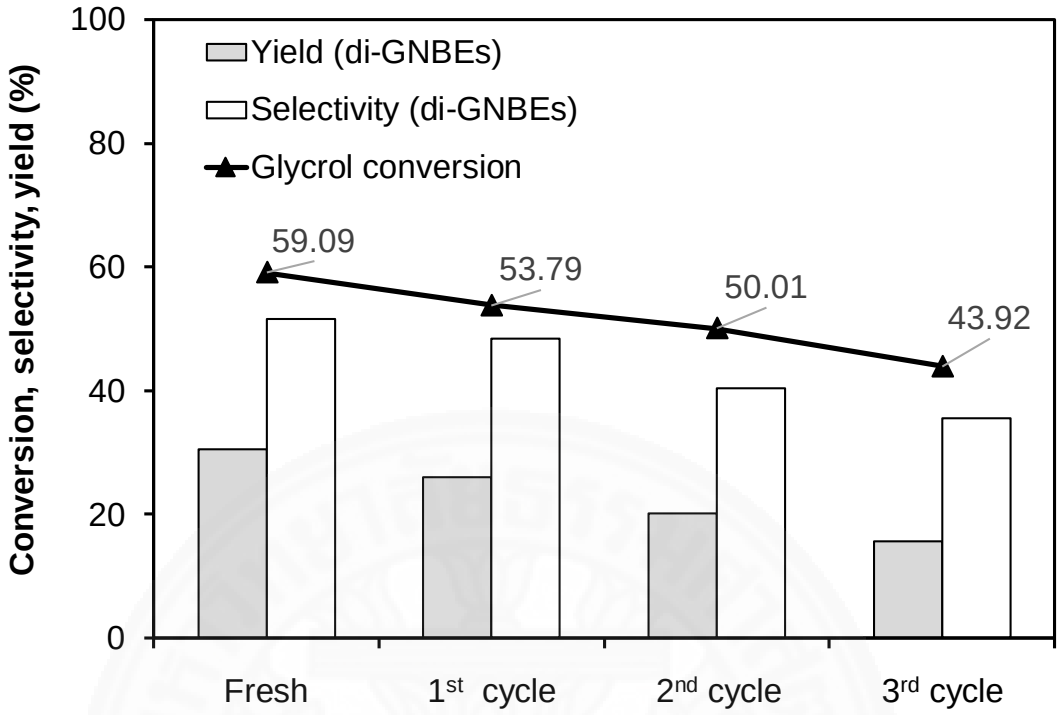

Figure 4.9 Catalytic activity of glycerol etherification of fresh and reused catalyst at 140 °C for 6 h under 10 wt.% 0.3-KIT-6-SO_3H catalyst loading

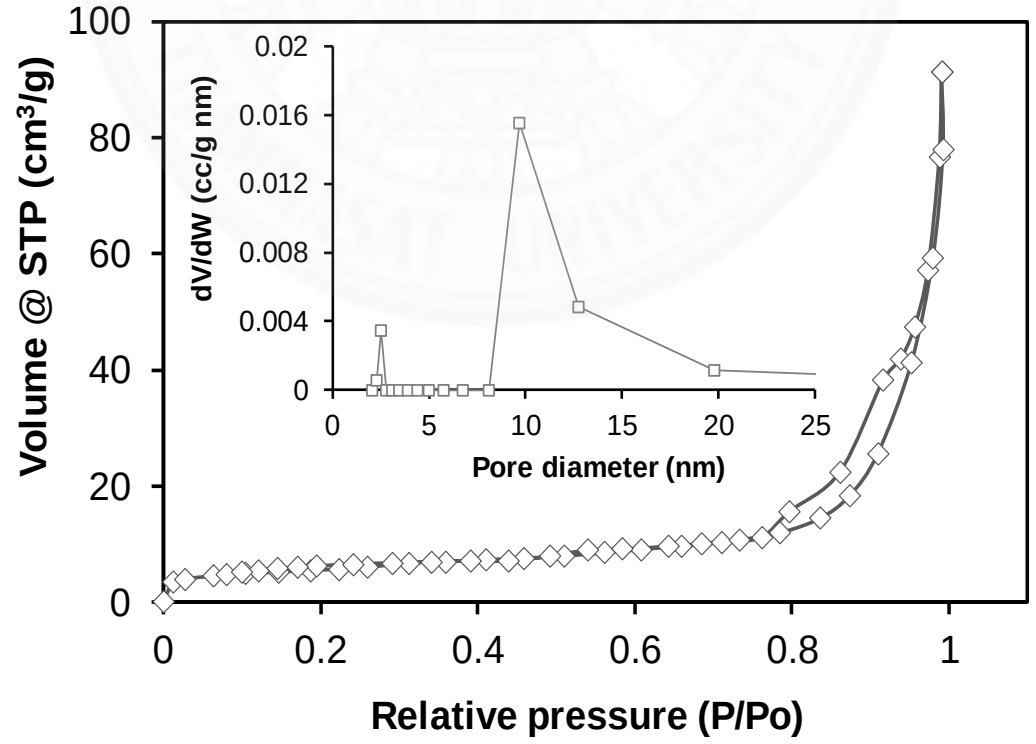

Figure 4.10 N_2 sorption and pore size distribution of 3rd used 0.3-KIT-6-SO_3H catalyst

Ref. code: 25625909320250YIN

4.6 Conclusions

The sulfonic acid functionalized mesoporous catalyst (KIT-6-SO_3H) was prepared by the co-condensation method with the different molar ratios of MPMDS: TEOS. The 0.3-KIT-6-SO_3H catalyst gave the highest acidity and was selected as a catalyst for synthesis the glycerol n-butyl ethers from etherification of glycerol and n-butanol. The number of acid sites, as well as the accessibility of reactants strongly affected the catalytic performance. The sulfonated functionalized mesoporous catalyst preferred to produce di-GNBEs production. The highest di-GNBEs selectivity was up to 51.50% at the optimized reaction condition of 140 ℃ for 6 h with a 9:1 molar ratio of n-butanol to glycerol and 10 wt.% catalyst loading. In conclusion, the KIT-6-SO_3H catalyst can be a candidate of solid acid catalyst for diglycerol n-butyl ethers production by etherification reaction.

Ref. code: 25625909320250YIN

4.7 References

Agency, U. S. E. P., & Laboratory, N. R. E. (2009). *State bioenergy primer: Information and resources for states on issues, opportunities, and options for advancing bioenergy, "Chapter 1: Introduction"*. Retrieved from State and Local Climate and Energy Program: https://www.nrel.gov/docs/fy10osti/44688.pdf

Bozbas, K. (2008). Biodiesel as an alternative motor fuel: Production and policies in the European Union. *Renewable and Sustainable Energy Reviews, 12* (2), 542-552. doi:https://doi.org/10.1016/j.rser.2005.06.001

Byrnett, D., Mulholland, D., Zinsmeister, E., Doris, E., Milbrandt, A., Stanley, R., & Vimmerstedt, L. (2009). *State bioenergy primer: information and resources for states on issues, opportunities, and options for advancing bioenergy*. Retrieved from

Cornejo, A., Barrio, I., Campoy, M., Lázaro, J., & Navarrete, B. (2017). Oxygenated fuel additives from glycerol valorization. Main production pathways and effects on fuel properties and engine performance: A critical review. *Renewable and Sustainable Energy Reviews, 79*, 1400-1413. doi:https://doi.org/10.1016/j.rser.2017.04.005

Demirbas, A. (2007). Progress and recent trends in biofuels. *Progress in Energy and Combustion Science, 33* (1), 1-18. doi:https://doi.org/10.1016/j.pecs.2006.06.001

Di Serio, M., Casale, L., Tesser, R., & Santacesaria, E. (2010). New process for the production of glycerol tert-butyl ethers. *Energy & Fuels, 24* (9), 4668-4672. doi:https://doi.org/10.1021/ef901230r

Dominguez, C. M., Romero, A., & Santos, A. (2019). Improved etherification of glycerol with tert-butyl alcohol by the addition of dibutyl ether as solvent. *Catalysts, 9* (4), 378. doi:https://doi.org/10.3390/catal9040378

Frusteri, F., Arena, F., Bonura, G., Cannilla, C., Spadaro, L., & Di Blasi, O. (2009). Catalytic etherification of glycerol by tert-butyl alcohol to produce oxygenated additives for diesel fuel. *Applied Catalysis A: General, 367* (1), 77-83. doi:https://doi.org/10.1016/j.apcata.2009.07.037

Gabriele, B., Mancuso, R., Salerno, G., Veltri, L., Costa, M., & Dibenedetto, A. (2011). A general and expedient synthesis of 5- and 6-membered cyclic carbonates by palladium-catalyzed oxidative carbonylation of 1,2- and 1,3-diols. *ChemSusChem, 4* (12), 1778-1786. doi:https://doi.org/10.1002/cssc.201100250

Gu, Y., Azzouzi, A., Pouilloux, Y., Jérôme, F., & Barrault, J. (2008). Heterogeneously catalyzed etherification of glycerol: new pathways for transformation of glycerol to more valuable chemicals. *Green Chemistry, 10* (2), 164-167. doi:10.1039/B715802E

Hermida, L., Abdullah, A. Z., & Mohamed, A. R. (2011). Synthesis of monoglyceride through glycerol esterification with lauric acid over propyl sulfonic acid post-synthesis functionalized SBA-15 mesoporous catalyst. *Chemical Engineering Journal, 174* (2), 668-676. doi:https://doi.org/10.1016/j.cej.2011.09.072

Huang, R., & Kim, E. Y. (2015). Catalytic synthesis of glycerol tert-butyl ethers as fuel additives from the biodiesel by-product glycerol. *Journal of Chemistry, 2015*. doi: https://doi.org/10.1155/2015/763854

Karinen, R. S., & Krause, A. O. I. (2006). New biocomponents from glycerol. *Applied Catalysis A: General, 306*, 128-133. doi:https://doi.org/10.1016/j.apcata.2006.03.047

Klepáčová, K., Mravec, D., & Bajus, M. (2005). Tert-butylation of glycerol catalysed by ion-exchange resins. *Applied Catalysis A: General, 294* (2), 141-147. doi:https://doi.org/10.1016/j.apcata.2005.06.027

Klepáčová, K., Mravec, D., Kaszonyi, A., & Bajus, M. (2007). Etherification of glycerol and ethylene glycol by isobutylene. *Applied Catalysis A: General, 328* (1), 1-13. doi:https://doi.org/10.1016/j.apcata.2007.03.031

Klepáþová, K., Mravec, D., Hajekova, E., & Bajus, M. (2003). Etherification of glycerol. *Petroleum and Coal, 45* (1-2), 54-57.

Kong, P. S., Aroua, M. K., & Daud, W. M. A. W. (2016). Conversion of crude and pure glycerol into derivatives: A feasibility evaluation. *Renewable and Sustainable Energy Reviews, 63*, 533-555. doi:https://doi.org/10.1016/j.rser.2016.05.054

Kumar, A., & Srivastava, R. (2019). $FeVO_4$ decorated $–SO_3H$ functionalized polyaniline for direct conversion of sucrose to 2,5-diformylfuran & 5-ethoxymethylfurfural and selective oxidation reaction. *Molecular Catalysis, 465*, 68-79. doi:https://doi.org/10.1016/j.mcat.2018.12.017

Lee, H. J., Seung, D., Filimonov, I. N., & Kim, H. (2011). Etherification of glycerol by isobutylene. Effects of the density of acidic sites in ion-exchange resin on the distribution of products. *Korean Journal of Chemical Engineering, 28* (3), 756-762. doi:https://doi.org/10.1007/s11814-010-0452-8

Ref. code: 25625909320250YIN

Lee, H. J., Seung, D., Jung, K. S., Kim, H., & Filimonov, I. N. (2010). Etherification of glycerol by isobutylene: Tuning the product composition. *Applied Catalysis A: General, 390* (1), 235-244. doi:https://doi.org/10.1016/j.apcata.2010.10.014

Liu, F., De Oliveira Vigier, K., Pera-Titus, M., Pouilloux, Y., Clacens, J.-M., Decampo, F., & Jérôme, F. (2013). Catalytic etherification of glycerol with short chain alkyl alcohols in the presence of Lewis acids. *Green Chemistry, 15* (4), 901-909. doi:10.1039/C3GC36944G

Liu, S., Chen, J., Peng, Y., Hu, F., Li, K., Song, H., . . . Li, J. (2018). Studies on toluene adsorption performance and hydrophobic property in phenyl functionalized KIT-6. *Chemical Engineering Journal, 334*, 191-197. doi:https://doi.org/10.1016/j.cej.2017.08.091

Luo, X., Ge, X., Cui, S., & Li, Y. (2016). Value-added processing of crude glycerol into chemicals and polymers. *Bioresource Technology, 215*, 144-154. doi:https://doi.org/10.1016/j.biortech.2016.03.042

Melero, J. A., Vicente, G., Morales, G., Paniagua, M., Moreno, J. M., Roldán, R., . . . Pérez, C. (2008). Acid-catalyzed etherification of bio-glycerol and isobutylene over sulfonic mesostructured silicas. *Applied Catalysis A: General, 346* (1), 44-51. doi:https://doi.org/10.1016/j.apcata.2008.04.041

Melero, J. A., Vicente, G., Paniagua, M., Morales, G., & Muñoz, P. (2012). Etherification of biodiesel-derived glycerol with ethanol for fuel formulation over sulfonic modified catalysts. *Bioresource Technology, 103* (1), 142-151. doi:https://doi.org/10.1016/j.biortech.2011.09.105

Moulder, J. F. (1995). Handbook of X-ray photoelectron spectroscopy. *Physical Electronics*, 230-232.

Nandiwale, K. Y., Patil, S. E., & Bokade, V. V. (2014). Glycerol etherification using n-butanol to produce oxygenated additives for biodiesel fuel over H-Beta zeolite catalysts. *Energy Technology, 2* (5), 446-452. doi:10.1002/ente.201300169

Ng, E. P., Mohd Subari, S. N., Marie, O., Mukti, R. R., & Juan, J.C. (2013). Sulfonic acid functionalized MCM-41 as solid acid catalyst for tert-butylation of hydroquinone enhanced by microwave heating. *Applied Catalysis A: General, 450*, 34-41. doi:https://doi.org/10.1016/j.apcata.2012.09.055

Ref. code: 25625909320250YIN

Pico, M. P., Romero, A., Rodríguez, S., & Santos, A. (2012). Etherification of glycerol by tert-butyl alcohol: Kinetic model. *Industrial & Engineering Chemistry Research, 51* (28), 9500-9509. doi:10.1021/ie300481d

Pirez, C., Caderon, J. M., Dacquin, J. P., Lee, A. F., & Wilson, K. (2012). Tunable KIT-6 mesoporous sulfonic acid catalysts for fatty acid esterification. *ACS Catalysis, 2* (8), 1607-1614. doi:10.1021/cs300161a

Rác, B., Molnár, Á., Forgo, P., Mohai, M., & Bertóti, I. (2006). A comparative study of solid sulfonic acid catalysts based on various ordered mesoporous silica materials. *Journal of Molecular Catalysis A: Chemical, 244* (1), 46-57. doi:https://doi.org/10.1016/j.molcata.2005.08.043

Román-Aguirre, M., Gochi, Y. P., Sánchez, A. R., de la Torre, L., & Aguilar Elguezabal, A. (2008). Synthesis of camphene from α-pinene using SO_3^{2-} functionalized MCM-41 as catalyst. *Applied Catalysis A: General, 334* (1), 59-64. doi:https://doi.org/10.1016/j.apcata.2007.09.031

Russo, P., Antunes, M., Neves, P., Wiper, P., Fazio, E., Neri, F., . . . Pinna, N. (2014). Solid acids with SO_3H groups and tunable surface properties.

Samoilov, V. O., Ramazanov, D. N., Nekhaev, A. I., & Maksimov, A. L. (2016). Heterogeneous catalytic conversion of glycerol with n-butyl alcohol. *Petroleum Chemistry, 56* (2), 125-130. doi:10.1134/S0965544116010060

Song, D., An, S., Lu, B., Guo, Y., & Leng, J. (2015). Arylsulfonic acid functionalized hollow mesoporous carbon spheres for efficient conversion of levulinic acid or furfuryl alcohol to ethyl levulinate. *Applied Catalysis B: Environmental, 179*, 445-457. doi:https://doi.org/10.1016/j.apcatb.2015.05.047

Srinivas, M., Sree, R., Raveendra, G., Kumar, C. R., Prasad, P., & Lingaiah, N. (2014). Selective etherification of glycerol with tert-butanol over 12-tungstophosphoric acid catalysts supported on Y-zeolite. *Indian Journal of Chemistry-Section A (IJC-A), 53A*, 524-529. doi:http://nopr.niscair.res.in/handle/123456789/28473

Wang, X., Lin, K. S. K., Chan, J. C. C., & Cheng, S. (2005). Direct synthesis and catalytic applications of ordered large pore aminopropyl-functionalized SBA-15 mesoporous materials. *The Journal of Physical Chemistry B, 109* (5), 1763-1769. doi:10.1021/jp045798d

Ref. code: 25625909320250YIN

Wang, Y., Wang, D., Tan, M., Jiang, B., Zheng, J., Tsubaki, N., & Wu, M. (2015). Monodispersed hollow SO_3H-functionalized carbon/silica as efficient solid acid catalyst for esterification of oleic acid *ACS Applied Materials & Interfaces, 7* (48), 26767-26775. doi:10.1021/acsami.5b08797

Zhao, W., Yang, B., Yi, C., Lei, Z., & Xu, J. (2010). Etherification of glycerol with isobutylene to produce oxygenate additive using sulfonated peanut shell catalyst. *Industrial & Engineering Chemistry Research, 49* (24), 12399-12404. doi:10.1021/ie101461g

Ref. code: 25625909320250YIN

CHAPTER 5
CONCLUSIONS AND RECOMMENDATIONS

5.1 Conclusions

The sulfonic acid functionalized mesoporous KIT-6 catalyst (x-KIT-6-SO_3H) was successfully synthesized by sequential co-condensation and oxidation method with different molar ratios between MPMDS and TEOS. The KIT-6 was presented with a pore size of 6.2 nm and a large surface area up to 872 m^2/g. The pore size of the KIT-6-SO_3H catalyst decreased from 4.70 nm to 4.50 nm with increased MPMDS:TEOS molar ratio from 0.1 to 0.3. However, both KIT-6 and KIT-6-SO_3H catalyst still presented the mesoporous structure with a cubic Ia3d symmetry three-dimensional structure. The 3D structure was discovered to be an important factor to enhance the catalytic performance. This catalyst contained high acidity up to 1.53 mmol/g at the MPMDS:TEOS molar ratio of 0.3. The conversion of sulfhydryl (-SH) groups successfully converted to the sulfonic acid (-SO_3H) group which could be confirmed by a single peak of S2p XPS spectra.

The KIT-6-SO_3H catalysts were studied their catalytic performance in xylose dehydration to synthesis furfural production. The catalyst performed good catalytic activity to obtain the highest furfural yield, furfural selectivity, and xylose conversion at optimized conditions were 92.5%, 94.7%, 97.7%, respectively. The 0.2-KIT-6-SO_3H catalyst was selected the best catalyst in term of xylose conversion, selectivity and yield of furfural, as well as the high TOF (10.43 h^{-1}) due to the highest acid density (0.008 mmol/m^2). The catalytic activity in the xylose dehydration route was affected by the number of acid sites per catalyst surface area or acid density. The reusability of catalyst was also investigated at the optimum condition (170 °C for 2 h, 25 wt.% catalyst loading) up to three cycles. The xylose conversion slightly decreased from 98.70% to 93.00% after three cycles. The deactivation was mainly caused by coke deposition to cover the active sites.

Ref. code: 25625909320250YIN

Besides, the KIT-6-SO_3H catalyst was applied to the catalytic performance in fusel oil esterification to synthesis isoamyl acetate. The 0.3-KIT-6-SO_3H catalyst performed good catalytic activity with a 95.05% yield of isoamyl acetate at the reaction condition of 80 °C for 3 h, 5 wt.% catalyst loading and 2:1 molar ratio of acetic acid to fusel oil. The acidity or number of acid sites, as well as the accessibility of reactants strongly affected the catalyst performance. The 0.3-KIT-6-SO_3H catalyst performed the highest isoamyl acetate yield, while 0.1-KIT-6-SO_3H gave the highest TOF (78.15 h^{-1}). The reusability of catalysts was also investigated at the optimum condition which could be reused up to three cycles. In the reusability study without re-oxidation, the isoamyl acetate yield decreased by 24.0% after three cycles. However, with the reusability study together with the re-oxidation of catalyst, there was no significant reduction of the isoamyl acetate yield (>92.00%) over the three cycles. Comparing to the Amberlyst-35 as conventional catalyst, the KIT-6-SO_3H catalyst showed a higher efficiency than the Amberlyst-35 catalyst.

The last part, KIT-6-SO_3H catalyst was applied to the glycerol etherification for synthesis glycerol n-butyl ethers production. The 0.3-KIT-6-SO_3H catalyst contained the highest acidity would be selected as a catalyst for synthesis the glycerol n-butyl ethers from glycerol and n-butanol via the etherification reaction. The sulfonated functionalized mesoporous catalyst was selective to produce di-GNBEs. The highest di-GNBEs selectivity was 51.50% at the optimized reaction condition of 140 °C for 6 h with a 1:9 molar ratio of glycerol to n-butanol and 10 wt.% catalyst loading.

In conclusion, the KIT-6-SO_3H catalyst could be a candidate catalyst to perform the good performance in acid catalyst related reactions including dehydration, esterification and etherification reaction. Moreover, the sulfonated mesoporous silica could be further applied as an alternative acid catalyst for various biomass conversion processes to produce bio-based chemicals and fuels.

Ref. code: 25625909320250YIN

5.2 Recommendations

The KIT-6-SO_3H can be further developed to improve the catalytic activity, acid strength, chemical and thermal stability of catalyst to obtain higher efficiency in the biomass conversion process.

The KIT-6 catalyst can be modified with different acid functional groups such as phosphoric (-PO_4), phenylboronic (-BO), carboxylic (-COO). Moreover, it could combination between Lewis acid and Brønsted acid sites to enhance the biomass conversion and product selectivity.

The removal of produced water in the reaction during dehydration, esterification and etherification process should be considered for preventing the catalyst deactivation and an improvement in production. Follow this idea, the mixture of zeolite as water adsorbents with the catalyst should be placed inside the flow reactor.

The xylose dehydration process can be investigated with different solvents such as butanol, alcohol, THF to comparison the furfural selectivity and optimized condition. The raw fusel oil can be pretreated to remove water and the impurities before studied the esterification reaction. Moreover, the author can study with the microwave-assisted system. The glycerol etherification could be investigated by adding a solvent (toluene, 1,4-dioxane, and ethanol) able to selectively dissolve ethers product generated in the progress of the reaction to improve the reaction rate.

Ref. code: 25625909320250YIN

APPENDICES

Ref. code: 25625909320250YIN

APPENDIX A

SYNTHESIS OF SULFONIC ACID FUNCTIONALIZED KIT-6 CATALYST FOR FURFURAL PRODUCTION BY XYLOSE DEHYDRATION REACTION

A.1 Xylose

Xylose, one of carbohydrate, is a monosaccharide of pentose sugar comprises five carbon atoms and a formyl or aldehyde functional group. It was originated in biomass hemicellulose with free carbonyl group can adopt various structures (Binder, Blank, Cefali, & Raines, 2010). Xylose is widely applied in industries include pharmaceutical (as intermediate in medicine manufacturing), food production (as sweetener in beverage and food), cosmetics (as additive used to reduce the loss of moisture in cleanser, fragrance ingredient, moisture creams and body lotions), human consumption, agriculture/animal feed, etc. ("Applications and uses of D-Xylose," 2015). Moreover, xylose is a precursor to synthetic polymers, solvent in industry and several chemicals such as furan-based biofuel, bioethanol, furfuryl alcohol, furfural, xylitol, THF, organic acids, carbon materials, etc.

The usage of xylose has drawn attention with the development of high-value utilization of biomass. Xylose can be transformed into a variety of valuable chemicals by different technique such as fermentation to ethanol, dehydration to furfural, electrochemical reduction of xylose to xylitol, hydrothermal carbonization. Acid catalyzed dehydration and hydrolysis of the pentose sugars draw up the basis of such industry.

A.2 Furfural

Furfural ($C_5H_4O_2$) is a cyclic formyl compound that can be derived from biomass hemicellulose (pentose sugar) such as wheat straw, sugarcane, corn stover, almond husks, wood, cottonseed hulls, rice husks, etc.) The furfural has been utilized as a biofuel precursor or furan-based chemicals with widely apply in an industry

Ref. code: 25625909320250YIN

comprised bioplastic, agrochemicals pharmaceuticals and organic solvent (tetrahydrofuran (THF), methyl tetrahydrofuran (MeTHF)), etc. In the world, about 60 – 70 % of furfural production has been converted to furfuryl alcohol. (Hoydonckx, Van-Rhijn, Van-Rhijn, De Vos, & Jacobs, 2007) The remaining part is used as

- "Extractant for aromatics from lubricating oils.
- Purification solvent for C4 and C5 hydrocarbons.
- Reactive solvent and wetting agent.
- Chemical feedstock for other furan derivatives.
- Nematode control agent".

To illustrate, a hemicellulose hydrolysis into monomeric sugars and the xylose dehydration into furfural and furfural undergoes with typical reactions will be shown in **Figure A.1**.

Furfural is a viscous, colorless liquid that has an aromatic scent similar to almonds which quickly darkens or black color when exposed to air. The physical properties of furfural will be shown in **Table A.1** (Hoydonckx et al., 2007)

A.2.1 Standard calibration curve for furfural production (HPLC)

First, a furfural solution was prepared 0.01 g of furfural (AR grade, 99%, Sigma-Aldrich) was dissolved in Toluene and titrated in 10 mL volumetric flasks. Then, using that solution to prepare several standard solutions in 10 mL volumetric flasks (0.2, 0.4, 0.6, 0.8 and 1.0 mM) follow by **Equation (3.5)**:

$$C_1V_1 = C_2V_2 \qquad (3.5)$$

C_1: Initial concentration of furfural solution (~10.05 mM)

V_1: Amount of initial furfural solution (mL)

C_2: Desired concentration of furfural solution (0.2 – 1 mM)

V_2: Amount of desired furfural solution (10 mL)

A.2.2 Standard calibration curve for xylose conversion (HS-GC-MS)

Xylose solution was prepared with xylose concentration (~5 – 30 ppm). First, the mixture of 1.0 mL xylose solution and 5.0 mL H_2SO_4 (98%, QReC) was transferred to the bottle. After that, the bottle was put in the water batch at 70 °C for

Ref. code: 25625909320250YIN

15 min. Finally, 100 μL of this product was pipetted into headspace vials that contained Na_2CO_3 anhydrous for analysis with HS-GC-MS.

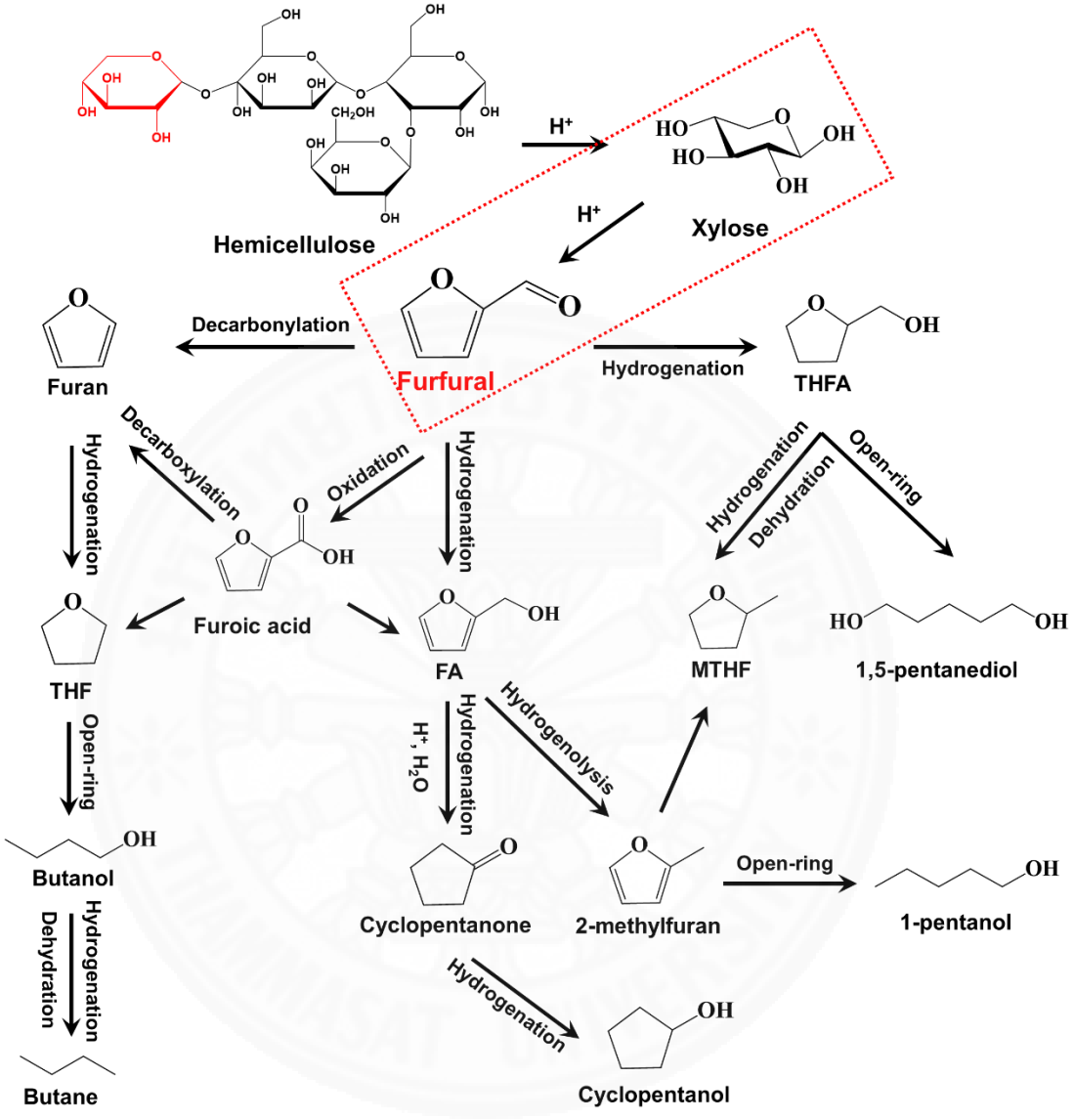

Figure A.1 Furfural derivatives from biomass hemicellulose

Ref. code: 25625909320250YIN

Table A.1 Physical properties of furfural production

Property	
Molar mass (g/mol)	96.08
Boiling point at 101.3 kPa (°C)	161.7
Flash point, tag closed cup (°C)	61.7
ρ at 20 °C (g/cm^3)	1.1598
Vapor density (Air = 1)	3.3
Critical pressure Pc (MPa)	5.502
Viscosity, 25°C (mPa.s)	1.49
Critical temperature Tc (°C)	397
Solubility, in water, wt.% (25 °C)	8.3
Ethyl alcohol, diethyl ether	∞
Spectroscopic polarity (E_T^N)	0.426
Dielectric constant at 20 °C	41.9
Heat of vaporization (liquid) (kJ/mol)	42.8
Heat capacity (liquid, 20 – 100 °C) ($Jg^{-1}K^{-1}$)	11.74
Heat of combustion (liquid) (kJ/mol)	2344
ΔH_f (l), (kJ/mol)	-201.65
ΔH_f (g), (kJ/mol)	-151.05
Explosion limits (in air), (vol.%)	2.1 - 19.3
Surface tension at 29.9 °C (mN/m)	40.7

Ref. code: 25625909320250YIN

APPENDIX B

PRODUCTION OF ISOAMYL ACETATE FROM FUSEL OIL ESTERIFICATION USING A SULFONIC ACID FUNCTIONALIZED KIT-6 CATALYST

B.1 Fusel oil

Fusel alcohols, fuselol or fusel oil are mixtures of several alcohols (chiefly amyl alcohol) such as isoamyl alcohol, isobutyl alcohol, and propanol obtained as a by-product during bioethanol fermentation. Fusel oil production is a natural part of fermentation, thus present in all wines, whiskey, rum, bourbon, vodka, beer, cider and other products. Fusel oil has a high boiling point between 130 and 132 °C and must be removed from the low volatility fractions during distillation. The GC-FID chromatogram of fusel oil compositions as shown in **Figure B.1**.

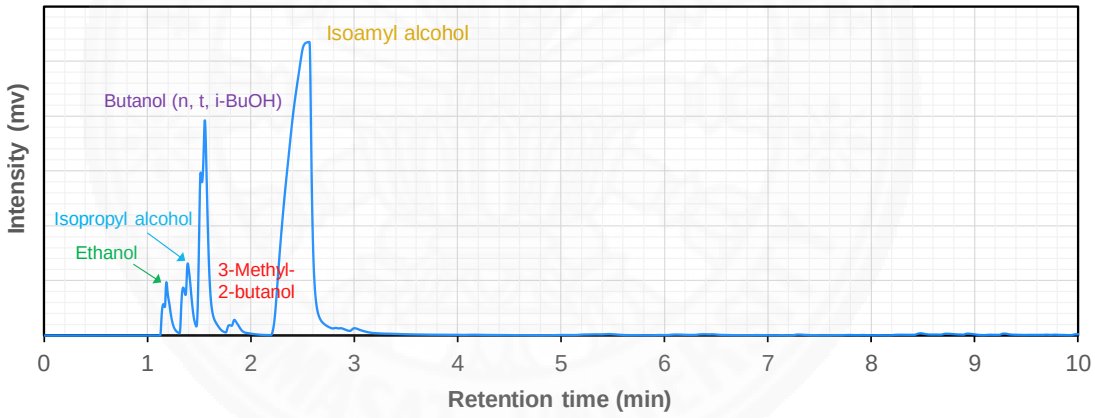

Figure B.1 The GC-FID chromatogram of raw fusel oil

B.2 Isoamyl acetate

Isoamyl acetate, isopentyl acetate or banana oil ($C_7H_{14}O_2$) is an organic compound that is the ester formed with reaction between isoamyl alcohol and acetic acid as shown in **Figure B.1**. It is a colorless liquid and slightly soluble in water but dissolved in most organic solvents. Isoamyl acetate has a strong odor which is also described as like both banana and pear. Isoamyl acetate is made naturally and

Ref. code: 25625909320250YIN

synthetically. The natural version has a sweet, fruity, fragrance. The synthetic version has a lighter scent. Whether natural or synthetic, it's used various ways.

Isoamyl acetate is a natural flavor ester, widely used as a source of banana flavor by the food industry. Moreover, isoamyl acetate are used in cements and glues, paper coatings, lacquers and paints, leather finishes, flavoring, perfume, nail enamels, plastic wood, textile sizing and finishes, printing compounds, and photographic film. They are used in extraction of penicillin, as a warning odor, as a solvent for nitrocellulose and ethyl cellulose, and as a solvent for phosphors in fluorescent lamps. (Quilter, Hurley, Lynch, & Murphy, 2003)

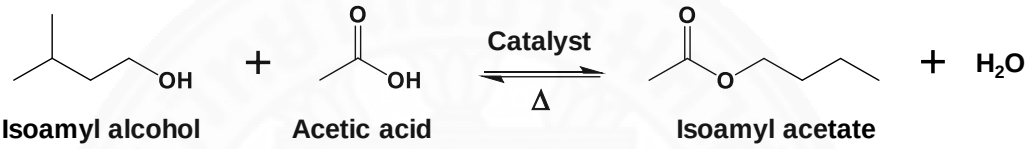

Figure B.2 Isoamyl acetate production from fusel oil esterification with acetic acid

Ref. code: 25625909320250YIN

APPENDIX C

GLYCEROL ETHERIFICATION USING A SULFONIC ACID FUNCTIONALIZED KIT-6 CATALYST FOR FUEL ADDITIVE

C.1 Glycerol

Glycerol or glycerin ($C_3H_8O_3$) is a simple polyol compound or sugar alcohol. It is a colorless, odorless, viscous liquid that is sweet-tasting and non-toxic. The glycerol backbone is found in those lipids known as glycerides. It is widely used in a variety of personal care products, including toothpaste, hair conditioner, cosmetics, and moisturizers. It can also be used as an effective marker to measure liver disease. It is also widely used as a sweetener in the food industry and as a humectant in pharmaceutical formulations. Owing to the presence of three hydroxyl groups, glycerol is miscible with water and is hygroscopic in nature. The U.S. Food and Drug Administration (FDA) is the primary regulator of over-the-counter products and food packaging materials. FDA has approved glycerol for use as an additive to food packaging materials. Glycerol also has been approved for use in skin care products. To illustrate, a transformation of glycerol into valuable chemicals with typical reactions will be shown in **Figure C.1**.

C.2 Glycerol n-butyl ethers

Glycerol n-butyl ethers-based fuel additives were tested as cold flow improvers on the viscosity of biodiesel (Bradin, Grune, & Trivette, 2009; García, Laca, Pérez, Garrido, & Peinado, 2008; Melero, Vicente, Morales, Paniagua, & Bustamante, 2010; Noureddini, 2000; Smith, Ngothai, Nguyen, & O'Neill, 2010). The blending of glycerol-based additives with diesel fuel has reduced the amount of particulate emissions (NO_x), increased the lubricity of diesel, increased engine performance, and increased the distillation temperature of diesel (Kesling, Karas, & Liotta, 1994; Lovestead & Bruno, 2011; Mukhopadhyay & Chakraborty, 2015; Oprescu et al., 2014).

Ref. code: 25625909320250YIN

Moreover, these additives also show increased performance for the wear preventive characteristics of lubricating grease (Samoilov, Ramazanov, Nekhaev, Maximov, & Bagdasarov, 2016) To illustrate, a side reaction of glycerol and n-butanol will be shown in **Figure C.2**.

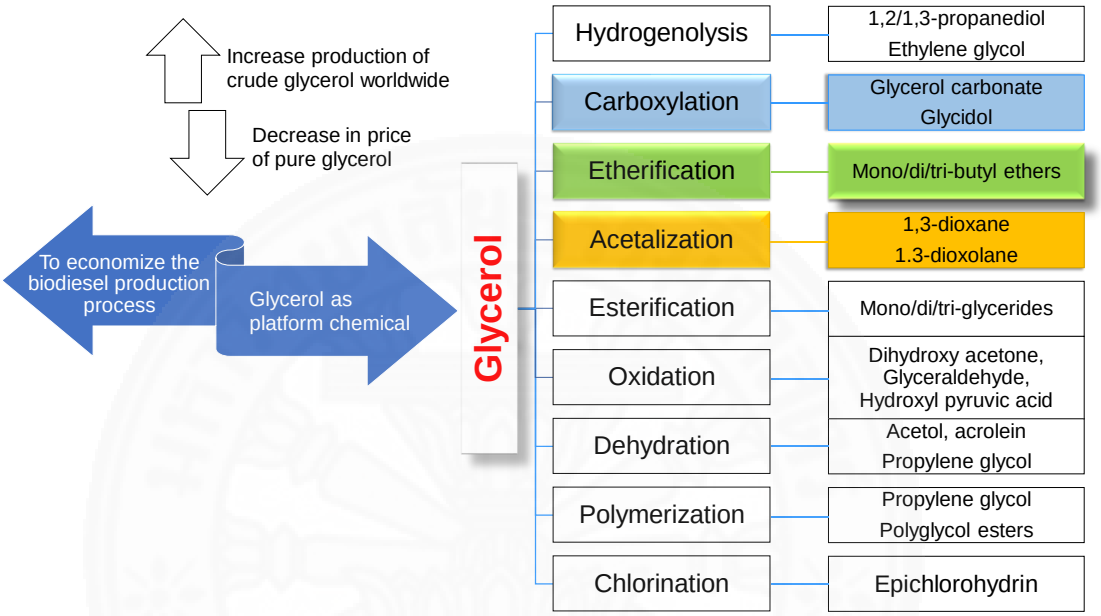

Figure C.1 The pathways for the transformation of glycerol into value-added chemicals and products

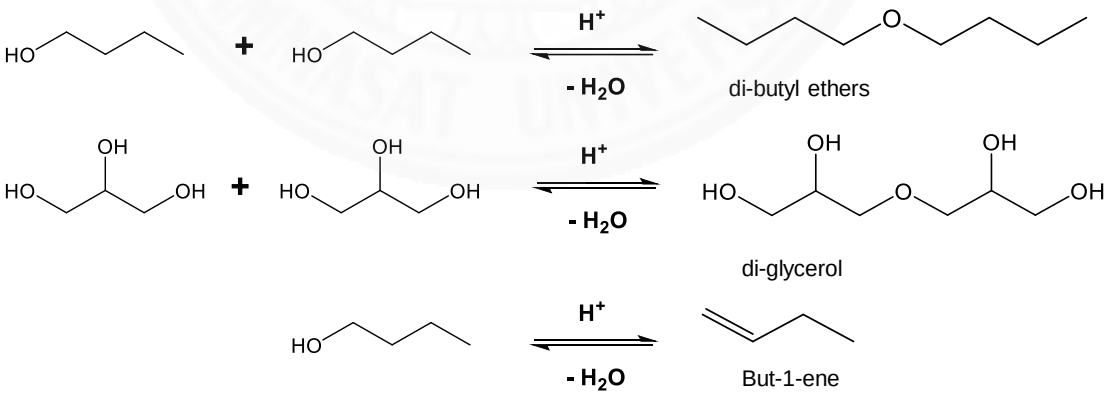

Figure C.2 The possible side reaction of etherification of glycerol and n-butanol

Ref. code: 25625909320250YIN

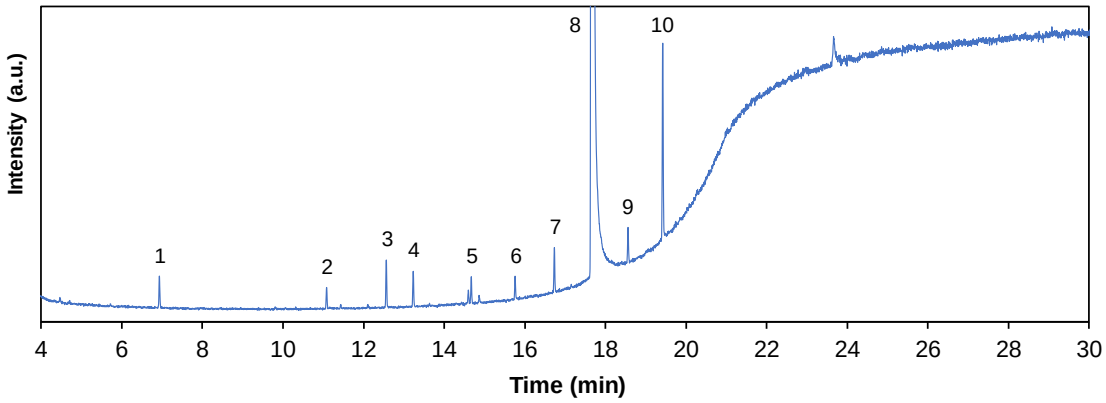

Peak #	Compounds
1	1,4,7,10,13,16-Hexaoxacyclooctadecane
2	Butane, 1,1-diethoxy-2-methyl-
3	[5-Hydroxymethyl)-1,3-dioxolan-4-yl]methanol
4	1,3-Dioxolane-4-methanol, 2-ethyl-
5	Ethanol, 2-(2-butoxyethoxy)-, acetate
6	Pentadecanoic acid, methyl ester
7	Hexadecanoic acid, methyl ester
8	Methyl heptadecanoate (Standard)
9	Nonadecanoic acid, methyl ester
10	1,3-dibutoxypropan-2-ol

Figure C.3 The GC-MS chromatogram of glycerol etherification at 140 °C – 6 h, 10 wt.% catalyst loading

Ref. code: 25625909320250YIN

References

Applications and uses of D-Xylose. (2015). In M.R.N.S.I.T. Rm503 (Ed.), *Use and application*. Newsee.

Binder, J. B., Blank, J. J., Cefali, A. V., & Raines, R. T. (2010). Synthesis of furfural from xylose and xylan. *ChemSusChem, 3* (11), 1268-1272. doi:10.1002/cssc.201000181

Bradin, D., Grune, G. L., & Trivette, M. (2009). Alternative fuel and fuel additive compositions. In: Google Patents.

García, E., Laca, M., Pérez, E., Garrido, A., & Peinado, J. (2008). New class of acetal derived from glycerin as a biodiesel fuel component. *Energy & Fuels, 22* (6), 4274-4280. doi:10.1021/ef800477m

Hoydonckx, H. E., Van Rhijn, W. M., Van Rhijn, W., De Vos, D. E., & Jacobs, P. A. (2007). *Furfural and Derivatives*. Weinheim, Wiley-VCH.

Kesling Jr, H. S., Karas, L. J., & Liotta Jr, F. J. (1994). Diesel fuel. In: Google Patents.

Lovestead, T. M., & Bruno, T. J. (2011). Comparison of diesel fuel oxygenate additives to the composition-explicit distillation curve method. Part 3: t-butyl glycerols. *Energy & Fuels, 25* (6), 2518-2525. doi:10.1021/ef200343a

Melero, J. A., Vicente, G., Morales, G., Paniagua, M., & Bustamante, J. (2010). Oxygenated compounds derived from glycerol for biodiesel formulation: Influence on EN 14214 quality parameters. *Fuel, 89* (8), 2011-2018. doi:https://doi.org/10.1016/j.fuel.2010.03.042

Mukhopadhyay, P., & Chakraborty, R. J. E. P. (2015). Effects of bioglycerol based fuel additives on diesel fuel property, engine performance and emission quality: a review. *79*, 671-676.

Noureddini, H. (2000). Process for producing biodiesel fuel with reduced viscosity and a cloud point below thirty-two (32) degrees Fahrenheit. In: Google Patents.

Oprescu, E.-E., Dragomir, R. E., Radu, E., Radu, A., Velea, S., Bolocan, I., . . . Rosca, P. (2014). Performance and emission characteristics of diesel engine powered with diesel–glycerol derivatives blends. *Fuel Processing Technology, 126*, 460-468. doi:https://doi.org/10.1016/j.fuproc.2014.05.027

Ref. code: 25625909320250YIN

Quilter, M., Hurley, J., Lynch, F., & Murphy, M. (2003). The production of isoamyl acetate from amyl alcohol by Saccharomyces cerevisiae. *Journal of the Institute of Brewing, 109* (1), 34-40.

Samoilov, V. O., Ramazanov, D. N., Nekhaev, A. I., Maximov, A. L., & Bagdasarov, L. N. J. F. (2016). Heterogeneous catalytic conversion of glycerol to oxygenated fuel additives. *172*, 310-319.

Smith, P. C., Ngothai, Y., Dzuy Nguyen, Q., & O'Neill, B. K. (2010). Improving the low-temperature properties of biodiesel: Methods and consequences. *Renewable Energy, 35* (6), 1145-1151. doi:https://doi.org/10.1016/j.renene.2009.12.007

Ref. code: 25625909320250YIN

BIOGRAPHY

Name	Miss Tran Thi Tuong Vi
Date of Birth	March 3, 1992
Citizenship	Vietnamese
Educational Attainment	2017 – 2020: Doctoral of Philosophy (Chemistry) Thammasat University, Thailand (International Program) 2014 – 2016: Master of Science (Chemistry), Thammasat University, Thailand (International Program) 2010 – 2014: Bachelor's degree of Petrochemistry Technology in Industrial University of HCM City, VietNam
Scholarship	2016 – 2019: Scholarships for Foreign Students Studying toward a Degree 2560 B.E in Thammasat University 2014 – 2016: ASEAN Economic Community Scholarship (AEC scholarship) in Thammasat University 2010: Industrial University of HCM City.

PUBLICATIONS

[1] C. Samart, **T.T.V. Tran**, S. Kongparakul, S. Karnjanakom, P. Reubroycharoen, Heterogeneous catalysis in hydroxymethylfurfural conversion to fuels and chemicals, in: S. Nanda, D.-V. N. Vo, P.K. Sarangi (Eds.), Biorefinery of Alternative Resources: Targeting Green Fuels and Platform Chemicals, Springer Singapore, Singapore, 2020, pp. 355-370. **Book Chapter**

[2] P. Waribam, S.D. Ngo, **T.T.V. Tran**, S. Kongparakul, P. Reubroycharoen, N. Chanlek, L. Wei, H. Zhang, G. Guan, C. Samart, Waste biomass valorization through production

Ref. code: 25625909320250YIN

of xylose-based porous carbon microspheres for supercapacitor applications, Waste Management 105 (2020) 492-500.

[3] S.D. Ngo, **T.T.V. Tran**, S. Kongparakul, P. Reubroycharoen, P. Kidkhuntod, N. Chanlek, J. Wang, G. Guan, C. Samart, Catalytic pyrolysis of Napier grass with nickel-copper core-shell bi-functional catalyst, Journal of Analytical and Applied Pyrolysis 145 (2020) 104745.

[4] **T.T.V. Tran**, S. Kongparakul, S. Karnjanakom, P. Reubroycharoen, G. Guan, N. Chanlek, C. Samart, Selective production of green solvent (isoamyl acetate) from fusel oil using a sulfonic acid-functionalized KIT-6 catalyst, Molecular Catalysis 484 (2020) 110724.

[5] L.K.H. Pham, **T.T.V. Tran**, S. Kongparakul, P. Reubroycharoen, S. Karnjanakom, G. Guan, C. Samart, Formation and activity of activated carbon supported Ni2P catalysts for atmospheric deoxygenation of waste cooking oil, Fuel Processing Technology 185 (2019) 117-125.

[6] L.K.H. Pham, S.D. Ngo, **T.T.V. Tran**, S. Kongparakul, P. Reubroycharoen, C. Chaiya, D.-V.N. Vo, G. Guan, C. Samart, Integrated catalytic hydrodeoxygenation of Napier grass pyrolysis vapor using a Ni2P/C catalyst, Journal of Analytical and Applied Pyrolysis 140 (2019) 170-178.

[7] W. Kettum, **T.T.V. Tran**, S. Kongparakul, P. Reubroycharoen, J. Wang, G. Guan, M. Ding, C. Samart, High selective monoaromatic hydrocarbon production via integrated pyrolysis and catalytic upgrading of Napier grass over Ca/Ni/boronic acid/KIT-6, Biomass Conversion and Biorefinery (2019).

[8] **T.T.V. Tran**, S. Kongparakul, S. Karnjanakom, P. Reubroycharoen, G. Guan, N. Chanlek, C. Samart, Highly productive xylose dehydration using a sulfonic acid functionalized KIT-6 catalyst, Fuel 236 (2019) 1156-1163.

[9] W. Kettum, **T.T.V. Tran**, S. Kongparakul, P. Reubroycharoen, G. Guan, N. Chanlek, C. Samart, Heavy metal sequestration with a boronic acid-functionalized carbon-based adsorbent, Journal of Environmental Chemical Engineering 6(1) (2018) 1147-1154.

[10] **T.T.V. Tran**, S. Kongparakul, P. Reubroycharoen, G. Guan, M.H. Nguyen, N. Chanlek, C. Samart, Production of furan-based biofuel with an environmental benign carbon catalyst, Environmental Progress & Sustainable Energy 37(4) (2018) 1455-1461.

Ref. code: 25625909320250YIN

[11] **T.T.V. Tran**, S. Kaiprommarat, S. Kongparakul, P. Reubroycharoen, G. Guan, M.H. Nguyen, C. Samart, Green biodiesel production from waste cooking oil using an environmentally benign acid catalyst, Waste Management 52 (2016) 367-374.

CERTIFICATIONS/AWARDS

[1] Best Oral Presentation Award for Oral Presentation in the 31st International Symposium on Chemical Engineering (ISChE) on Dec 30–2, 2018, Chiang Mai, Thailand.

[2] Scholarship for youth chemists participating at the 8th IUPAC International Conference on Green Chemistry (ICGC) on Sep 9–14, 2018, Bangkok, Thailand.

[3] Best Oral Presentation Award for Oral Presentation in the 30th International Symposium on Chemical Engineering (ISChE) on Dec 1–3, 2017, Deajeon, Korea.

[4] Best Student Paper Award for Oral Presentation in the 3rd Asian Conference on Biomass Science (ACBS) on January 19, 2016, Niigata, Japan.

[5] Quality Assurance and Accreditation ISC/IEC 17025 and ISO/IEC 17020, April 2016, Thammasat University, Thailand.

CONFERENCES

[1] Oral presentation in topic: “Esterification of Fusel Oil and Acetic Acid via Sulfonated KIT-6 Mesoporous Silica” in the 1st Thailand Biorefinery Conference on July 25-26, 2019, Suranaree University of Technology, Nakhon Ratchasima, Thailand.

[2] Oral and poster presentation in topic: “Esterification of Fusel Oil by Heterogeneous Sulfonated KIT-6 Mesoporous Catalyst” in the 8th International Symposium on Catalysis and Fine Chemicals (C&FC) on December 10-14, 2018, Chulalongkorn University, Bangkok, Thailand.

[3] Oral presentation in topic: “Esterification of Fusel Oil by Sulfonated KIT-6 Mesoporous Silica Catalyst” in the 31st International Symposium on Chemical Engineering (ISChE) on November 30 – December 2, 2018, ChiangMai, Thailand.

[4] Oral presentation in topic: “Dehydration of D-xylose into Furfural Production over KIT-6 Mesoporous Sulfonic Acid Catalyst” in the 8th IUPAC International Conference on Green Chemistry (ICGC) on September 9-14, 2018, Shangri-La Hotel, Bangkok, Thailand.

[5] Poster presentation in topic: “Furfural Production with MPr-SO_3H-KIT-6 Mesoporous Catalyst via Xylose Dehydration Process” in the PACCON 2018 on February 7-9, 2018, Songkla University, Hat Yai, Thailand.

Ref. code: 25625909320250YIN

[6] Oral presentation in topic: “Dehydration of D-xylose into Furfural Production over KIT-6 Mesoporous Sulfonic Acid Catalyst” in the NSYSU-TU Bilateral Workshop on Chemical Science on January 15-18, 2018, National Sun Yat-sen University, Kaohsiung, Taiwan.

[7] Oral presentation in topic: “Preparation of KIT-6 Mesoporous Catalysts for Furfural Production from Xylose Dehydration” in the 30th International Symposium on Chemical Engineering (ISChE) on December 1-3, 2017, KAIST Daejeon, Korea.

[8] Innovative Green Chemistry Research Unit, Faculty of Science and Technology, Thammasat University, Workshop, 2017, Thailand.

[9] 1st HORIBA-TU Science Forum, Green Catalysis and Clean Energy toward Sustainable Society, Workshop, Aug 2016, Thailand.

[10] Oral presentation in topic: “Development Sulfonated Carbon Microsphere for the Catalyst of Biodiesel Production” in the 3rd Asian Conference on Biomass Science (ACBS 2016), January 19, 2016, Niigata, Japan.

[11] Oral presentation in topic: “Cleaner Biodiesel Production from Waste Cooking Oil using a Carbon Solid Acid Catalyst” in the 5th International Conference on Green and Sustainable Innovation (ICGSI 2015), November 8 – 10, 2015, Pattaya, Thailand.

[12] Oral presentation in topic: “Sulfonated Carbon Microsphere Catalyst for Biodiesel Production from Waste Cooking Oil” in the AUN/SEED-NET Regional Conference on Materials Engineering (RCME 2015), October 29 – 30, 2015 Bangkok, Thailand.

[13] Oral presentation in topic: “Green Production of Carbon Microsphere by Hydrothermal Carbonization of Xylose” in Biotechnology International Congress (BIC 2015), TU-TSB Special Session on Biomass Utilization, September 10, 2015, BITEC, Bangkok, Thailand.

[14] ACS/CST BOOST Skills Workshop for Young Thai Scientists and Engineers, July 2015, Thammasat University, Thailand.

[15] Poster presentation in topic: “Green Production of Carbon Microsphere by Hydrothermal Carbonization of Xylose” in Paccon Conference 2015, January 21 – 23, 2015 Bangkok, Thailand.

Ref. code: 25625909320250YIN